Title
Mechanisms of Large COPII-coated Procollagen I Carrier Formation

Author
Yuan, Lin

Publication Date
2017

Peer reviewed|Thesis/dissertation

Mechanisms of Large COPII-coated Procollagen I Carrier Formation

By

Lin Yuan

A dissertation submitted in partial satisfaction of the

requirements for the degree of

Doctor of Philosophy

in

Molecular and Cell Biology

in the

Graduate Division

of the

University of California, Berkeley

Committee in charge:

Professor Randy Schekman, Chair
Professor Michael Rape
Professor Gregory Barton
Professor Ke Xu

Summer 2017

Abstract

Mechanisms of Large COPII-coated Procollagen I Carrier Formation

by

Lin Yuan

Doctor of Philosophy in Molecular and Cell Biology

University of California, Berkeley

Professor Randy Schekman, Chair

The coat protein complex II (COPII) mediates ER-to-Golgi transport in protein secretion. Genetic diseases affecting COPII function have demonstrated a requirement for COPII in secretion of bulky cargos, such as the 300-nm procollagen I (PC1), which is 5 times the diameter of an average COPII vesicle. Although large COPII vesicles were previously observed in cells overexpressing KLHL12, a substrate adaptor of the E3 ligase CUL3, the role of large COPII vesicles as PC1 transport carriers was not unambiguously demonstrated, and the mechanism of cargo packaging and vesicle enlargement required further elucidation.

The research presented in this dissertation reports the existence of bona fide large COPII carriers of PC1 with evidence from multiple advanced microscopy techniques. By developing a cell-free COPII vesicle budding reaction, we demonstrated that the capture of PC1 into large COPII vesicles requires COPII proteins and the GTPase activity of the COPII subunit SAR1. This reaction was then used to show the co-packaging of PC1 with its cargo adaptor TANGO1 and the SAR1 nucleotide exchange factor (GEF) SEC12 into large COPII carriers. Coordinated cargo-sensing by TANGO1 and vesicle size regulation by SEC12 through its GEF activity was further shown to be important for PC1 secretion. In an independent effort to understand how the CUL3-KLHL12 complex regulates the size of COPII and PC1 secretion, we discovered that monoubiquitylation of SEC31A can inhibit its stimulatory effect on SAR1-GTP hydrolysis. Together, the study of two independent regulatory pathways revealed a converging mechanism on COPII size regulation by adjusting the local concentration of SAR1-GTP.

Table of Contents

List of Figures

Acknowledgements

Thank you to my mentor Randy Schekman. You gave me freedom to think and work independently as well as guidance at critical moments. You taught me to focus especially during hard times, to persevere without losing the big picture, and to communicate effectively in science and in life.

Thank you to my thesis committee members Michael Rape, Greg Barton, and Ke Xu for your insights and advice. I would like to thank Sam Kenny and Ke Xu for your expertise on STORM, which provided the earliest evidence of large COPII coated PC1 carriers and the beautiful STORM images in Chapters 2 and 3. I would like to thank Colleen McGourty, Nia Teerikorpi, and Michael Rape for your help on setting up ubiquitylation assays in Chapter 4 and Lentiviral protocols as well as valuable discussions. I would like to thank Greg Barton for the inspiration of using flow cytometry to quantify COPII vesicles in Chapter 2.

Thank you to all past and present Schekman lab members. I would like to thank our lab manager Bob Lesch for always looking out for our best interests and pampering us with well-organized inventories and meeting schedules. I would like to thank Amita Gorur, the co-first author of Chapter 2, for being a dependable collaborator and a caring friend; Kanika Bajaj and Satoshi Baba for pioneering the PC1 budding reaction; Min Zhang, David Melville, and Pengcheng Zhang for teaching me molecular and biochemical techniques when I started in the lab; Liang Ge, Dan Sirkis, Johannes Freitag and Matt Shurtleff for discussions that I benefited greatly from; Livy Wilz Brier and Morayma Temoche-Diaz for all the lab fun; Juliet Hemmati for putting up with an inexperienced mentor and helping with the construction of plasmids used in Chapters 3 and 4.

Thank you to Vivek Malhotra for the interesting discussions and debates during your sabbatical at our lab, which have inspired hypotheses and experiments. I also appreciate the generous sharing of plasmids and antibody information from your lab.

Thank you to Susan Marqusee and Jeremy Thorner for kindly providing their fluorometers for the Tryptophan fluorescence experiments in Chapters 3 and 4. Thank you to Shawn Shirazi for helping me with 3D printing, which was essential for the setup of the Tryptophan fluorescence experiments.

Thank you to staff at UC Berkeley shared facilities: Ann Fisher and Alison Kililea at the Tissue culture facility; Steven Ruzin and Denise Schichnes at the CNR

Biolgoical Imaging Facility; Kartoosh Heydari at the Flow cytometry facility; Holly Aaron and Jen-Yi Lee at the Molecular Imaging Center; Reena Zalpuri at the Electron Microscopy Lab, Lori Kohlstaedt at the Vincent J. Coates Proteomics/Mass Spectrometry Laboratory, and Mary West at the Viral Packaging Facility.

Thank you to Nadine Tang and Leslie Tang, the founders of the Tang family fellowship, for your generosity and warmth. I appreciate your support and life advices.

I am extremely grateful to my entire family, as I cannot imagine the journey to this dissertation without you. I would like to thank my parents for the continual support, without which I may not have the opportunity to study abroad. Finally, I would like to thank my husband Tim for your love and encouragement, which had helped me to overcome challenges throughout my graduate career.

Chapter 1: Introduction

As an essential step in conventional protein secretion, coat protein complex II (COPII) mediates vesicular transport from the ER to the Golgi apparatus in eukaryotes. The GTPase SAR1, inner coat proteins SEC23/SEC24, and outer coat proteins SEC13/SEC31 are five cytosolic components of the COP II complex, and they are sufficient to generate COPII-coated vesicles from synthetic liposomes (Matsuoka et al., 1998; Kim et al., 2005). COPII vesicles were observed by EM to be ~60–80 nm in diameter, which potentially limits the transport of large cargos such as the 300-nm-long procollagen I (PC1) rigid rod (Bächinger et al., 1982; Barlowe et al., 1994; Kim et al., 2005; Noble et al., 2013). However, human genetic evidence showed that COPII is required to secrete procollagens. Mutations in genes that code for the human COPII paralogs SEC23A and SEC24D were identified as causing the genetic diseases cranio-lenticulo-sutural dysplasia (CLSD) and osteogenesis imperfecta and their characteristic collagen deposition defects during development (Boyadjiev et al., 2006; Kim et al., 2012; Garbes et al., 2015).

The requirement for COPII to secrete PC has been independently demonstrated in multiple model systems. Mutation of the *sec-23* gene in *Caenorhabditis elegans* disrupts collagen secretion and leads to aberrant cuticle, dissociated hypodermal cells, and late embryonic lethality (Roberts et al., 2003). In *Drosophila melanogaster*, tissue-specific knockdown of Sar1 or Sec23 in collagen-secreting fat body cells leads to intracellular accumulation of collagen and cell lethality (Pastor-Pareja and Xu, 2011). The zebrafish mutants *crusher* and *bulldog* result from mutations in *sec23a* and *sec24d* genes, respectively, and their chondrocytes retain procollagen II in the ER. These mutants also show defects during craniofacial development, with phenotypes reminiscent of human cranio-lenticulo-sutural dysplasia (Lang et al., 2006; Sarmah et al., 2010). Sec23A-null mice are embryonically lethal, and skin fibroblasts accumulate ER-localized collagen I and III (Zhu et al., 2015). Knockdown of SEC13 in primary human dermal fibroblasts also selectively blocks PC1 secretion (Townley et al., 2008). Hence, the requirement for COPII in the ER exit of PC is evolutionarily conserved in metazoans.

The necessary role of COPII in large-cargo secretion is further supported by the discovery of a large transmembrane protein, TANGO1 (MIA3), which has been shown to have a general role in the secretion of large cargos, including many

members of the collagen family, laminin, and large lipoprotein complexes such as prechylomicrons (Saito et al., 2009; Wilson et al., 2011; Petley-Ragan et al., 2016; Santos et al., 2016). The luminal Src homology 3 (SH3) domain of TANGO1 interacts with the PC-specific chaperone HSP47 to recognize a broad range of PC isoforms (Saito et al., 2009; Ishikawa et al., 2016). The cytosolic side of TANGO1 was shown to interact with multiple COPII components: its proline-rich domain (PRD) binds to the inner COPII coat protein SEC23 directly, and its second coiled-coil domain recruits cTAGE5, a spliced variant of a TANGO1 isoform, which binds SEC12, an initiating factor of COPII assembly (Saito et al., 2009, 2011, 2014; Ma and Goldberg, 2016). Therefore, TANGO1 plays an important role in coordinating large-cargo sensing and COPII recruitment, which further supports the involvement of COPII in large-cargo secretion.

Despite the abundant evidence supporting the importance of COPII in PC secretion, the exact role that the COPII complex plays was not demonstrated. This is in part due to the lack of microscopy evidence to identify PC carriers in the early secretory pathway in vivo. An in vitro assay was also needed to test the molecular requirements for the generation of such carriers. In this dissertation, I report our discovery of functional large COPII coated PC1 carriers using a combination of in vivo morphological analyses and in vitro reconstitution studies. The tools that we developed have helped us to further elucidate the mechanism underlying cargo-packaging and provided evidence towards the understanding of vesicle enlargement.

Chapter 2: COPII-coated membranes function as transport carriers of intracellular procollagen I

Introduction

Although the requirement for COPII to export the large cargo PC out of the ER is clear, the precise role that COPII plays in this process is poorly understood. A conventional model was proposed in which COPII concentrates large cargos at ER exit sites (ERESs) and orchestrates the packaging of large cargos into vesicles and the formation of vesicles with structured coats (Fromme and Schekman, 2005). An alternative model suggests that COPII functions only to concentrate large cargos and other factors required for the ER export at ERESs, and large cargos exit the ER in carriers not coated with COPII proteins (Mironov et al., 2003; Siddiqi et al., 2003, 2010).

The conventional model is paradoxical unless a cellular mechanism exists to increase the size of COPII-coated vesicles. The Rape and Schekman laboratories previously reported that the E3 ubiquitin ligase, CUL3, and one of its substrate adaptors, KLHL12, regulate the size of COPII-coated vesicles and collagen I and IV secretion (Jin et al., 2012). Overexpression of KLHL12 induces the formation of large COPII structures that are decorated with KLHL12. Most of these structures are more than 300 nm in diameter and large enough to accommodate cargo of the size of PC1. Unfortunately, the coincident localization of PC1 in these large carriers was not clearly elucidated in that work. Here, we reexamined these large COPII structures and showed that they are bona de membranous carriers of PC1 in cells. Moreover, we reconstituted PC1 capture into vesicles formed in a cell-free reaction. These carriers were isolated and visualized as large COPII-coated vesicles.

The work presented in this chapter has been published previously as part of the following paper: Gorur A, Yuan L, Kenny SJ, Baba S, Xu K, Schekman R. 2017. COPII-coated membranes function as transport carriers of intracellular pro-collagen I. J Cell Biol. Apr 20. doi:10.1083/jcb.201702135.

Results

Large COPII vesicles co-localize with PC1

The ubiquitin ligase CUL3 and its substrate adaptor KLHL12 were shown to regulate collagen secretion and the size of COP II vesicles, possibly through the monoubiquitylation of the COP II protein SEC31A (Jin et al., 2012). To study whether the large COPII vesicles observed after overexpression of KLHL12 are collagen carriers, we engineered human fibrosarcoma cells (KI6) to stably overexpress the human pro-α1(I) collagen and inducible KLHL12 under doxycycline-controlled transcriptional activation. KI6 cells synthesized PC1 in contrast to the parent cell line as confirmed by an immunofluorescence (IF) signal for PC1 (Fig. 2.S1 A) and immunogold-labeled PC1 in the ER and large vesicles (Fig. 2.S1 B). KLHL12 overexpression was reported to accelerate the ER export of PC1: more cells had secreted PC1 after 30 min of ascorbate treatment when KLHL12 was overexpressed, and no significant difference was observed at a later time point (1 h) after ascorbate treatment (Jin et al., 2012). Consistent with our previous study, we also observed accelerated ER-to-Golgi trafficking of PC1 in KI6 cells 20 min after ascorbate treatment in cells that had induced KLHL12 overexpression for 7.5 h (Fig. 2.S1 C; Jin et al., 2012). KI6 cells secreted PC1 through the conventional secretory pathway, shown by the inhibitory effect of brefeldin A (BFA) on the ex- port of PC1 into the culture medium (Fig. 2.S1 D). Because TANGO1-knockout mice are defective in collagen I secretion, we knocked down TANGO1 in KI6 cells and observed a decreased level of PC1 secretion, as detected by immunoblots of the culture medium, with a corresponding intracellular accumulation of PC1 detected in cell lysates (Fig. 2.S1 E; Wilson et al., 2011).

In our previous study (Jin et al., 2012) using a polyclonal antibody (LF-67) raised against synthetic human α1(I) collagen C-telopeptide (Bernstein et al., 1996), we observed partial co-localization between PC1 and KLHL12 but could not unambiguously document that the large COPII vesicles, generated by overexpression of KLHL12, carried PC1. In contrast, with the use of two monoclonal antibodies raised against N- or C-pro- peptides of PC1 (Fig. 2.S2 A; Foellmer et al., 1983), we observed clear co-localization of PC1 and KLHL12 in KI6 cells after 7.5 h of induction (Figs. 2.1 A and 2.S2 B). Puncta positive for both PC1 and KLHL12 also co-localized with SEC31A, a subunit of the outer coat of COPII vesicles (Fig. 2.1 B).

We reasoned that if large COPII vesicles are functional secretory transporters of collagen, they should also contain HSP47, a collagen-specific chaperone. HSP47 binds to the triple helical region of PC in the ER and promotes the correct folding of trimerized PC (Nagai et al., 2000; Tasab et al., 2000, 2002; Ishida and Nagata, 2011; Ono et al., 2012; Widmer et al., 2012). HSP47 accompanies PC to the ER–Golgi intermediate compartment (ERGIC) or cis-Golgi membrane, where it dissociates because of a lower pH, after which it is recycled back to the ER via its C-terminal RDEL sequence (Satoh et al., 1996; Oecal et al., 2016). We found that HSP47 co-localized with the large COPII vesicles as visualized by triple IF labeling of HSP47, SEC31A, and KLHL12 in KI6 cells, consistent with a role for the large COPII vesicles as secretory carriers of PC1 (Fig. 2.1 C).

Large COPII vesicles are hollow membranous containers

Given that conventional confocal microscopy images revealed co-localized diffraction-limited puncta with no discernible morphological details, we sought to resolve these structures using stochastic optical reconstruction microscopy (STORM; Rust et al., 2006; Huang et al., 2008), a type of superresolution microscopy, and correlative light and electron microscopy (CLEM). With 3D STORM analysis, we observed large, hollow, cage-like COPII structures that are 300–1,000 nm in diameter, using a SEC31A antibody and a secondary antibody conjugated with Alexa Fluor 647 fluorophore in KI6 cells induced for the overexpression of KLHL12 (Fig. 2.2 A). A virtual z-stack of a single structure confirmed the cage-like COPII protein localization completely surrounding a cavity in three dimensions. Similar analysis was conducted on vesicles immunolabeled with FLAG antibody, which targeted the overexpressed KLHL12-FLAG, and large hollow cages that were 300–1,000 nm in diameter were also observed (Fig. 2.2 B).

We observed a similar morphological feature by CLEM on regions of co-localized endogenous PC1 and SEC31A without KLHL12 overexpression in human osteosarcoma Saos-2 cells, a cell line that secretes endogenous PC1 (Fig. 2.2 C; Pautke et al., 2004). Correlative serial thin-section EM revealed that fluorescent puncta containing co-localized PC1 and SEC31A were large, single membrane–bounded compartments and were not clusters of small vesicles. These correlated structures were spherical to ovoid in shape and 350 nm to 1.7 µm in diameter, decorated with what may be remnants of coat protein. Collectively, the diffraction-limited PC1 and COPII co-localized puncta were

resolved by STORM and CLEM to be large protein-coated, single membrane–bounded containers.

PC1 is completely encapsulated in large COPII-coated membranes

We next sought to dissect the precise localization of PC1 with respect to the COPII coat within puncta that showed co-localization of the two markers. To achieve this, we performed dual- and triple-color 3D STORM imaging on SEC31A/PC1 co-localizing puncta from cells with overexpressed and endogenous levels of KLHL12. Large COPII cages with hollow cavities were observed in KI6 cells (Fig. 2.3 Aix), consistent with our observation using single-color STORM (Fig. 2.2, Aiii and Aiv), and PC1 was resolved to be inside of the hollow cavities, entirely encapsulated by the COPII cage (Fig. 2.3, Av–Ax; and Video 1). This was also evident in KLHL12/SEC31A/PC1 co-localizing puncta in Saos-2 cells, where endogenous KLHL12 and SEC31A was found surrounding the endogenous PC1 (Fig. 2.3, Bvi–Bxiii). The appearance of confined labeling of the PC1 fiber in relation to the expansive COPII coat may reflect a restricted orientation of the fiber within the vesicle or steric hindrance of the PC1 monoclonal antibody by the polyclonal antibody used to label the coat. In contrast, we did not observe PC1 in canonical COPII cages ranging in size from 80 to 100 nm (Fig. 2.3, Aii–Aiv). Interestingly, we also observed puncta that appeared to have the COPII coat only partially enveloping PC1, possibly representing an intermediate in the shedding of COPII subunits or a nascent budding event at the ERES (Fig. 2.3, Bii–Bxiii; and Fig. 2.S3, A–C).

PC1-containing giant COPII vesicles exhibit movement

The dynamic nature and organization of ER-to-Golgi transport have been visualized previously with the use of fluorescent labeling and time-lapse microscopy (Presley et al., 1997; Scales et al., 1997; Shima et al., 1999). We sought to understand whether the large COPII vesicles were capable of functioning as mobile transport carriers independent of the ER. The localization of large COPII vesicles relative to the ERES and ER was examined in KI6 cells by dual-color confocal and STORM microscopy using antibodies against SEC31A, SEC16A, a scaffolding protein at the ERES, and KDEL, the ER retrieval signal at the C terminus of ER resident proteins. Images from both approaches showed clear separation of large COPII and ERES or ER marker proteins (Fig. 2.4, A and B). Large puncta positive for both SEC31A and SEC16A were also observed by confocal microscopy (Fig. 2.4 A). These coincidently labeled

structures may represent prebudding complexes of COPII vesicles that remained attached to the ER.

We then visualized the spatiotemporal dynamics of these vesicles by imaging YFP-tagged, SEC31A-labeled structures with time-lapse microscopy. KLHL12 was induced in KI6 cells for 7.5 h, and the cells were treated with ascorbate for 10 min to promote the formation of hydroxyproline residues essential to the folding and ER exit of PC1 (Stephens and Pepperkok, 2002). We observed large COPII vesicles exhibiting both long-range (>2 µm displacement) and short-range (<2 µm displacement) transport, as previously observed for fluorescently tagged small COPII vesicles (Fig. 2.4, C and D; and Video 2 Stephens et al., 2000). Long-range transport was not evident in cells treated with nocodazole, a microtubule-depolymerizing agent, as determined by particle tracking of individual vesicles (Fig. 2.4, C and D; and Video 3). The long-range mobility of large COPII vesicles was observed to be independent of a CFP-tagged ER marker (Stephens et al., 2000), which is consistent with our observations in fixed samples (Video 4). To confirm that these large mobile COPII vesicles are PC1 carriers, we tracked vesicles positive for both YFP-tagged SEC31A and CFP-tagged PC1, which also exhibited directional movements (Fig. 2.4 E and Video 5).

COPII is required to package PC1 into vesicles that bud from the ER in a cell-free reaction

To further investigate whether the large-cargo PC1 exits the ER within COPII-coated vesicles, we modified a cell-free reaction designed to detect the formation of transport vesicles that bud from ER membranes in a preparation of permeabilized cells (Fig. 2.5 A; Kim et al., 2005; Merte et al., 2010). Donor ER membrane was prepared from IMR-90 cultured human fibroblasts and incubated at 30°C with purified recombinant human COPII proteins, cytosol, and nucleotides for 1 h to allow the formation of transport vesicles. Budded vesicles were isolated by a modification of our previous procedures to allow the detection of large vesicular carriers. A low centrifugal speed of 7,000 g was used to sediment donor membrane from a complete incubation, and the supernatant fraction, which contained budded vesicles, was applied to the bottom of an Optiprep step flotation gradient. After a high-speed centrifugation step of 250,000 g, 12 fractions were collected, and their contents were analyzed by immunoblotting (Fig. 2.5 B). Because lipid vesicles are buoyant, they floated to the top of the gradient as shown by the enrichment of a standard COPII cargo SEC22B in fraction 1. In contrast, a soluble cytosolic protein marker, vinculin, was observed at the bottom of the gradient in fractions 7–12. Most PC1 signal

floated to the top of the gradient and cofractionated with SEC22B, indicating that most PC1 in the reaction was associated with membrane.

To test whether PC1 detected in the floated fractions was packaged inside of intact membrane vesicles, we used a collagenase protection assay. When the top floated fraction was treated with collagenase at 30°C, most of the PC1 was protected from collagenase digestion and became susceptible only when detergent (1% Triton X-100) was included to lyse the membrane (Fig. 2.5 C). Because collagenase digestion was specific to collagens, another standard COPII cargo, ERGIC53, was used as loading control.

We tested the requirement for COPII in PC1 packaging by supplementing the reaction with the inhibitory SAR1B H79G GTPase-defective mutant protein in place of wild-type SAR1B (Fig. 2.5 D). Significantly less PC1 was detected in the top floated fraction, consistent with the observation that microinjection of SAR1 H79G into live cells arrested PC in the ER (Stephens and Pepperkok, 2002). As further controls, the cell-free reaction was performed in the absence of donor membrane, cytosol, or purified recombinant COPII proteins, respectively. Immunoblotting of the top floated fractions showed that donor membrane, cytosol, purified COPII proteins, and a physiological temperature of 30°C were required to reconstitute export of PC1 (Fig. 2.5 D). PC1 packaging appears to be completely dependent on both cytosolic proteins and COPII for packaging; thus, soluble factors in addition to the COPII coat may be essential to sort PC1 for transport.

PC1 is known to trimerize in the ER, and only the correctly folded PC1 trimers are chaperoned by HSP47 to exit the ER en route to the Golgi membrane. Consistent with our observation in cells where HSP47 was found to be present on the large COPII vesicles, the budding of HSP47 was also observed in the cell-free reaction, which required similar conditions as the budding of PC1 (Figs. 2.5 D and 1 C). To further demonstrate the physiological relevance of our cell-free reaction, we analyzed the content of the floated fractions under a nonreducing, denaturing condition, which would preserve the interchain disulfide bonds and allow the detection of trimeric PC1 (Fig. 2.S2 A). In cell-free reactions supplemented with wild-type SAR1B, lower-mobility ~ 570-kD PC1 (the predicted size of PC1 trimer) was detected in the floated fraction under the nonreducing, denaturing condition, whereas monomeric ~ 190-kD PC1 was detected under a reducing, denaturing condition (Fig. 2.5 E). Consistent with observations under the reducing, denaturing condition, the amount of trimeric PC1 observed in the floated fraction was significantly decreased upon

incubation with SAR1B H79G (Fig. 2.5 E). Thus, we conclude that the COPII-dependent packaging of trimeric PC1 and its chaperone HSP47 is sustained in our cell-free reaction.

PC1 is exported from the ER in large COPII-coated vesicles

To visualize the morphology of vesicular PC1 carriers in the floated fraction, we modified the cell-free reaction so that both the COPII coat and the large-cargo PC1 were fluorescently labeled. For fluorescence visualization of isolated COPII-coated vesicles, we added purified Alexa Fluor 647–conjugated SEC23A/24D to the reaction mixture (Bacia et al., 2011). For fluorescence visualization of PC1, we prepared donor membrane from cells that were transiently transfected with a C-terminally GFP-tagged construct of the pro-α1(I) chain of human PC1. This construct was shown to produce GFP signal that exits the ER in cells incubated in ascorbate-containing medium (Stephens and Pepperkok, 2002). We confirmed that the GFP tag did not interfere with trimerization and ER-to-Golgi transport of PC1-GFP, as GFP signal was found at the Golgi apparatus after the addition of ascorbate (Fig. 2.S4 A). Moreover, PC1-GFP was packaged in a COPII-dependent manner in the vesicle budding reaction, as detected by immunoblotting of GFP in the floated fraction (Fig. 2.S4 B).

Vesicles observed by structured illumination microscopy (SIM) displayed PC1 co-localized with large COPII-coated structures of ~ 400 nm in diameter (Fig. 2.6 A). With the resolution of SIM, the PC1-GFP signal appeared fully within the signal of SEC23A/24D (Fig. 2.6 A and Videos 6 and 7). Smaller COPII structures devoid of PC1-GFP, likely to be conventional COPII vesicles, were also observed. Not all large COPII structures observed contained the PC1-GFP signal (quantified in Fig. 2.6, Biii and Biv), possibly because only 10–30% of the donor membrane contained GFP signal as a result of low transfection efficiency. It is also possible that PC1 was not the only large cargo exiting the ER in large COPII-coated vesicles. Not all PC1-GFP observed co-localized with SEC23A/24D: the nonoverlapping GFP signal may represent PC1 not enclosed within membranes, possibly coinciding with the amount of PC1 that was sensitive to collagenase digestion (Fig. 2.5 C); alternatively, the signal may emanate from transport vesicles from which the COPII coat had been shed (Fig. 2.3 B; Fig. 2.S3, A–C; and Fig. 2.S5 A).

We developed an unbiased flow cytometry approach to quantify the relative fluorescence signal associated with both conventional and large COPII vesicles. Single particles (singlets) were gated for their content of fluorescently labeled COPII proteins SEC23A/24D and the fluorescent lipid dye FM4-64. Particles that

satisfied such criteria accounted for ~ 0.7% of all singlets detected in the 7,000-g supernatant fraction (Fig. 2.6 Bi). Of these COPII-coated vesicles, 9.6% were GFP+, indicating that they carried the large cargo PC1-GFP (Fig. 2.6 Bii). This population of collagen-carrying COPII vesicles exhibited higher side and forward light scatter, both of which positively correlate with larger particle sizes (Fig. 2.6, Biii and Biv). The sizes of reconstituted COPII-coated vesicles were estimated using nanoparticle tracking analysis (NTA), which tracks and analyzes the Brownian motion of each particle (Fig. 2.S5 A; Dragovic et al., 2011). COPII-coated vesicles in the range of 50–150 nm were ~ 17.6× more prevalent than larger COPII-coated vesicles in the range of 300–1,000 nm. A medium-sized category of 150–300 nm was also observed, and it was ~ 4.3× less prevalent than the 50- to 150-nm category and 4.1× more numerous than the larger vesicles. We used thin-section EM to independently confirm the existence of medium to large coated membrane vesicles, with a coat of 10–15 nm (Fig. 2.S5 B).

Recruitment of functional KLHL12 to COPII-coated vesicles

To test whether our cell-free COPII vesicle formation reaction reconstitutes the cellular behavior of KLHL12, we supplemented the reaction with cytosol collected from cells transfected with either FLAG-tagged wild-type KLHL12 or a mutant, FG289AA, that fails to promote the formation of large COPII vesicles (Jin et al., 2012; Fig. 2.7). Densitometry analyses of immunoblots showed 6.8× more wild-type KLHL12 in the vesicle floated fraction compared with the FG289AA mutant protein ($P < 0.0001$, paired t test, $n = 7$; Fig. 2.7, A and B). This result coincided with our previous observation that KLHL12 FG289AA mutant protein rarely co-localized with COPII markers in cells (Jin et al., 2012). The relative budding efficiency of PC1 and control COPII cargos was also calculated from densitometry analyses of immunoblots, and PC1 budding was only marginally stimulated by KLHL12 wild-type cytosol compared with KLHL12 FG289AA cytosol ($P = 0.0412$, paired t test, $n = 7$; Fig. 2.7, A and C). Thus, although we have reconstituted the association of functional KLHL12 with budded vesicles, we were unable to assess the role of this protein in the capture of PC1 in our cell-free reaction. There may be other rate-limiting components, such as the calcium-binding coadaptors PEF1 and ALG2, which may fail to be recruited to the site of vesicle budding under the conditions of this incubation (McGourty et al., 2016).

Discussion

The function of canonical (60- to 80-nm) COPII vesicles in conventional cargo transport is well established: COPII subunits concentrate cargo proteins into vesicles that bud from the ER and form a structure that dictates the size and contour of the bud and completed vesicle (Zanetti et al., 2011). Although a wide range of studies have shown that PC secretion is COPII dependent, it has remained unclear whether COPII coats the membranes surrounding the large cargo or instead plays an indirect role in cargo packaging and transport carrier biogenesis. A primary requirement for the transport of large cargos would be to overcome the structural constraints of a small cage (Noble et al., 2013). KLHL12 was previously shown to fulfill this requirement, as overexpressing KLHL12 induced the formation of large COPII structures (Jin et al., 2012). Here, we confirmed that these large COPII-coated structures appeared hollow, presumably with a space to contain large cargos (Fig. 2.2, A and B). Similar observations were also made in PC1-secreting osteosarcoma cells (Saos-2) without any overexpression of KLHL12 (Figs. 2.2 C and 2.3 B). Notably, CLEM analysis of these structures in Saos-2 showed a COPII-coated single-membrane bilayer envelope surrounding a lumenal space filled with PC1 (Fig. 2.2 C).

Evidence for the contrary model that PC is transported out of the ER in non-COPII carriers came from studies of fibroblasts released from a PC1 hydroxylation block (Mironov et al., 2003). That study reported that PC1 exits from saccular extensions of the ER that appeared devoid of the COPII coat based on IF microscopy and immunogold EM studies. Those conclusions were based on the use of a polyclonal antibody, LF-68, that was generated against synthetic peptides of a unique sequence selected from the C-telopeptide (nontriple-helical segment exposed on the C terminus of mature collagen after a C-terminal propeptide is cleaved) of human α1(I) collagen (Fig. 2.S2 A; Fisher et al., 1995; Bernstein et al., 1996). Here, using two monoclonal antibodies, QED-42024 and sp1.d8, directed against C- and N- terminal propeptides cleaved from triple-helical PC1, respectively (Fig. 2.S2 A; Foellmer et al., 1983), we observed co-localization with large COPII structures in KI6 cells where both PC1 and KLHL12 were overexpressed (Fig. 2.1, A–C; and Fig. 2.3 A), natural collagen I–secreting svIMR-90 cells that overexpressed KLHL12 (Fig. 2.S2 C), and natural collagen I–secreting Saos-2 and IMR-90 cells where PC1 and KLHL12 are expressed endogenously (Figs. 2.2 C, 2.3 B, and 2.S2 D). We have independently confirmed the results of Mironov et al. (2003) using the same

polyclonal antibody (LF-68) for IF localization (Fig. 2.S2 E). However, we suspect that the C-telopeptides are not fully accessible in nondenatured PC1 trimers, possibly hindered by the presence of C-terminal propeptides, which are cleaved in post-Golgi vesicles or after secretion to the extracellular space (Fig. 2.S2 A). Thus this polyclonal antibody may have limited utility in IF detection of folded PC1 species in early secretory transport vesicles.

Independent of PC1 antibody labeling, the co-localization of PC1-CFP and the COPII coat protein SEC31A-YFP was also observed in live cells (Fig. 2.4 E). Moreover, the PC-specific chaperone HSP47 also co-localized with KLHL12 and COPII (Fig. 2.1 C). HSP47 binds to trimerized PC in the ER and assists its correct folding by preventing lateral aggregation (Nagai et al., 2000; Tasab et al., 2000; Ono et al., 2012; Widmer et al., 2012). This chaperone traverses the early secretory pathway with PC to ERGIC or cis-Golgi membranes, where it is released because of lower pH, before being recycled back to the ER via its C-terminal RDEL sequence (Satoh et al., 1996; Oecal et al., 2016). In HSP47-knockout mouse embryonic fibroblasts, misfolded PC1 trimers were observed to accumulate in the ER and were degraded by autophagy, independent of the ERAD-mediated clearance of monomeric PC1 aggregates (Ishida et al., 2006). Hence, the observation of HSP47 co-localized with large COPII confirms that these large COPII structures contain correctly folded triple helical PC1 and are physiologically relevant.

STORM and CLEM analyses revealed the ultrastructural details of these large COPII structures: collagen became completely encapsulated in a large COPII coat during vesicle formation, suggesting that COPII proteins acted directly by forming a complete cage around a single membrane bilayer vesicle that carried PC1 (Fig. 2.2). Furthermore, fluorescently labeled large COPII vesicles showed microtubule-dependent vectorial movement in live cells (Fig. 2.4, C–E). To sum up, bona fide large COPII-coated single-membrane carriers of PC1 were observed in fixed as well as live cells.

In an independent effort to test the role of COPII-coated vesicles in the sorting of PC1, we used a cell-free transport vesicle budding assay that was previously developed in our laboratory to probe the requirements for sorting of conventional COPII cargo proteins (Kim et al., 2005; Merte et al., 2010). Here, we report an alternative fractionation method to detect the ER export of the large-cargo PC1 and its chaperone HSP47 (Fig. 2.5). Using the combination of a buoyant density flotation protocol, a collagenase protection assay, and SIM, we showed that PC1 exits the ER inside of large membrane vesicles that are coated

with COPII proteins (Fig. 2.5, B and C; and Fig. 2.6 A). Furthermore, the packaging of PC1 requires the addition of recombinant COPII proteins, as well as other unspecified cytosolic proteins, and depends on the GTPase activity of SAR1, the GTP-binding protein that initiates the assembly of the COPII coat (Fig. 2.5 D).

Although we were unable to identify a function for KLHL12 in our cell-free reaction, we observed the wild-type but not a ubiquitylation-defective mutant form of the protein recruited to budded vesicles (Fig. 2.7). The requirement for cytosolic proteins in addition to COPII is consistent with reports in the literature of other factors such as Sedlin, Sly1, TFG, ALG2, and PEF1 in the export of PC from the ER (Venditti et al., 2012; Nogueira et al., 2014; McCaughey et al., 2016; McGourty et al., 2016). Further resolution of the cytosolic proteins required in the cell-free reaction may illuminate those that cooperate with KLHL12 to stimulate PC1 packaging.

In summary, we examined the role of COPII during the ER export of large-cargo PC1 using a combination of in vivo morphological analyses and in vitro reconstitution studies. Our results support the conventional model in which COPII participates directly by forming a large COPII-coated membrane vesicle to transport bulky cargo out of the ER. Although the exact mechanism by which the size of COPII vesicles is regulated awaits further investigation, the cell-free PC1 budding reaction described here should aid in such studies.

Materials and methods

Antibodies and plasmids

Commercially available antibodies used for IF and immunoblotting (IB) were as follows: mouse anti-PC1 (clone 42024; QED Biosciences; 1:200 [1 mg/ml stock concentration] for IF); rabbit anti-SEC31A (Bethyl Laboratories; for IF, at 1:200 for confocal and 1:2,000 for STORM); mouse anti-FLAG (Thermo Fisher Scientific; 1:5,000 for IB); goat anti-FLAG (Novus Biologicals; for IF at 1:1,000 for confocal and 1:5,000 for STORM); chicken anti-KLHL12 (Novus Biologicals; for IF at 1:200 for confocal and 1:2,000 for STORM); mouse anti-KLHL12 (clone 2G2; Cell Signaling Technology; at 1:1,000 for IB); rabbit anti-calnexin (Abcam; at 1:200 for IF); mouse anti-HSP47 (Enzo Life Sciences; at 1:200 for IF and 1:5,000 for IB); sheep anti-TGN46 (AbD Serotec; at 1:200 for IF); mouse anti-KDEL (clone 10C3; Enzo Life Sciences; at 1:200 for IF); mouse anti-vinculin

(Abcam; 1:5,000 for IB); and rabbit anti-GFP (Torrey Pines Biolabs; at 1:1,000 for IB). Rabbit anti–ribophorin I, ERGIC53, and SEC22B were made in-house and used at 1:5,000 for IB. Rabbit anti–PC1 LF-41, -67, and -68 antibodies were a gift from L. Fisher (National Institute of Dental and Craniofacial Research, Bethesda, MD; Fisher et al., 1989, 1995; Bernstein et al., 1996). LF-67 and LF-68 were raised against the same synthetic peptide of the human α1(I) collagen C-telopeptide (aa 1,192–1,218; Bernstein et al., 1996), and LF-68 was used at 1:1,000 for IF only to repeat previous studies (Mironov et al., 2003; Jin et al., 2012). LF-41 was raised against a synthetic peptide of the C terminus of the human α1(I) collagen (aa 1,443–1,464; Fisher et al., 1989) and was used for all anti-PC1 IB at 1:5,000, but not for IF in this study. The mouse anti-PC1 antibody sp1.d8 was purified in-house from culture medium of mouse hybridoma cells obtained from Developmental Studies Hybridoma Bank at the University of Iowa (Iowa City, IA) using standard procedures and used at 3.75 ng/µl for IF. Expression constructs for SEC31A-YFP, PC-CFP, PC-GFP, and pCFP-ER (encodes a fusion protein consisting of enhanced CFP flanked by an N-terminal signal peptide of calreticulin and a C-terminal ER retrieval sequence, KDEL) were provided by D. Stephens (University of Bristol, Bristol, England, UK).

Cell culture, transfection, and drug treatments

Human lung fibroblasts IMR-90 and svIMR-90 (IMR-90 immortalized with SV-40) were obtained from Coriell Cell Repositories at the National Institute on Aging, Coriell Institute for Medical Research. Human osteosarcoma Saos-2 and U-2OS and human fibrosarcoma HT-1080 were obtained from ATCC. IMR-90, svIMR-90, Saos-2, U-2OS, and HT-1080 were maintained in DMEM plus 10% FBS (GE Healthcare). The HT-PC1.1 cell line was generated from HT-1080 as previously described (Jin et al., 2012) by stable expression of COL1A1 in a pRMc/CMV plasmid (gift from N. Bulleid, University of Glasgow, Glasgow, Scotland, UK) and maintained in 0.4 mg/ml G418. The doxycycline-inducible KLHL12-3xFLAG stable cell line (KI6) was generated through sequential clonal selection of HT-PC1.1 cells that stably integrated pcDNA6/TR and KLHL12-3xFLAG in a pcDNA5/FRT/TO vector (Flp-In T-REx Core kit; Thermo Fisher Scientific) and were selected in the presence of 6 µg/ml blasticidin and 0.2 mg/ml hygromycin, respectively. Cells were kept in a 37°C incubator with 5% CO2. Transfection of DNA constructs into svIMR-90 and KI6 cells was performed using Lipofectamine 2000 as detailed in the manual provided by Invitrogen. Transfection of DNA constructs to Saos-2, svIMR-90, and U-2OS cells for donor membrane preparation and HEK293T cells for cytosol preparation was performed using

polyethylenimine (PEI) at a DNA/PEI ratio of 1:3. Ascorbate treatment used 0.25 mM ascorbic acid (Sigma-Aldrich) and 1 mM ascorbic-2-phosphate (Sigma-Aldrich) were used for ascorbic treatment. This concentration was in addition to the amount of ascorbic acid present in FBS (0.08 mM) as supplied by the manufacturer. Doxycycline (Sigma-Aldrich) was used at 1 µg/ml. BFA (Sigma-Aldrich) was used at 10 µg/ml. Nocodazole (Sigma-Aldrich) was used at 5 µM.

Immunofluorescence

Cells growing on poly-l-lysine–coated glass coverslips were fixed in 4% PFA for 20 min at RT or 30 min at 4°C, washed five times with PBS, and incubated with permeabilization buffer (PBS containing 0.1% Triton X-100 and 0.2 M glycine) at RT for 15 min. Cells were incubated with blocking buffer (0.5% BSA in PBS) for 30 min at RT followed by incubation for 1 h each at RT with primary antibody and then secondary antibody. Antibody incubations were followed by five washes with PBS. Coverslips were mounted in ProLong-Gold antifade mountant with DAPI (Thermo Fisher Scientific) overnight, before imaging. Images were acquired using Zen 2010 Software on an LSM 710 confocal microscope system (ZEISS). The objectives used were Plan-Apochromat 100×, 1.4 NA, and Plan-Apochromat 100×, 1.4 NA. The excitation lines and laser power used were 488 (4%), 543 (6%), 405 (2%), and 633 (6%). Co-localization analysis was performed using the spots detection algorithm in the image-processing module Imaris 8.1.2. In brief, a total number of KLHL12 labeled puncta in the z-stack was obtained, and the percentage of puncta positive for both KLHL12 and PC1 was calculated.

Immunoblotting

Standard immunoblotting procedures were followed. In brief, samples were heated at 65°C for 10 min, resolved on 4–20% polyacrylamide gels (15-well, Invitrogen; 26-well, Bio-Rad Laboratories), and transferred to PVDF (EMD Millipore) at constant 0.15A for 16 h. The PVDF membrane was incubated with antibodies (primary for 2.5 h and secondary for 1 h at RT), and bound antibodies were visualized by the enhanced chemiluminescence method (Thermo Fisher Scientific) on a ChemiDoc Imaging System (Bio-Rad Laboratories) with ImageLab software v4.0 (Bio-Rad Laboratories).

Immunoelectron microscopy

KI6 cells were grown on 35-mm glass-bottom dishes (MatTek Corp.) and fixed with 4% PFA and 0.05% glutaraldehyde for 30 min. Cells were washed with PBS and incubated with blocking buffer (0.5% BSA and 0.02% saponin in PBS) at RT for 20 min. Primary antibody labeling was done at RT for 1 h followed by overnight incubation at 4° C in the presence of saponin. Secondary antibody labeling (1:50 dilution of 1.4 nm Nanogold-conjugated goat anti-mouse Fab′ fragment; Nanoprobes) was done at RT for 2 h. The Nanogold particles were gold enhanced in the dark for 5–7 min per the manufacturer's instructions using GoldEnhance (Nanoprobes). Cells were postfixed with 1% osmium tetroxide and processed for thin-section EM.

Correlative light and electron microscopy

Saos-2 cells were grown on gridded 35-mm glass-bottom dishes (MatTek Corp.) and fixed with PFA (4% in culture medium; Electron Microscopy Sciences). The cells were processed for IF as described earlier with the exception that 0.02% saponin was used as the permeabilizing agent, a concentration well below the established protocol, which typically uses 0.1% saponin (Mironov et al., 2005). The cells (in PBS) displaying co-localized PC1/SEC31A spots were imaged at RT on a Zeiss 710 confocal microscope using a C-Plan Apochromat 63×/1.2 W objective followed by marking the alphanumeric location using a 5×/0.12-NA objective. A z-stack series of the cell of interest was also collected using Zen 2010 software. The cells were then fixed for 30 min in 0.1 M cacodylate buffer, pH 7.2, containing 2% glutaraldehyde and washed with 0.1 M sodium cacodylate buffer before postfixation with 1% osmium tetroxide for 30 min on ice. This was followed by staining with 1% aqueous uranyl acetate for 30 min at RT. For dehydration with progressive lowering of temperature, each incubation period was 10 min, with exposure to 35% ethanol at 4°C, 50% ethanol and 70% ethanol at −20°C, and 95% and 100% ethanol at −35°C. Cells were restored to RT in 100% ethanol before embedding in an epon resin. The cell of interest was identified by the grid location on the resin and thin (70- to 100-nm) serial sections were collected on Formvar-coated 200-mesh copper grids and poststained with 2% aqueous uranyl acetate and 2% tannic acid. The sections were imaged at 120 kV using a Tecnai 12 Transmission Electron Microscope (FEI). Regions of interest were identified manually by correlating the z-slices of the confocal stack with the serial sections and laying the fluorescent image over the TEM image by marking down prominent cell landmarks such as the nuclear boundary, vacuoles, and mitochondria. The overlay was confirmed using the Icy software package (de Chaumont et al., 2012).

STORM imaging

Immunofluorescently labeled cell samples were mounted on glass slides with a standard STORM imaging buffer consisting of 5% (wt/vol) glucose, 100 mM cysteamine, 0.8 mg/ml glucose oxidase, and 40 μg/ml catalase in Tris-HCL, pH 7.5 (Rust et al., 2006; Huang et al., 2008), and sealed using Cytoseal 60 (Thermo Fisher Scientific). STORM imaging was performed on a home-built setup based on a modified Eclipse Ti-U inverted fluorescence microscope (Nikon) using a Nikon CFI Plan Apo λ 100× oil-immersion objective (NA 1.45). Dye molecules were photo switched to the dark state and imaged using either 647- or 560-nm lasers (MPB Communications); the lasers were passed through an acousto-optic tunable filter and introduced through an optical fiber into the back focal plane of the microscope and onto the sample at intensities of ~2 kW/cm. A translation stage was used to shift the laser beams toward the edge of the objective so that light reached the sample at incident angles slightly smaller than the critical angle of the glass-water interface. A 405-nm laser was used concurrently with either the 647- or 560-nm lasers to reactivate fluorophores into the emitting state. The power of the 405-nm laser (typical range 0–1 W/cm) was adjusted during image acquisition so that at any given instant, only a small, optically resolvable fraction of fluorophore in the sample was in the emitting state. For 3D STORM imaging, a cylindrical lens was inserted into the imaging path so that images of single molecules were elongated in opposite directions for molecules on the proximal and distal sides of the focal plane (Huang et al., 2008). The raw STORM data were analyzed according to previously described methods (Rust et al., 2006; Huang et al., 2008). Data were collected at a frame rate of 110 Hz using an iXon Ultra 897 EM-CCD camera (Andor), for a total of ~80,000 frames per image. Three-color imaging was performed on targets labeled by Alexa Fluor 647, CF680, and CF568 via sequential imaging with 647- and 560-nm excitation. With 647-nm excitation, a ratiometric detection scheme (Bossi et al., 2008; Testa et al., 2010) was first used to concurrently collect the emission of single Alexa Fluor 647 and CF680 molecules. Emission of single molecules was split into two light paths (channels) using a long-pass dichroic mirror (T685lpxr; Chroma), each of which was projected onto one-half of an iXon Ultra 897 EM-CCD camera. We performed fluorophore assignment by localizing and recording the intensity of each single molecule in the two channels. Excitation at 560 nm was subsequently used to image CF568 through the reflected light path of the dichroic mirror.

Live-cell imaging, particle tracking, and image analysis

KI6 cells were transfected with plasmids encoding SEC31A-YFP and PC1-CFP for a period of 9 h and induced for 7.5 h with doxycycline within that time period to induce the overexpression of KLHL12. The cells were imaged using a temperature-controlled LSM 710 Axio Observer microscope (ZEISS; Plan-Apochromat 63×, 1.4 NA oil DIC M27; standard ZEISS PMT detectors) at 37°C in prewarmed phenol red–free culture medium. Main beam splitters were MBS-405 and MBS-458/514. Emission wavelengths collected were at 454–516 nm and 519–621 nm. Cells were imaged every 5 s for 2 min starting at the end of 10-min treatment with ascorbate and recorded using Zen 2010 software. For experiments requiring nocodazole treatment, the drug was added for 30 min before imaging. Particle detection and tracking were performed using Imaris v8.1 (Bitplane USA). Images were first subjected to background subtraction, and the Spots module was used to automatically detect point-like particles with spot diameter of 200 nm. Appropriate threshold values were confirmed. Object tracing through sequential time frames was done using an autoregressive motion particle-tracking algorithm. A maximum search distance of 5 µm was defined. A gap-closing algorithm was also implemented to link track segment ends to track segment starts. Track outputs were then visually inspected.

Vesicle budding reaction

Vesicle budding reactions were performed as previously described in Kim et al. (2005) with the following modifications. Donor ER membrane was prepared fresh for each reaction by permeabilizing young (under PDL 37.5) IMR-90 cells (95% confluent in 3 × 10-cm dishes) treated with 20 µg/ml digitonin (5 min on ice) in B88 (20 mM Hepes, pH 7.2, 250 mM sorbitol, 150 mM potassium acetate, and 5 mM magnesium acetate) and washed with 0.5 M LiCl in B88 then B88 and resuspended in 200 µl B88-0 (20 mM Hepes, pH 7.2, 250 mM sorbitol, and 150 mM potassium acetate) to a final concentration of OD600 2–6. Each 100-µl reaction contained ATP regeneration system (1 mM ATP, 40 mM creatine phosphate, and 0.2 mg/ml creatine phosphokinase), 3 mM GTP, purified human COPII proteins (2 µg SAR1B, 1 µg SEC23A/24D, and 1 µg SEC13/31A), cytosol (2 µg/µl unless otherwise stated, see “Cytosol preparation” for details), and a final concentration of 5 OD600/ml donor ER membrane in B88-0. Vesicles generated in vitro were isolated from the reaction mixture in two steps. First, donor membranes were sedimented by centrifuging twice at 7,000 g at 4°C for 5 min each in a swinging bucket rotor (S-24-11-AT; Eppendorf). Then, 85 µl of the supernatant was mixed with 50 µl of 60% OptiPrep (Sigma-Aldrich) gently until

homogeneous, placed at the bottom of a 7 × 20-mm tube (Beckman Coulter), and overlaid with 100 µl of 18% and 10 µl of 0% OptiPrep in B88. The OptiPrep gradient was centrifuged at 250,000 g for 90 min at 4°C (Beckman TLS-55 with adaptors for 7 × 20-mm tubes) with slow acceleration and deceleration, after which 20-µl fractions were collected from the top and mixed with sample buffer for immunoblotting analysis. When a vesicle budding reaction was analyzed by SIM or flow cytometry, the donor ER membrane was prepared from cells (2 × 10-cm, 80% confluent Saos-2, 40% confluent U-2OS, or 60% confluent svIMR-90 at the time of transfection) transiently transfected with 7.5 µg COL1A1-GFP per 10-cm plate using PEI (Sigma-Aldrich) for 72 h when cells were 100% confluent. The reaction was supplemented with fluorescently labeled SEC23A/24D. Fluorescent SEC23A/24D was produced as previously described in Bacia et al. (2011) using Alexa Fluor 647 C2 maleimide (Thermo Fisher Scientific).

Protein purification

Human SAR1 proteins were overexpressed in Escherichia coli and purified as cleaved GST-fusions, as described for hamster Sar1 purifications in Kim et al. (2005). In brief, a bacterial lysate was first centrifuged at 43,000 g for 15 min, then the supernatant fraction was further centrifuged at 185,000 g for 1 h. The supernatant was incubated with prewashed glutathione agarose (1 ml slurry/l bacteria; Thermo Fisher Scientific) for 1 h at 4°C. Agarose was washed with wash buffer (50 mM Tris, pH 7.4, 150 mM NaCl, 0.1% Tween, 5 mM MgCl2, and 100 µM GDP), and SAR1 was eluted by cleaving with 20 U/ml thrombin (Roche) in TCB (50 mM Tris, pH 8, 250 mM KoAc, 5 mM CaCl2, 5 mM MgCl2, and 100 µM GDP). Human SEC13/31A and SEC23A/24D were purified from lysates of baculovirus-infected insect cells, as described previously (Kim et al., 2005). In brief, insect cell lysates were centrifuged at 185,000 g for 1 h, and 30% ammonium sulfate was added to the supernatant fraction at 4°C. The precipitant was collected by centrifugation at 30,000 g for 30 min and solubilized in no-salt buffer (20 mM Hepes, pH 8, 10% glycerol, 250 mM sorbitol, 0.1 mM EGTA, 5 mM β-mercaptoethanol, and 10 mM imidazole). The solubilized 30% ammonium sulfate precipitant was cleared at 30,000 g for 20 min, and the supernatant was incubated with prewashed Ni-NTA resin (1.25 ml slurry/l insect cells; Thermo Fisher Scientific) for 1 h at 4°C. Ni-NTA was washed with 20 mM Hepes, pH 8, 10% glycerol, 250 mm sorbitol, 500 mM KoAc, 0.1 mM EGTA, 5 mM β-mercaptoethanol, and 50 mM imidazole and eluted with 250 mM imidazole. Ni-

NTA–eluted protein was further purified using an anion exchange column (MonoQ) on an AKTA FPLC system (GE Healthcare).

Cytosol preparation

Plates (20 × 15 cm) of HT-1080 or HT-PC1.1 cells were cultured to confluence, washed with PBS, and gently scraped in B88 with protease inhibitors (Roche). Plates (5 × 15 cm) of HEK293T cells were transiently transfected with 18 µg of empty pEGFP_n1 plasmid, wild-type, or mutant KLHL12-3xFLAG in a pcDNA5/FRT/TO vector per 15-cm plate, and cells were collected 24 h after transfection by pipetting with PBS after gently washing with PBS. The collected cells were permeabilized with gentle rocking for 30 min in 80 µg/ml digitonin in 5 ml B88 per five 15-cm plates with protease inhibitors at the concentration suggested by manufacturer (Roche) at 4°C. The cell lysate was collected as a supernatant fraction after centrifugation at 300 g for 5 min. Digitonin was removed from the cell lysate by incubating with washed Bio-Beads SM2 (dry weight of 1 g beads per five 15-cm dishes; Bio-Rad Laboratories) at 4°C overnight. Bio-Beads were removed by centrifugation at 300 g for 5 min. The supernatant fraction was further centrifuged at 160,000 g for 30 min, and the clarified supernatant was collected and concentrated with an Amicon Ultra-3k (EMD Millipore) filter to 40–80 mg/ml. Small aliquots were frozen in liquid nitrogen and stored at −80°C for future use in vesicle budding reactions.

Collagenase protection assay

Top fractions collected after Optiprep gradient flotation were pooled and redistributed to each reaction to ensure that all samples had the equal starting material. Samples were mixed with or without 0.1 U/µl collagenase (Sigma-Aldrich) in the presence or absence of 1% Triton X-100 (Sigma-Aldrich) and incubated at 0°C or 30°C for 10 min.

Structured illumination microscopy Imaging

Donor ER membrane isolated from cells that expressed PC-GFP was incubated with purified Alexa Fluor 647–conjugated SEC23A/24D and other components, as specified, and budded vesicles were isolated from the top of the flotation gradient as described in “Vesicle budding reaction.” Budded vesicles were mounted in Prolong Diamond (Invitrogen) under no. 1.5H coverslips (ZEISS) and set for at least 5 d before imaging to eliminate drift. z-stacks of 1–2 µm were

collected in three rotations and five phases using the 100×/1.46 objective on Elyra PS.1 superresolution microscope (ZEISS) with less than 2% laser power and less than 400-ms exposure in all channels, which was determined using no fluorescence and single-channel fluorescence controls. Images were reconstructed and channels were aligned using Zen Black software (ZEISS). Images and videos of 3D iso-surface renderings of each channel were done using Imaris v8.1 (Bitplane USA). Image acquisition, processing, and 3D rendering were done using equipment and software in the CNR Biological Imaging Facility at the University of California, Berkeley.

Flow cytometry

Vesicle budding reactions were scaled up 6× for flow cytometry analyses. After a 7,000-g, 10-min centrifugation of a 600-µl cell-free reaction, 540 µl supernatant was collected from the top. The lipid dye FM4-64 (Thermo Fisher Scientific) was added to the supernatant at 5 µg/ml immediately before the flow cytometry analyses. 100,000 particles were collected for each sample. FSC-A and FSC-H were used to gate for single particles (singlets), which were used for further analysis. Gating of each fluorescent channel was determined by comparing a control sample without any fluorescent labeling and a control that was labeled in a single channel. Data were collected on a BD LSR Fortessa (BD) and analyzed by FlowJo software. Instrument and software were provided by the LKS flow core facility at the University of California, Berkeley.

Nanoparticle tracking analysis

Size of vesicles budded in vitro were estimated using the NanoSight NS300 instrument equipped with a 405-nm laser (Malvern Instruments). Qdot525-positive particles were analyzed with a 500-nm filter (fluorescent mode); nonfluorescent particles were analyzed in the scatter mode without a filter. Silica 100-nm microspheres (Polysciences) were analyzed to check instrument performance and determine the viscosity coefficient of B88. Vesicles were collected from the top 20 µl of the flotation gradient as described in the Vesicle budding reaction section and diluted 40× with 780 µl filtered B88 (0.02 µm; Whatman). To label COPII with the fluorescent Qdot525, the 7,000-g supernatant fraction was incubated with mouse anti-SEC31A primary antibody (1:100; BD) and donkey anti–mouse IgG secondary antibody Qdot525 conjugate (1:100; Thermo Fisher Scientific) for 1 h at RT. As a labeling control, primary antibody was omitted. The labeled supernatants were used as inputs for flotation (see details in Vesicle budding reaction), and 2× top 20 µl of floated

fractions was collected from duplicates, to double the labeling material, and diluted 20× with 760 µl filtered B88 (0.02 µm; Whatman). The samples were automatically introduced into the sample chamber at a constant flow rate of 50 (arbitrary manufacturer unit, ~10 µl/min) during five repeats of 60-s captures at camera level 13 in scatter mode and level 15 in fluorescent mode with Nanosight NTA 3.1 software (Malvern Instruments). Each sample was measured at two different positions of the syringe introduction to minimize the heterogeneous flow of vesicles. The particle size was estimated with detection threshold 3 for fluorescent mode and 5 for scatter mode using the Nanosight NTA 3.1 software, after which "experiment summary" and "particle data" were exported. Particle numbers in each size category was calculated from the particle data, in which "true" particles with track length >3 were pooled, binned, and counted with Excel (Microsoft). GraphPad Prism 7 was used for graphing and statistical analyses.

Electron microscopy of budded vesicles

For morphological analysis of the budded vesicles, the top 80 µl of a supernatant fraction after the 7,000-g, 10-min spin of a 100-µl reaction was fixed with 2% PFA and 0.2% glutaraldehyde in B88 buffer for 15 min at 4°C and centrifuged at 25,000 g (Beckman TLS-55 with adaptors for 11 × 34-mm tubes) for 30 min with slow acceleration and deceleration on to a 0.5-ml agarose bed (2% low melting point; Sigma-Aldrich). This centrifugation speed was optimized to collect large COPII-coated vesicles. After three washes in B88 buffer, the pellet was embedded in 12% gelatin, cut in small blocks, and infiltrated with 2.3 M sucrose in 0.1 M phosphate buffer at pH 7.4 overnight at 4°C. The blocks were mounted on pins and stored frozen in liquid nitrogen. Ultrathin cryosections were collected on Formvar and carbon-coated nickel grids, poststained with 2% uranyl acetate, and imaged at 120 kV using a Tecnai 12 Transmission Electron Microscope.

Figures

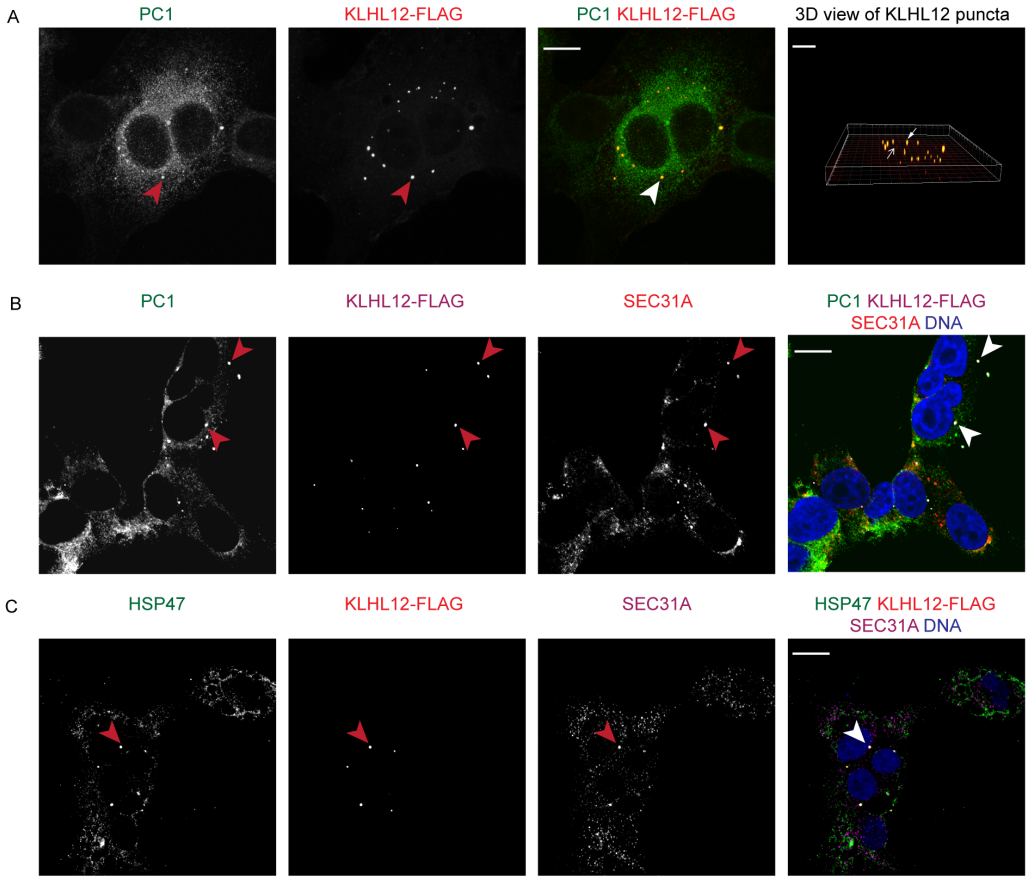

Figure 2.1. Large COPII vesicles co-localize with PC1.
(A) PC1 (green) and KLHL12 (red) co-localize in KI6 cells that were treated with doxycycline for 7.5 h to induce the expression of KLHL12. Images shown are average intensity projected views of a Z stack shown for each and merged channel. 3D view of KLHL12 puncta was obtained from the Z stack using the Spot feature in Imaris 8.1.2. Examples of co-localizing "yellow" puncta are indicated by a closed arrow, and KLHL12 positive puncta not co-localizing with PC1 are indicated by an open arrow. Total number of KLHL12 positive puncta determined in the Z stack was 27 and 78% of these spots were positive for PC1 calculated using CoLoc feature in Imaris 8.1.2. (B) PC1 (green), KLHL12 (magenta) and SEC31A (red) co-localize in KI6 cells (closed arrows). DAPI is shown in blue. Half of the total number of KLHL12 positive puncta (n=14) were positive for PC1 and SEC31A. (C) HSP47 (green), KLHL12 (red) and SEC31A (magenta) co-localize in KI6 cells (close arrow). Of the total number of KLHL12

positive puncta (n=24) counted in 11 cells, 79 % were positive for both SEC31 and HSP47. Scale bar: 10 μm. n=3.

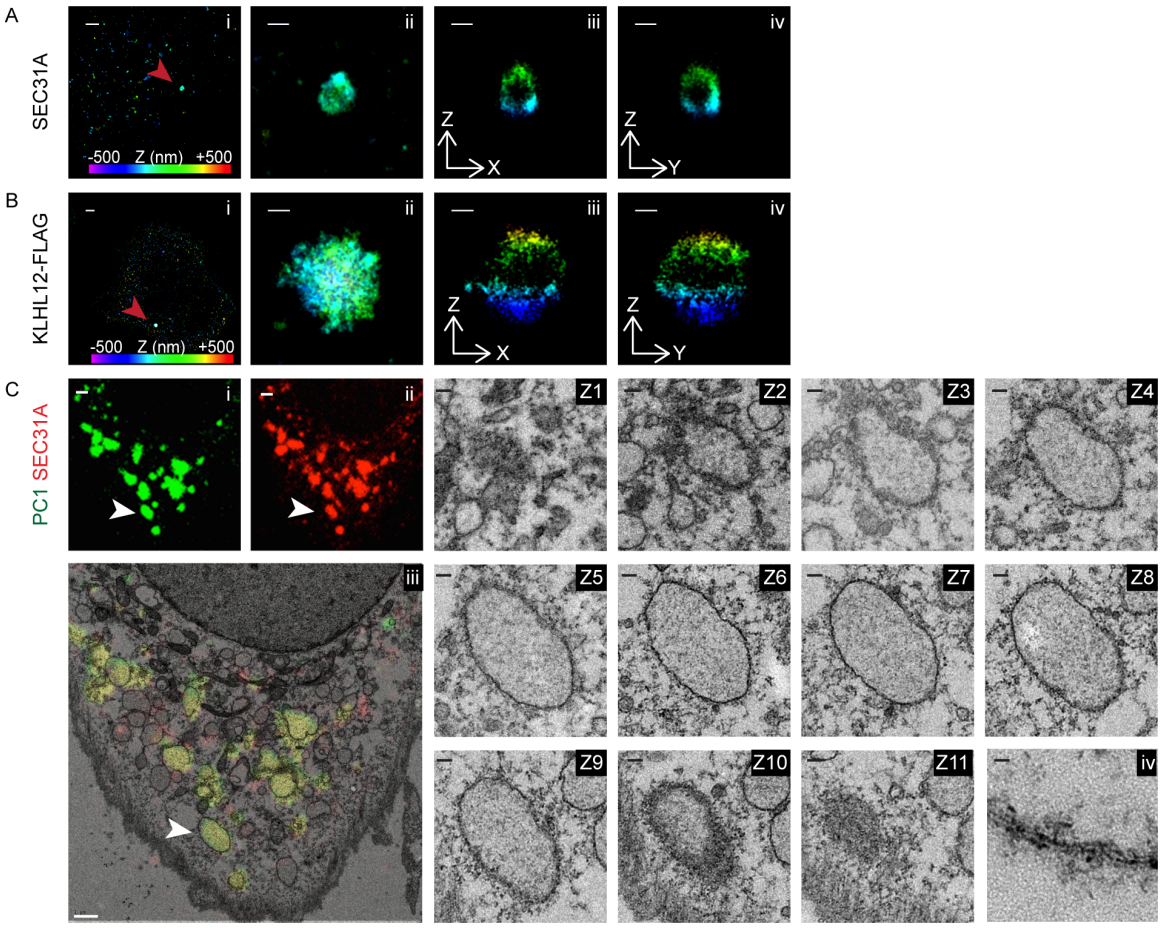

Figure 2.2. Large COPII vesicles are hollow membranous containers.
3D STORM images of large SEC31A (A) or KLHL12-FLAG (B) puncta in KI6 cells after 7.5 h induction. Position in depth (Z axis) is represented by color according to the color scale bar in (Ai and Bi). (i) Overview of an area of the cell imaged by STORM: SEC31A (A) or FLAG (B). (ii) Magnified maximum XY-projection of a large SEC31A (A) or FLAG (B) structure. Virtual cross-sections of this structure in XZ (iii) and YZ (iv) planes reveal a hollow compartment encapsulated by SEC31A (A) or KLHL12-FLAG (B). (C) CLEM resolved overlapping immunofluorescent (i) PC1 (green) and (ii) SEC31A (red) puncta as single membrane bound compartments in cultured Saos-2 cells expressing endogenous levels of PC1 and KLHL12. (iii) A representative cell showing co-localizing puncta (n=36; indicated by white arrow) was processed for CLEM. Image shows overlay of the merged fluorescent channels (green and red) on a thin section (70 nm) TEM image (Z1-11) Serial sections of 70 nm thicknesses through structure of interest. (iv) Magnified view of lipid bilayer from an area of the single membrane enclosing the organelle. n=2. Scale bars in (A i): 1 μm; (B i):

1 μm; (A ii-iv): 200 nm, (B ii-iv): 200 nm; (C i-iii): 1 μm ; Z1 –Z11: 100 nm , (C iv): 10 nm

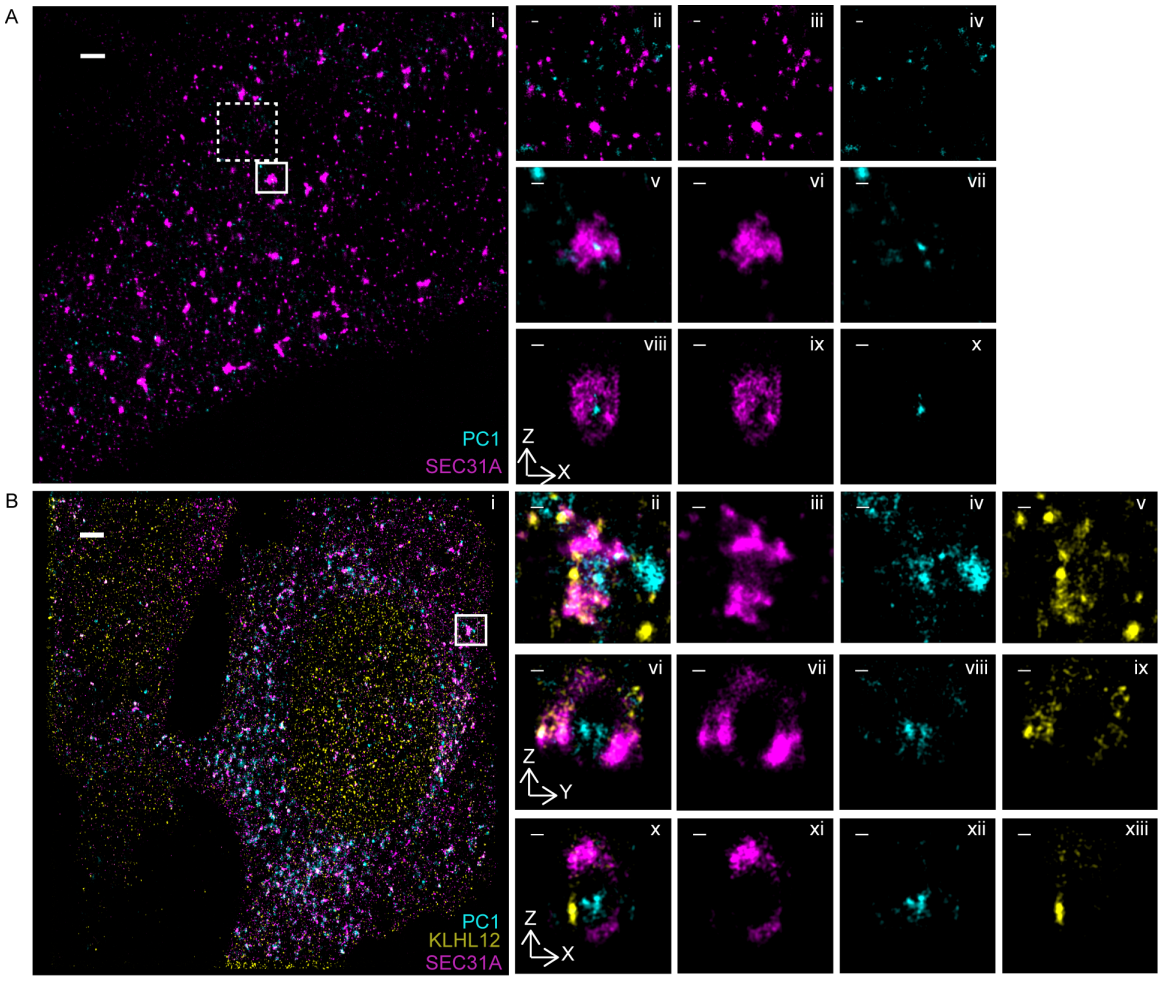

Figure 2.3. PC1 is completely encapsulated in large COPII-coated vesicles. (A) Two-color 3D STORM revealed PC1 (cyan) residing inside of large SEC31A (magenta) cages in KI6 cells after 7.5 h of induced KLHL12 overexpression. (i) Overview of an area of the cell imaged by STORM. Small (80-100 nm diameter) canonical SEC31A puncta did not co-localize with PC1 (0%, n=76 puncta, N=8 experiment). Examples in dashed inset are magnified in (ii) as merged image, (iii) as SEC31A, and (iv) as PC1. Large SEC31A puncta of diameter above 300 nm co-localized with PC1 (76.3%, n=36 puncta, N=8 experiments). An example in solid inset is magnified in (v) as merged image, (vi) as SEC31A, (vii) as PC1. A virtual cross-section in the XZ plane of the large COPII vesicle shown in (viii) as merged image (ix) as SEC31A; (x) as PC1. (B) Triple-color 3D STORM imaging shows endogenous PC1 (cyan) encapsulated by endogenous KLHL12 (yellow) and SEC31A (magenta) in Saos-2 cells grown at steady state. XY maximum projection of the overview is shown in (i), and of a magnified vesicle was shown

in (ii-v). Virtual cross-sections in the XZ plane were shown in (x-xii) and YZ in (vi-ix). Merged three-color channel is shown in (i, ii, vi, and x), SEC31A in (iii, vii, xi), PC1 in (iv, viii, xii), and KLHL12 in (v, ix, xiii). Scale bars in (A i): 1 μm, (B i): 2 μm, and in magnified views: 100 nm

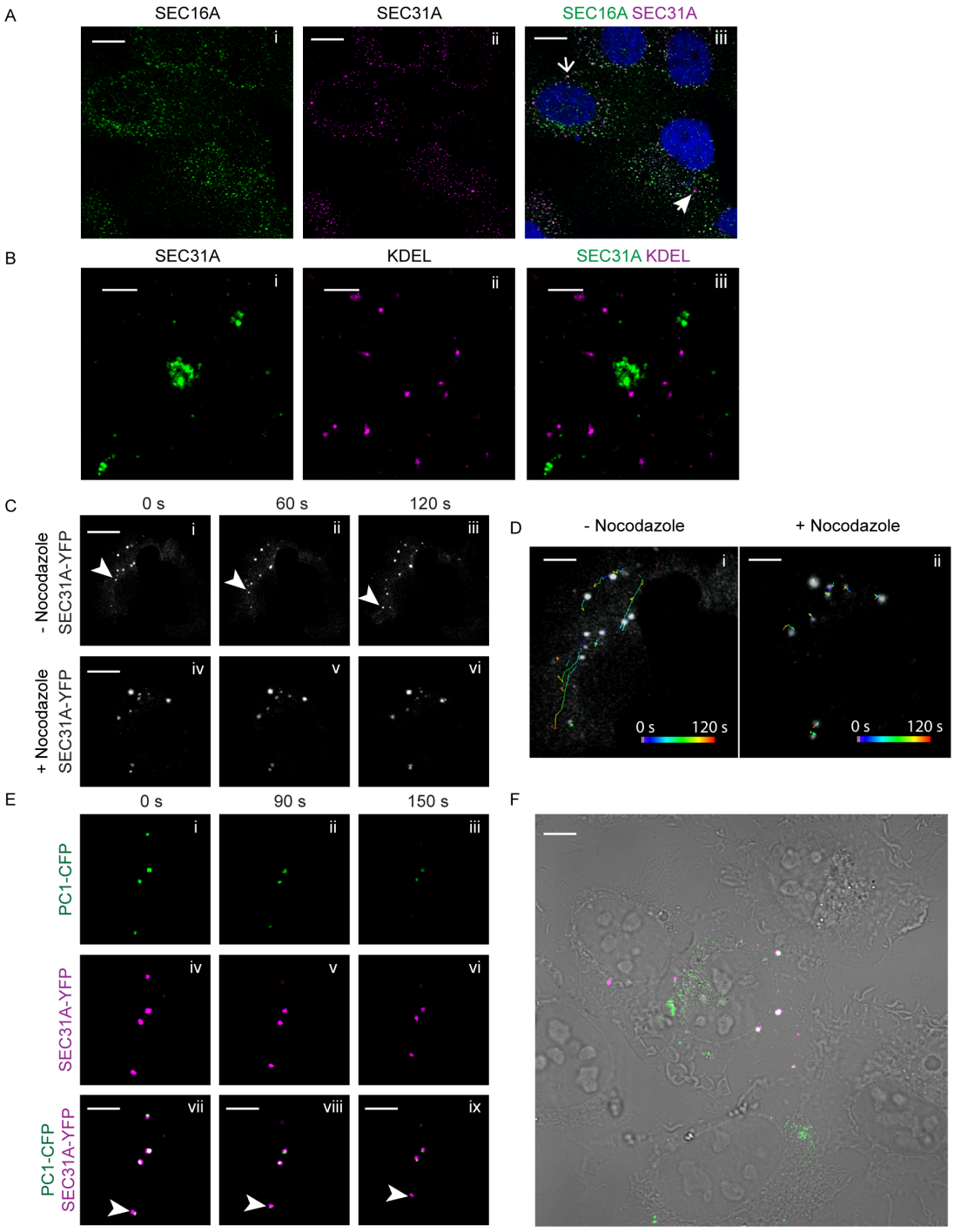

Figure 2.4. Procollagen carrying vesicles exhibit movement.
(A) Confocal microscopy imaging on KI6 cells treated with doxycycline for 7.5 h were labeled with SEC16A and SEC31A antibodies. Open arrow in merged image points to a co-localized spot; closed arrow points to a large SEC31A-labeled vesicle not co-localizing with SEC16A. (B) Two-color STORM imaging

was performed on KI6 cells induced for KLHL12 overexpression for 7.5 h and then labeled with KDEL and SEC31A antibodies. Panels show magnified XY view of (i) a SEC31A (green)-labeled large COPII cage (ii) KDEL marker labeling ER (magenta) and (iii) merged image of the two channels. (C) KI6 cells were transfected with YFP-tagged SEC31A and induced for KLHL12 expression for 7.5 h. (i-iii) show time lapse imaging of SEC31A-YFP puncta in cells not treated with nocodazole. Arrow indicates a puncta exhibiting long-range transport (>10 μm distance). n=3 (iv-vi) show time lapse images of SEC31A-YFP puncta after the treatment of 5 μM nocodazole for 30 min. (D) Images shown are the first frame of the time-lapse movie overlayed with the trajectories of SEC31A-YFP puncta in the absence (i) and presence (ii) of nocodazole. Trajectories in time (0-120 s) is represented by color according to the scale bar in (D). n=3 (E) Time lapse imaging of SEC31A-YFP and PC1-CFP positive puncta in KI6 cells. Arrows point to a vesicle that displays a spatial displacement in time. (F) Overview of the cell imaged in (E); overlay of merged fluorescent image over DIC image shows PC1-CFP in green and SEC31A-YFP in magenta. Scale bars in (A): 5 μm, (B): 500 nm, (C):10 μm, (D-F): 5 μm.

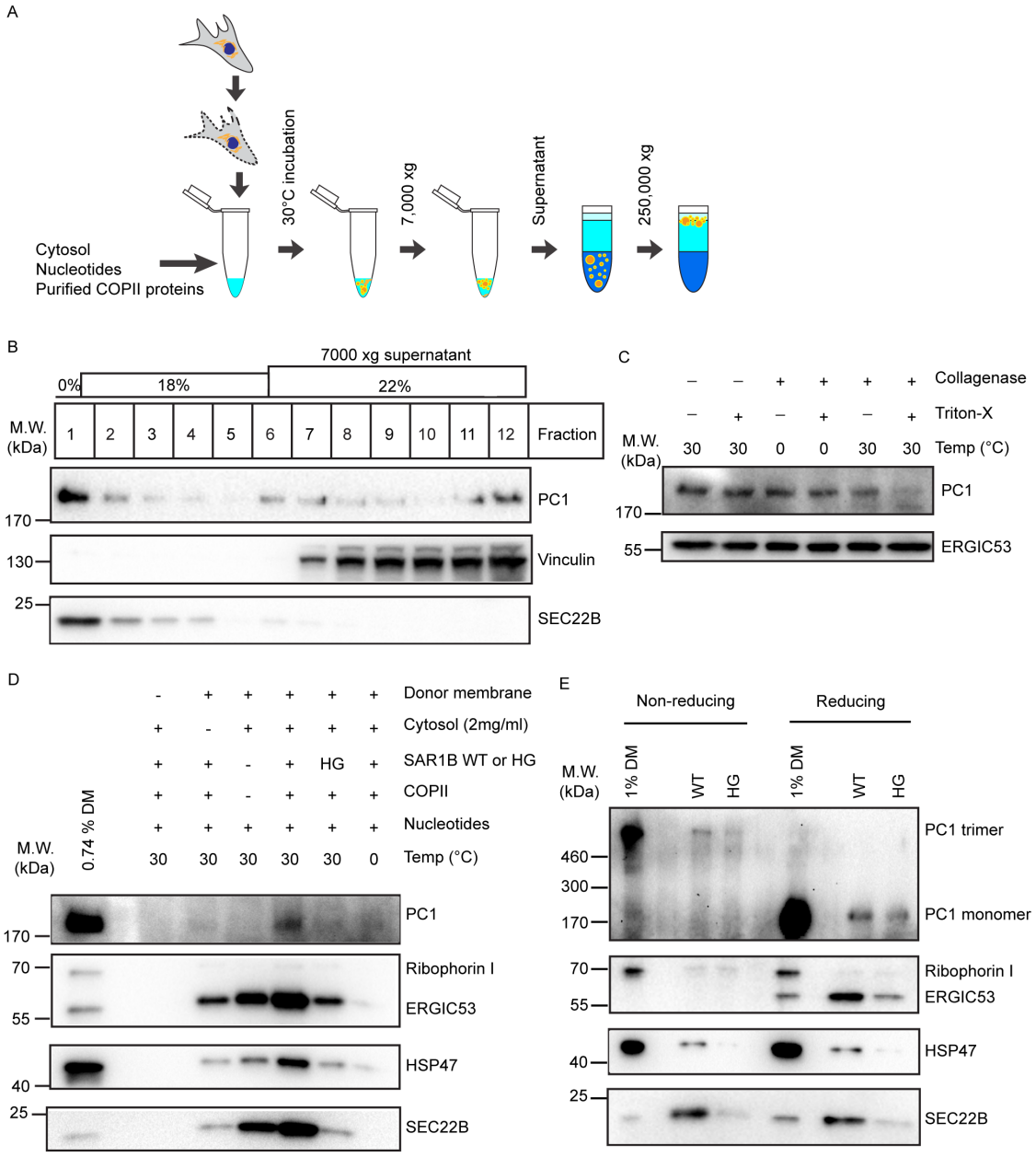

Figure 2.5. COPII is required to export PC1 in vesicles that bud from the ER in a cell-free reaction.

(A) Scheme depicting the experimental procedure of the cell-free vesicle budding reactions. Briefly, donor membrane prepared from IMR-90 cells were incubated at 30°C with cytosol (from HT1080 or HTPC1.1 cells), nucleotides (an ATP regenerating system and GTP), and purified recombinant human COPII

proteins. Vesicles in 7000 xg supernatant fractions from budding reactions were isolated by flotation. (B) Fractions (12) were taken from the top of an Optiprep gradient after flotation and analyzed by immunoblotting. SEC22B is found in conventional COPII vesicles and serves as a positive control. Vinculin serves as a control for cytosolic proteins that do not float with vesicles. n=3. (C) Top floated fraction was treated with or without collagenase (0.1 U/µl) in the presence or absence of the detergent Triton X (1%) at the indicated temperature for 10 min. ERGIC53 is found in conventional COPII vesicles and serves as loading control. n=4. (D) Budding requirements of PC1 and HSP47 were assessed under different incubation conditions. The top fraction after flotation was taken from each sample and analyzed by immunoblotting. Ribophorin I is an ER resident protein that serves as a negative control. ERGIC53 and SEC22B are found in conventional COPII vesicles and serve as positive controls. n=3. (E) To detect trimeric PC1, we treated donor membrane or floated fractions with non-reducing denaturing sample buffer before gel electrophoresis. Donor membrane or floated fractions treated with reducing denaturing sample buffers were used as controls. n=2.

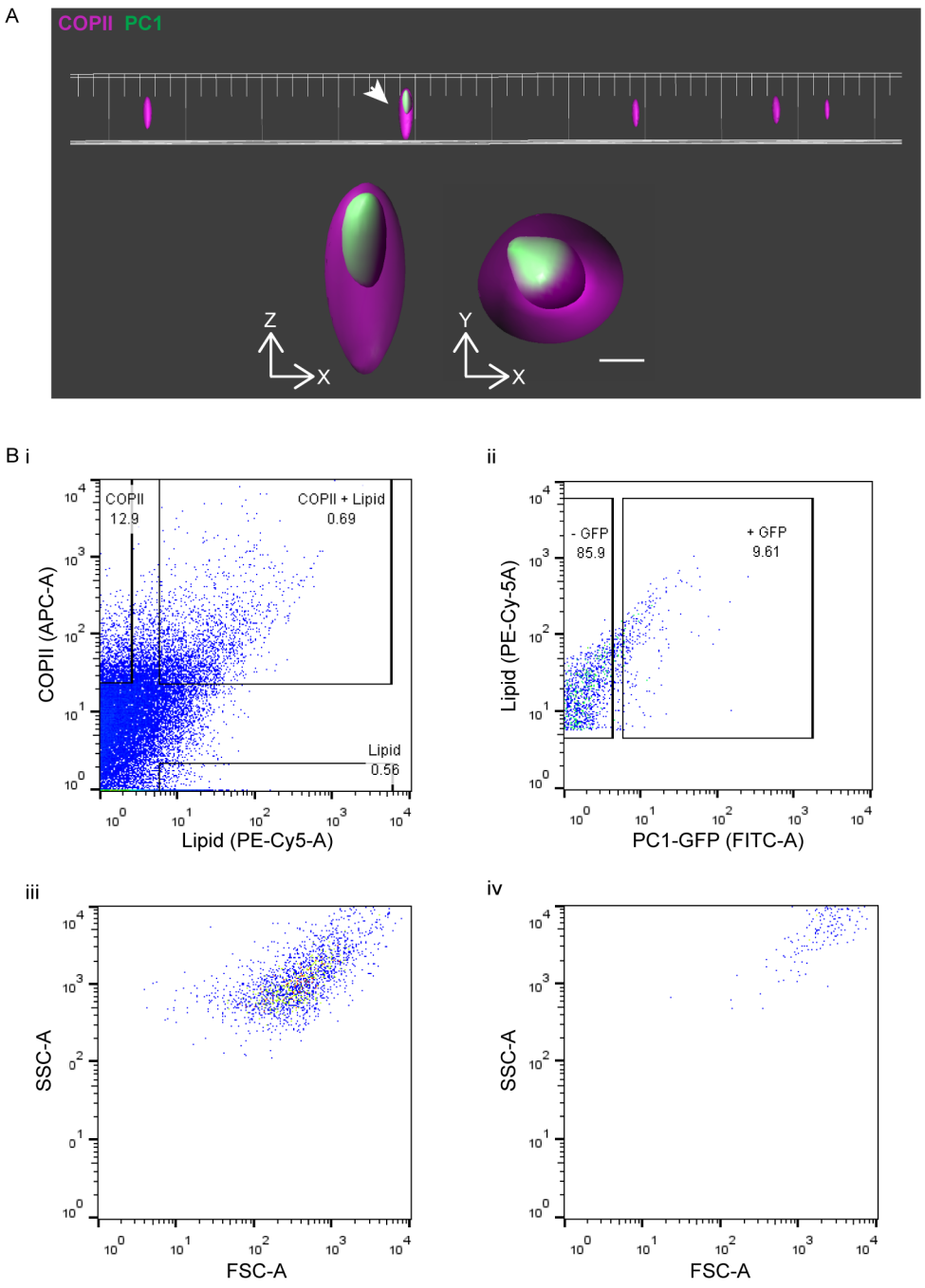

Figure 2.6. PC1 is exported out of the ER in large COPII-coated vesicles.
(A) A representative field of COPII vesicles isolated from cell-free vesicle budding reaction visualized by SIM. One of them indicated by the arrow contained PC1-GFP (green) that was entirely encapsulated by the COPII inner coat proteins SEC23A/24D-647 (magenta). The magnified XZ and YZ views are displayed underneath the overview. Around 20 images were collected from each

experiment with fluorescence controls. n=3. Bar: 200 nm. (B) Relative size of COPII carriers of PC1 compared to regular COPII vesicles quantified by flow cytometry, and numbers in graphs represent the percentage of particles in the respective subpopulation. (i) Singlets were plotted for the fluorescence intensities of the COPII coat proteins SEC23A/24D-647 (APC-A) and the lipid dye FM4-64 (PE-Cy5-A). (ii) Particles positive for both “COPII” and “lipid” are COPII vesicles and were plotted for the fluorescence intensity of PC1-GFP (FITC-A). (iii-iv) The values of side scatter (SSC-A) versus forward scatter (FSC-A) of COPII vesicles that are PC1-GFP negative (iii) or GFP positive (iv) are plotted. n=3.

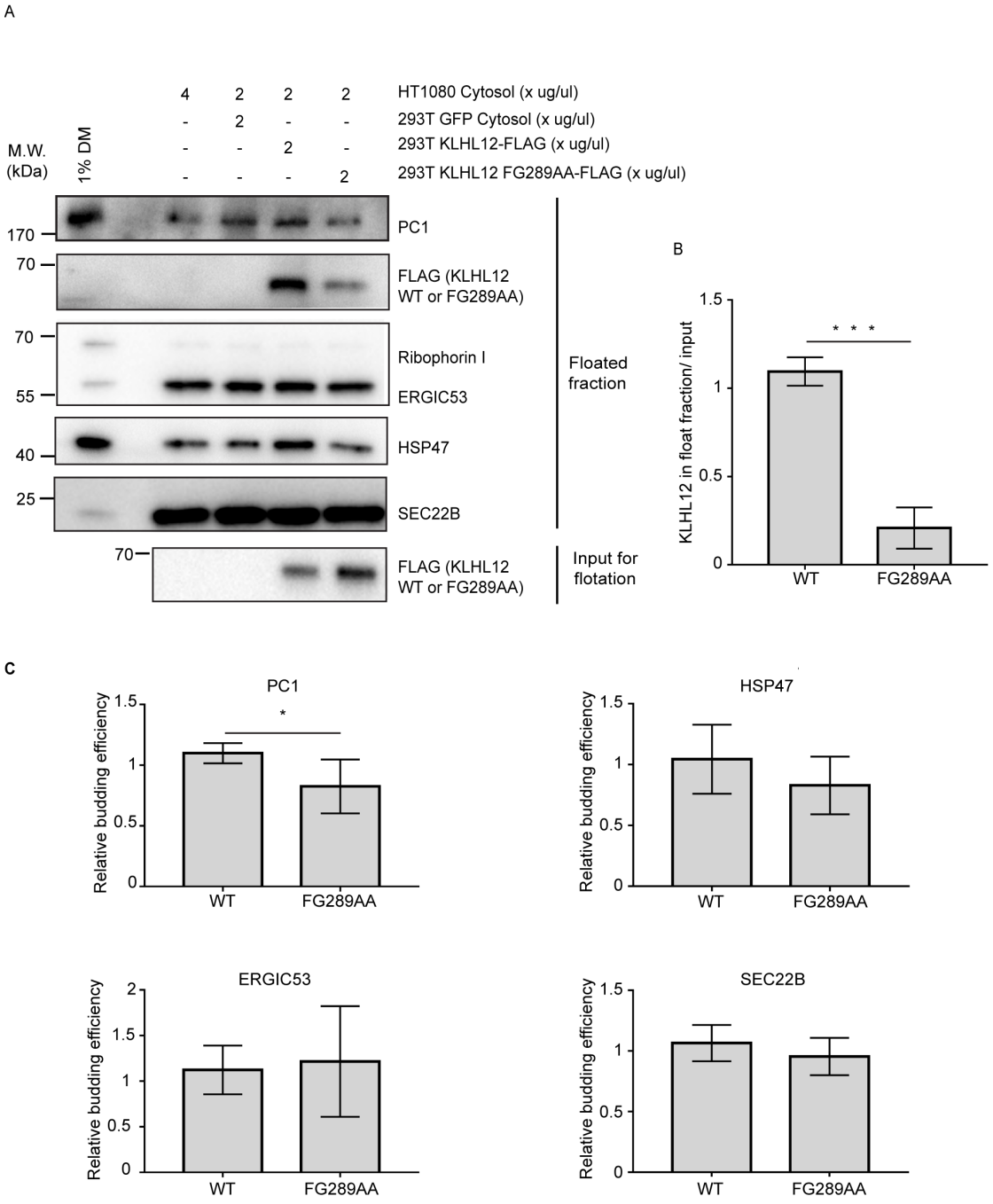

Figure 2.7. The cellular behavior of KLHL12 is recapitulated in the cell-free reaction.

(A) Budding reactions were supplemented with 2μg/ul 293T cytosol containing FLAG-tagged KLHL12 wild-type or FG289AA mutant in addition to 2μg/ul HT1080 cytosol. Cytosol (293T cells) that contained GFP and 4μg/μl HT1080 cytosol were used as controls with endogenous levels of wild-type KLHL12. Top

fractions were collected after density gradient flotation for immunoblotting analyses. A representative experiment out of 7 independent repeats. (B) Relative enrichment of KLHL12 detected in the floated fraction. Densitometry quantification of FLAG intensities in the floated fraction was divided by the corresponding FLAG intensity in the 7000 xg supernatant (input for flotation). Error bars: SD. Paired t-test. $p<0.0001$. $n=7$. Average of wild-type / average of FG289AA = 6.80. (C) Relative budding efficiency of PC1, HSP47, ERGIC53 and SEC22B in reactions that were supplemented with 293T cytosol that contained wild-type KLHL12 or KLHL12 FG289AA. Vesicle budding efficiencies were calculated from densitometry quantification relative to the control lane where 293T cytosol that contained GFP was supplemented. Paired t-test was used to analyze the difference between wild-type and FG289AA samples of each cargo and the p values were 0.0412 for PC1, 0.1215 for HSP47, 0.5307 for ERGIC53, and 0.2993 for SEC22B. Error bars: SD. $n=7$.

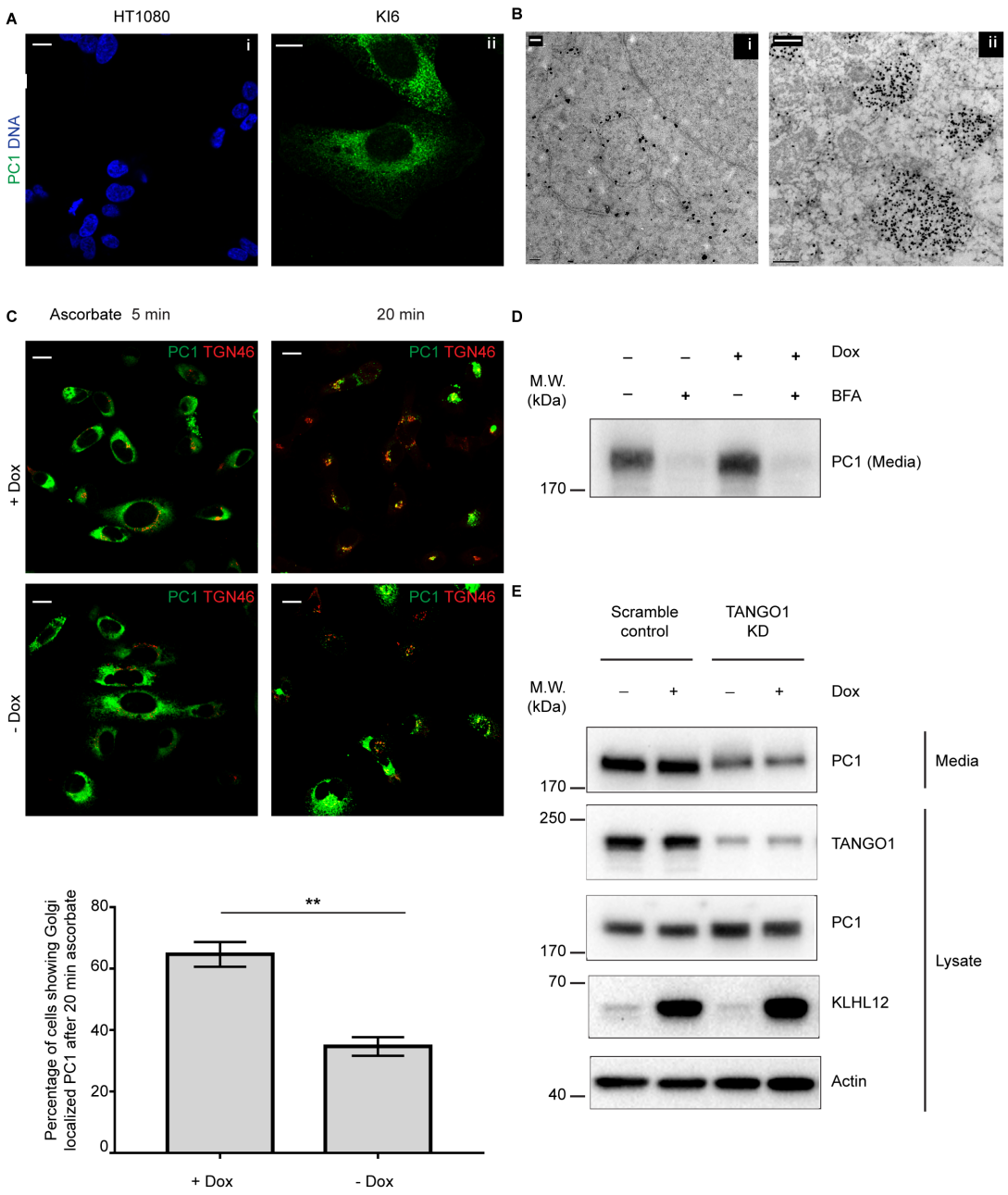

Figure 2.S1. Generation of human fibrosarcoma (KI6) cell line stably transfected with PC1 and doxycycline inducible KLHL12.

(A) No PC1 immunofluorescence signal was observed in parent cell line (HT1080) (i), while a uniform reticular pattern was observed in KI6 cells (ii). (B) Pre-embedding immunogold labeling using PC1 antibody in KI6 cells showing reticular pattern in (i) and in large vesicles (ii). (C) KI6 cells treated with doxycycline for 7.5 h (+Dox) and compared with cells without doxycycline (-Dox) after double-immunostaining with PC1 and Golgi marker TGN46 and ascorbate

treatments of 5 min and 20 min, respectively. Quantification below shows fraction of cells of a random sampling of 150 cells showing Golgi-localized PC1 in induced versus uninduced cells. Error bar: SD, n=3. (D) Immunoblotting analysis of PC1 in the pre-cleared culture medium secreted by KI6 cells with and without doxycycline induction in the presence or absence of BFA for 8 h. (E) Scramble or TANGO1 siRNA was transfected to KI6 cells for 72 h, and KLHL12 overexpression was induced during the last 7.5 h of knockdown. Pre-cleared culture medium and lysates were collected for immunoblotting analyses. PC1 secretion was inhibited after TANGO1 knockdown in KI6 cells. Scale bars in (A and C): 5 μm, (Bi): 0.2 μm, (Bii): 0.5 μm.

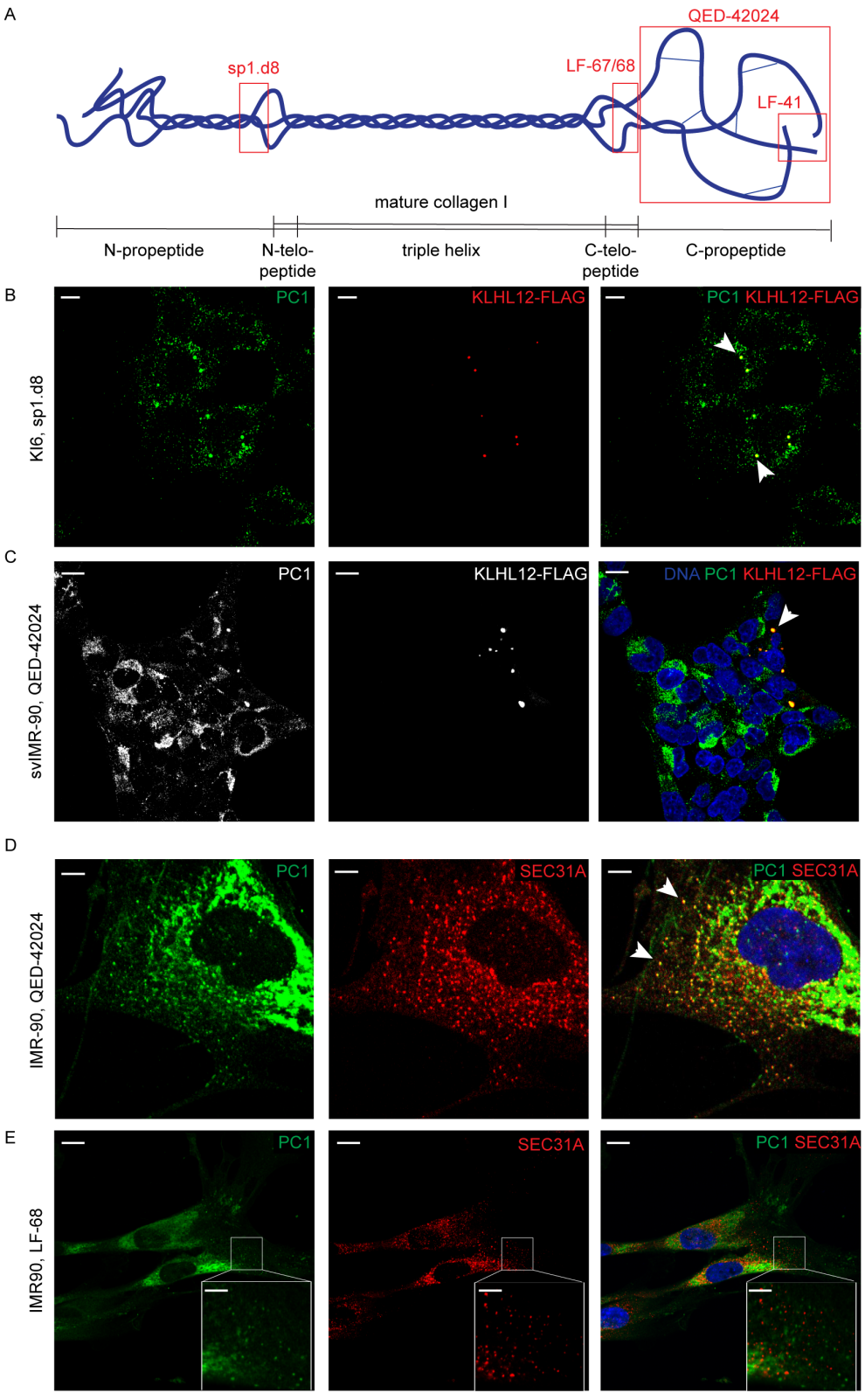

Figure 2.S2: Comparative IF analysis using different PC1 antibodies.

(A) Schematic illustration shows PC1 domain structure and sites recognized by different PC1 antibodies discussed in this report (not drawn to scale). Mature collagen I is generated after N and C-propeptides are cleaved from PC1, and the non-triple-helical ends of the mature collagen I are termed N and C-telopeptides. Inter-chain disulfide bonds between C-propeptides are important for trimerization. LF-67 and LF-68 were immunized with the same synthetic peptide sequence of the C-telopeptide and they were used in Jin et al., 2012 and Mironov et al., 2003 respectively. QED-42024 and sp1.d8 are monoclonal antibodies targeting C or N-propeptides respectively. LF-41 was made from synthetic peptide of the end of C-propeptides, and it was exclusively used to label PC1 in all immunoblotting and none of the immunofluorescent experiments in this study. (B) KI6 cells were induced for KLHL12 expression for 7.5 h with doxycycline and labeled with the monoclonal PC1 antibody sp1.d8. Arrows indicate puncta co-localizing for Klhl12 and PC1. (C) svIMR-90 cells were transfected with KLHL12-FLAG. Double immunofluorescence using PC1 (QED-42024) and FLAG antibodies revealed puncta that co-localized for both markers (indicated by arrow). (D, E) Panels show comparison of labeling using two PC1 antibodies: QED-42024 and LF-68. Arrow indicates SEC31A/PC1 co-localizing puncta. Scale bars in (B and D): 5 μm; (C and E): 10 μm, inset: 5μm.

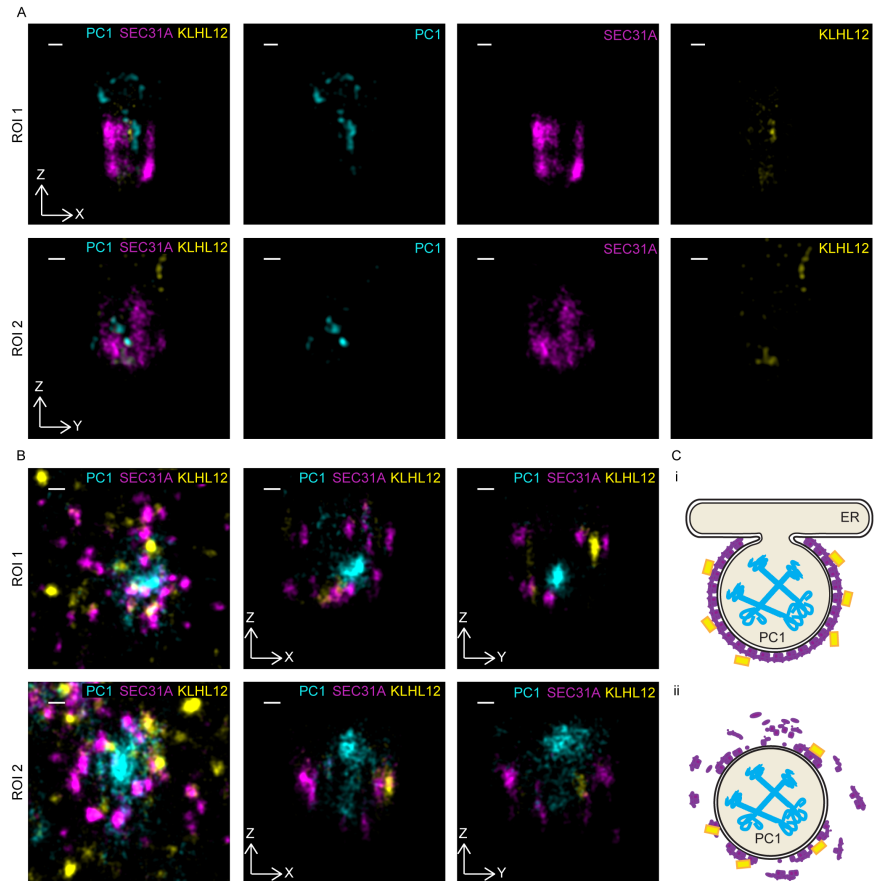

Figure 2.S3. Large partially COPII-coated PC1 carriers observed by STORM. Saos-2 cells were grown at steady state and immunostained for PC1 (cyan), SEC31A (magenta) and KLHL12 (yellow). (A) Two examples of half coated spheres are shown in magnified virtual cross-sections. (B) Two examples of PC1 surrounded by patchy coats in XY maximum projection, and virtual cross-sections in XZ and YZ planes in Saos-2 cells. (C) Schematic illustration of nascent budding events (i) observed in (A), and COPII vesicles in the process of decoating (ii) observed in (B). PC1 is drawn in blue, COPII coats in magenta, and KLHL12 in yellow. Scale bars: 100 nm.

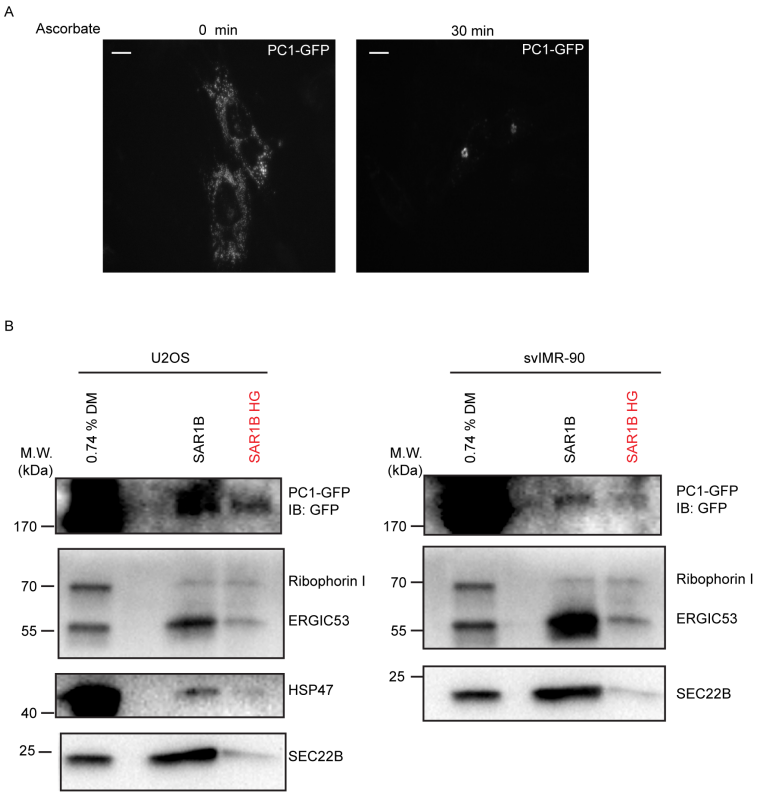

Figure 2.S4. PC1-GFP exits the ER in cells and in the vesicle budding assay. (A) Localization of PC1-GFP was examined in Saos-2 cells transiently transfected with PC1-GFP. The GFP signal localized to the Golgi apparatus after 30 min ascorbate treatment. Scale bar: 5 μm (B) Cell-free reaction using donor membrane harvested from cells that overexpressed PC1-GFP and GFP signal at the expected size was detected to exit the ER in a COPII dependent manner.

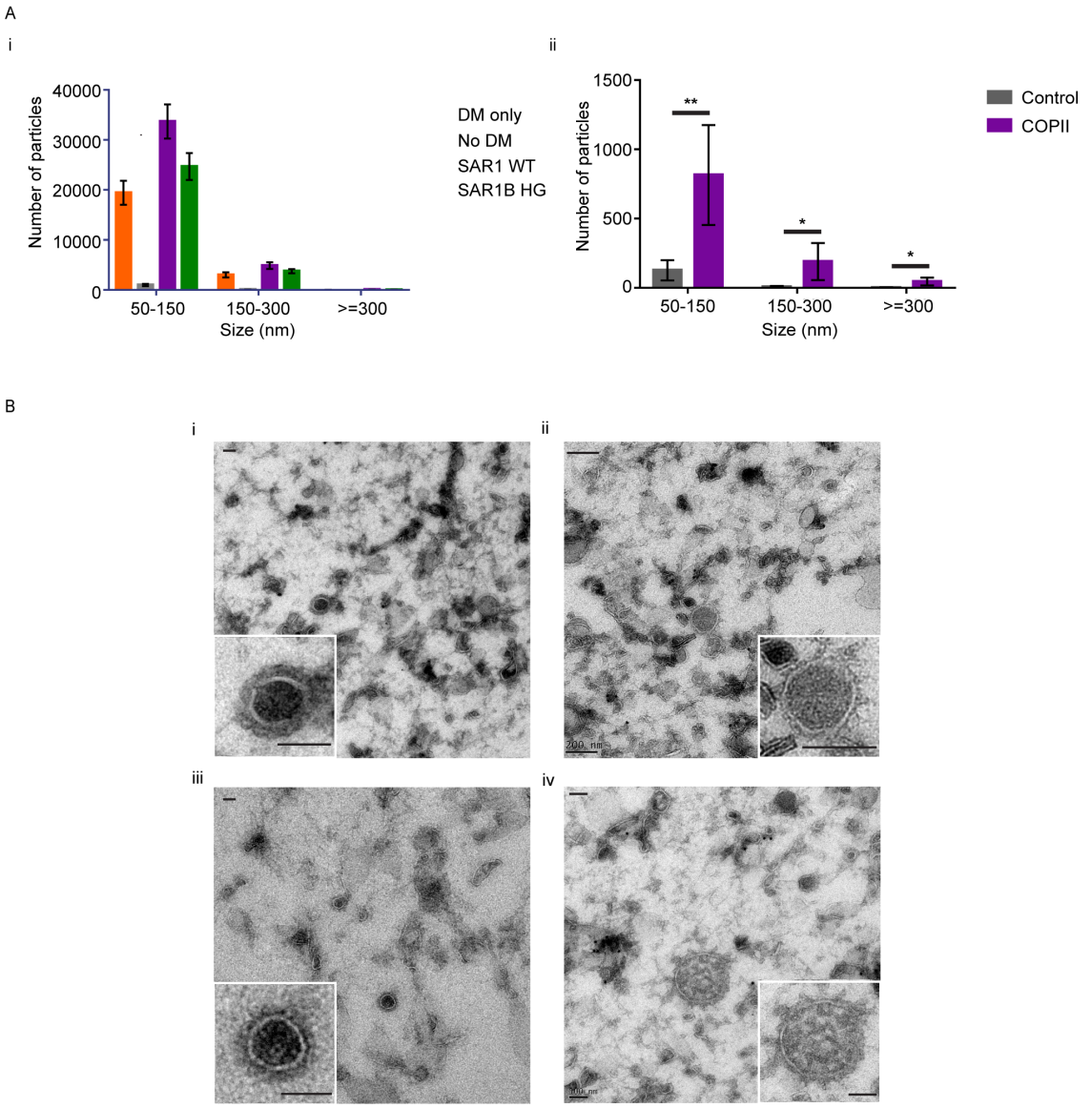

Figure 2.S5. Size distribution of vesicles in the floated fraction.
(Ai) Vesicle sizes were measured by nanoparticle tracking analysis (NTA). Bar graphs represent the average number of particles in each size category (n=3, Error bar: SD). Budding reactions with donor membrane, nucleotides, recombinant COPII, and cytosol ("Everything", purple) was used as positive control. Reactions using only donor membrane ("DM only", orange), everything but the donor membrane ("No DM", gray), and everything but SAR1B H79G instead of wild-type SAR1B ("HG control", green) were negative controls. The donor membrane itself (orange) contributed an averaged 57.2% (SD=2.64%, n=3) of all particles detected in the positive control (purple). An average of

27.0% (SD=1.36%, n=3) particles detected in the budding reaction were COPII vesicles, deduced from the differences between the positive and HG controls. (Aii) Size distribution of COPII carriers in the floated fraction quantified by fluorescent NTA to overcome high background of non-COPII particles. COPII carriers were labeled with mouse anti-SEC31A primary antibody and Qdot525 conjugated anti-mouse IgG secondary antibodies (Purple). Controls were incubated without primary antibodies (Gray). Bar graphs represent the average number of fluorescent particles in each size category and the antibody labeling of COPII vesicles was successful shown by the statistical significance compared with the controls (n=5, Error bar: SD, paired t-test, p=0.0094, 0.0346, 0.0242 for categories 50-150 nm, 150-300 nm, and >=300 nm respectively). COPII vesicles in the range of 50-150 nm were about 18 times more enriched on average than large COPII that are 300-1000 nm. The amount of conventional COPII estimated by fluorescence NTA appears to under-represent the amount deduced from scatter NTA in (Ai), possibly due to the dynamic shedding of the COPII coat and limitation of antibody affinities. The intensity of luminal GFP was too weak to be detected by fluorescent NTA. Due to this technical limitation, we were not able to quantify the size distribution of PC1-carrying COPII by NTA. (B) Morphology of membrane vesicles generated from *in vitro* budding reaction (i-iv) Ultrathin cryo-sections of sample collected from an in vitro budding reaction show an overview of differently sized membrane vesicles and an inset showing a magnified view of a single vesicle (i) coated ~150 nm membrane vesicle (ii) uncoated or partially coated ~200 nm vesicle (iii) coated ~225 nm membrane vesicle and (iv) ~300 nm vesicle. Scale bars in (i and iv, including insets): 100 nm; (ii and iii, including insets): 200 nm.

Acknowledgments

We thank the staff at UC Berkeley shared facilities including Ann Fisher and Alison Kililea (Tissue culture facility), Steven Ruzin and Denise Schichnes (CNR Biolgoical Imaging facility), Kartoosh Heydari (Flow cytometry facility) and Reena Zalpuri (Electron Microscopy lab). We are grateful for advice and guidance by Manfred Auer (LBNL) and Kent McDonald (Director, Electron Microscopy Lab). Research reported in this publication was performed in part at CRL Molecular Imaging Center and The CNR Biological Imaging facility, supported in part by the Gordon and Betty Moore Foundation and The National Institutes of Health S10 program under award numbers 1S10RR026866-01 and 1S10OD018136-01. We also thank past and present members of the Schekman Lab in particular Kanika Bajaj, Yusong Guo, Liang Ge and David Melville. RS is supported as an Investigator of the Howard Hughes Medical Institute and the UC Berkeley Miller Institute of Science. LY was supported in part by the Tang family fellowship. AG was supported in part by the Employee Development Program at Berkeley Lab. S.K. and K.X. acknowledge support from NSF under CHE-1554717, the Pew Biomedical Scholars Award, and the Sloan Research Fellowship. The authors declare no competing financial interests.

Author contributions

A. Gorur, L. Yuan, K. Xu, and R. Schekman conceptualized the experiments. A. Gorur and L. Yuan identified the monoclonal antibodies for collagen 1 and performed the immuno-fluorescence assays. A. Gorur performed electron microscopy and live-cell imaging. S.J. Kenny performed and analyzed STORM micros- copy data. L. Yuan established the in vitro budding protocol. L. Yuan performed and analyzed data from in vitro budding experiments. S. Baba carried out the initial optimization of the in vitro budding experiments. A. Gorur, L. Yuan, and R. Schekman prepared the original draft and revised the manuscript.

Chapter 3: The TANGO1/cTAGE5/SEC12 complex is co-packaged with PC1 to increase COPII size

Introduction

COPII vesicles are usually of uniform size as a result of the coordinated COPII budding machinery (Barlowe et al., 1994). Vesicles generated by purified COPII from mammalian ER average around 80 nm in diameter, yet large COPII vesicles of at least 300 nm in diameter were observed to transport the large cargo PC1 (Kim et al., 2005; Gorur et al., 2017). The occasional enlargement beyond the uniform size suggests that the cell only increases COPII size upon the demand of large cargo for secretion. To achieve this, the cell would require a sensor in the ER lumen to detect the presence of large cargos, an effector in the cytoplasm to regulate the COPII machinery that is responsible for membrane budding, and a transducer to relay the information across the ER membrane.

TANGO1 (MIA3) is a large transmembrane protein that was originally identified as a regulator of Golgi morphology and has since been implicated in collagen secretion (Bard et al., 2006; Saito et al., 2009; Wilson et al., 2011). TANGO1 can interact with a broad range of PC isoforms in the ER lumen by binding to the PC-specific chaperone HSP47 via its distal SH3 domain (Saito et al., 2009; Ishikawa et al., 2016). Its cytosolic domains were shown to interact with the COPII inner coat protein SEC23A directly and recruits the COPII initiating factor SEC12 indirectly through cTAGE5 (Saito et al., 2009, 2011, 2014; Ma and Goldberg, 2016). Currently, TANGO1 is thought to organize the biogenesis of large cargo carriers by encircling the neck of the budding membrane without leaving the ER (Saito et al., 2009; Raote et al., 2017).

It is puzzling how PCs are packaged into the budding membrane when TANGO1 does not depart with it, as the timing of cargo release and membrane fission could be challenging. One possibility is that TANGO1 recruits an additional protein to anchor PCs to the budding membrane and ensures its packaging. To identify the postulated PC1 anchor that would be co-packaged into the large carriers, a proximity labeling method using the engineered peroxidase APEX2 was employed. APEX2 reacts with biotin phenol (BP) and hydrogen peroxide (H_2O_2) to generates biotin phenol radicals, which biotinylate neighboring proteins in a 20-nm radius. Because the biotin phenol radicals are not membrane permeable and only react with proteins in a confined area, it has been used in

combination with mass spectrometry to identify and map proteins at subcellular localizations that are hard to purify such as the inner mitochondria membrane and the mitochondria-ER contact sites (Lam et al., 2015; Hung et al., 2017).

Here, we describe our effort to identify the hypothesized luminal anchor of PC1 by targeting APEX2 to the lumen of large COPII carriers. Surprisingly, TANGO1 and its interaction partners cTAGE5 and SEC12 were all observed to be co-packaged with PC1 into large COPII carriers. Our data suggests a model in which the co-packing of TANGO1 leads to the concentrated sorting of SEC12 into the PC1 containing buds, which increases the local SAR1-GTP level as well as the size of COPII.

Results

Targeting of APEX2 to large COPII carriers and characterization of proximity labeling

PCs fold into long rigid rods before they exit the ER, therefore tagging one end of PCs with APEX2 may not efficiently label proteins in the lumen of the large carrier. Practically, the size of collagen encoding genes also well exceed the effective packaging limit of the Lentivirus. For these reasons, APEX2 was fused to the C-terminus of the collagen specific chaperone HSP47 (Fig. 3.1 A). HSP47 binds to the triple helical region of folded PC trimers and accompanies PCs to ERGIC or cis-Golgi where it dissociates due to lower pH (Nagai et al., 2000; Ono et al., 2012; Widmer et al., 2012; Oecal et al., 2016). Following dissociation from PCs, HSP47 is recycled back to the ER via its C-terminal RDEL sequence, which is omitted from HSP47-APEX2 as we focus on the anterograde PC secretion pathway (Fig. 3.1 A) (Satoh et al., 1996).

To check if HSP47-APEX2 can be targeted to large COPII carriers of PC1, we examined its subcellular localization by electron and fluorescence microscopy. For EM, APEX2 catalyzes localized polymerization of diaminobenzidine (DAB), which then reacts with osmium to generate contrast. Darkened regions were observed inside the ER of cells that was transduced with Lentivirus carrying HSP47-APEX2, which was not observed in non-transduced controls (Fig. 3.1. B i,ii). Moreover, probable large COPII carriers with darkened lumen were observed between ER cisternae and the cis-face of Golgi (Fig. 3.1. B iii). For fluorescence microscopy, biotinylated proteins were visualized with streptavidin fluorophore conjugates after the addition of BP and H_2O_2 (Fig. 3.1 C).

Biotinylated proteins were detected in and around cells that expressed HSP47-APEX2 by microscopy, showing that HSP47-APEX2 was successfully secreted. Proximity biotinylation was also confirmed by streptavidin enrichment and immunoblotting against known interaction partners and marker proteins along the secretory pathway (Fig. 3.1 D,E).

Fractionation of large and regular COPII by rate-zonal sedimentation

In a living cell, newly generated COPII-coated vesicles are targeted for fusion with its destination organelle, making it challenging to label proteins in the lumen of such a short-lived transport vehicle. Therefore, we took advantage of a cell-free reaction that was developed to generate large COPII coated PC1 carriers (Gorur et al., 2017). Because this process is dependent on GTP hydrolysis, a reaction supplemented with GMP-PNP, the non-hydrolyzable GTP analogue, can be used as a negative control.

To enrich for large COPII, a rate-zonal sedimentation scheme was developed to fractionate the cell-free reaction (Fig 3.2 A). Following a 10-min centrifugation at 7000 g, vesicles in the supernatant were sedimented through a step density gradient at 250,000 g for 1 h to separate large and regular COPII membranes. Fractions taken after sedimentation were used as input for flotation to separate vesicles from soluble proteins and the floated sedimentation (FS) fractions were analyzed by immunoblots (Fig 3.2 B). Most PC1 was observed at the lower density interphase in FS fraction 4. In contrast, most control COPII cargos ERGIC53 and SEC22B were observed at the higher density interphase in FS fraction 8. When GMP-PNP was supplemented instead of GTP, the amount of PC1 in FS fraction 4 decreased, which suggested that the PC1 signal detected in this fraction represented COPII carriers of PC1 (Fig 3.2 C).

To identify the putative luminal anchor in large COPII carriers, I prepared donor membrane from cells transduced with HSP47-APEX2. BP and H_2O_2 was added to FS fraction 4 to biotinylate proteins in the lumen of large COPII carriers and biotinylated proteins were visualized by streptavidin blotting (Fig 3.2 D). Budding reaction supplemented with GMP-PNP and the FS fractions 8 were used as negative controls. In addition to the strong band at the molecular weight of PC1 (190 kD) in FS fraction 4 from a reaction that was supplemented with GTP, a unique band at the molecular weight of TANGO1 was also observed (Fig 3.2 D).

TANGO1/cTAGE5/SEC12 exit the ER in large COPII coated PC1 carriers

To test whether TANGO1 exit the ER with its cargo PC1, I performed cell-free reactions to reconstitute the packaging of PC1 into large COPII carriers under different incubation conditions (Gorur et al., 2017). TANGO1 was detected in the floated fraction under the most optimal incubation condition by immunoblotting (right most lane, Figure 3.3 A). The amount of TANGO1 detected in the floated fraction decreased when recombinant COPII was omitted or when the SAR1B H79G mutant deficient in its GTPase activity was supplemented instead of the wild-type SAR1B. Together with its dependency on physiological temperature, we concluded that COPII dependent budding of TANGO1 can be detected in the cell-free reaction.

Because TANGO1 forms a stable complex with cTAGE5 and SEC12 (Maeda et al., 2016), we immunoblotted for them in the floated fraction and both cTAGE5 and SEC12 were detected in vesicles formed in a COPII dependent manner (Figure 3.3 A). Interestingly, molecules that are implicated in PC1 secretion, namely PC1, HSP47, TANGO1, cTAGE5 and SEC12, showed similar sensitivity to the omission of recombinant COPII compared to the controls for regular COPII vesicle cargo, ERGIC53 and SEC22B (Figure 3.3 A). To test whether TANGO1/cTAGE5/SEC12 were co-packaged with PC1, I separated PC1 carriers from regular COPII by rate-zonal sedimentation (Fig. 3.2. A). TANGO1, cTAGE5 and SEC12 co-fractionated with PC1, as they were more abundant in the FS fraction 4 at the lower density interphase (Fig. 3.3 B). Moreover, less TANGO1, cTAGE5 and SEC12 were detected in the FS fraction 4 when SAR1B H79G mutant was supplemented to the reaction.

To examine the localization of TANGO1 and SEC12 in cells, I employed stochastic optical reconstruction microscopy (STORM), a technique that allowed the resolution of the coat and cargo proteins in large COPII carriers (Gorur et al., 2017). Both TANGO1 and SEC12 were observed on large COPII carriers by STORM (Fig. 3.3 C,D). Moreover, SEC12 was especially enriched in large COPII carriers observed in KI6 cells after the induced overexpression of KLHL12 for 8 h as well as in Saos-2 cells without any overexpression (Fig. 3.3. D,E). In summary, evidence from reconstitution of PC1 budding and fluorescence microscopy supported the conclusion that the cargo receptor TANGO1 was co-packaged with its cargo PC1 into large COPII-coated vesicles.

TANGO1 is recycled back to the ER in via HSP47

Unlike most cargo adaptors, TANGO1 does not contain a C-terminal KKXX or KDEL retrieval signal. Because TANGO1 interacts with HSP47 via its SH3 domain, I hypothesized that TANGO1 could be recycled back to the ER with HSP47 (Ishikawa et al., 2016). When the C-terminal RDEL sequence is omitted, HSP47ΔRDEL is readily secreted and can be observed in the extracellular matrix (Fig. 3.1 C; Sato et al., 1996).

To test whether TANGO1 is retrieved via its interaction with HSP47, I examined TANGO1 localization in cells that overexpressed HSP47ΔRDEL-StrepII. To my surprise, most intracellular TANGO1 disappeared from cells that have secreted HSP47ΔRDEL-StrepII (Fig. 3.4 A,B). Further, co-localization between TANGO1 and a Golgi marker Golgin97 was observed when cells overexpressing HSP47ΔRDEL were shifted to 19.5°C for 3 h to block cargos in the Golgi (Fig 3.4 C).

COPI dependent retrieval of TANGO1 was further demonstrated by the transfection of the GTP-locked ARF1 Q71L mutant. Overexpression of ARF Q71L inhibits retrograde trafficking and leads to accumulation of COPI cargos in the Golgi membrane. ERGIC53 is a COPII cargo adaptor for glycoproteins and is actively retrieved back to the ER by COPI (Barlowe and Helenius, 2016). In cells that overexpressed ARF1 Q71L, Golgi accumulation of ERGIC53 was observed, as it co-localized with ARF1 Q71L (Fig 3.4 D). Moreover, a fraction of TANGO1 co-localized with ARF1 Q71L and ERGIC53 in the same cells, showing that the retrieval of TANGO1 depended on ARF1-GTP hydrolysis and COPI budding (Fig 3.4. D).

TANGO1 concentrates SEC12 to generate large COPII coated PC1 carriers

SEC12 initiates COPII biogenesis by activating the GTPase SAR1, which subsequently induces membrane curvature and recruits downstream COPII components to complete vesicle budding (Nakano et al., 1988; Barlowe and Schekman, 1993; Weissman et al., 2001). Unlike other COPII components, SEC12 is not actively packaged into conventional COPII coated vesicles (Barlowe et al., 1994, Futai et al., 2004, Sato et al., 1996). The contrary was observed for large COPII, as SEC12 signal was particularly enriched at PC1 puncta and was resolved to coat around the entire large COPII membrane surface by STORM (Fig. 3.3 D,E).

Previously, SEC12 was shown to be recruited to ERES by interacting with cTAGE5, which is recruited by its interaction with TANGO1 (Saito et al., 2014; Maeda et al., 2016, 2017). Therefore, I hypothesize that SEC12 is actively packaged into PC1-containing large COPII vesicles by TANGO1. I tested this model by characterizing the overexpression phenotype with confocal microscopy. When cells were transfected with SEC12 alone, overexpressed SEC12 localized diffusely across the ER (Fig 3.5 A). However, when TANGO1 was co-transfected with SEC12, overexpressed SEC12 was concentrated into large punctate structures that co-localized with TANGO1 and endogenous PC1 (Fig 3.5 B).

To test the functional significance of concentrating SEC12 at PC1 containing sites, I monitored PC1 secretion under different transfection conditions. Overexpression of wild-type SEC12 alone did not have an effect on PC1 secretion compared to a control that was transfected with empty plasmids (Fig 3.5 D). In contrast, co-overexpression of SEC12 and TANGO1 stimulated PC1 secretion compared to overexpressing TANGO1 with an empty plasmid. Moreover, co-overexpressing TANGO1 and the SEC12 GEF mutant I41A, which is deficient in SAR1 activation did not promote PC1 secretion (Fig 3.5 C,D).

Discussion

The COPII complex mediates the ER to Golgi trafficking of secretory proteins by deforming the ER membrane into transport vesicles and by sorting selective cargo proteins into the vesicles. The formation of COPII coated vesicles is a coordinated process initiated by SEC12 and orchestrated by the GTPase SAR1, the inner coat protein SEC23, and the outer coat protein SEC31, whereas the selective cargo sorting is mainly driven by the inner coat protein SEC24. Some secretory cargos can interact with SEC24 directly via their cargo sorting signals, such as the diacidic DXE motif, others indirectly via cargo receptors including but not limited to ERGIC53 and p24 proteins for soluble cargos and Cornichon and SCAP for transmembrane cargos (Miller et al., 2003; Barlowe and Helenius, 2016). Most cargo receptors contain both COPII and COPI sorting signals and are efficiently recycled back to the ER by COPI vesicles (Barlowe and Helenius, 2016).

TANGO1 has been depicted as an unconventional cargo receptor for PCs, as it is thought to be retained in the ER (Saito et al., 2009). This conclusion was mainly derived from the result that TANGO1 was not detected by immunoblotting in COPII vesicles reconstituted from ER membrane that expressed collagen VII. However, packaging of the cargo collagen VII was not detected by this assay either. We recently developed an improved method to reconstitute and detect the capture of PC1 into large COPII carriers (Gorur et al., 2017). Using this method, we show the co-packaging of TANGO1 with PC1 in COPII carriers, as TANGO1 co-fractionated with PC1 rather than regular COPII markers and it was labeled by proximity biotinylation of HSP47-APEX2 (Fig. 3.2 D, Fig. 3.3 A,B). This result was confirmed by the co-localization of TANGO1 on large COPII in PC1 secreting cells (Fig. 3.3 C). Furthermore, we discovered that TANGO1 was recycled back to the ER by hitchhiking along with HSP47, which contains a RDEL retrieval signal, into COPI vesicles (Fig. 3.4). In summary, we have provided evidence for TANGO1 as a conventional cargo receptor for PC1.

Interestingly, the COPII initiating factor SEC12 was also detected in large COPII carriers (Fig. 3.3). Unlike regular COPII, large COPII was enriched with SEC12, as its extensive surface coverage was revealed by STORM (Fig. 3.3 D,E). The concentrated sorting of SEC12 to PC1-containing membranes was mediated by TANGO1 (Fig. 3.5 A,B). Highly concentrated SEC12 at PC1-containing membrane stimulated PC1 secretion, possibly by increasing the local concentration of SAR1-GTP (Fig. 3.5 C,D).

Addition of a soluble cytosolic domain fragment of SEC12 to a liposome budding reaction promotes bud formation and inhibits vesicle fission, making SEC12 an ideal candidate to enlarge COPII vesicles (Futai et al., 2004). The enrichment of SEC12 at PC1-containing membrane also provided a context for the otherwise puzzling observation concerning the TRAPP component Sedlin, which is also recruited by TANGO1 (Venditti et al., 2012). Sedlin controls PC export but not regular cargos by accelerating the dissociation of SAR1-GTP and inducing membrane scission, which would be specifically necessary for PC secretion due to the inhibitory effect of SEC12 on vesicle fission (Venditti et al., 2012).

We propose a speculative model on the enlargement of COPII for PC secretion initiated when TANGO1 via its interaction with HSP47 senses the presence of folded PC trimers in the ER lumen. TANGO1 interacting with cTAGE5 would then recruit SEC12 to PC1-containing membrane. The concentrated sorting of SEC12 may then promote the formation of larger-than normal COPII coats by

virtue of a persistent recharging of SAR1 on the coated membrane surface. Sedlin may counteract this by promoting the discharge of SAR1-GTP at the bud neck leading to vesicle fission. The packaging of PC would thus be ensured by the co-packaging of its adaptor TANGO1 into COPII vesicles, which is retrieved with HSP47 in COPI vesicles.

Materials and methods

Plasmids

HSP47ΔRDEL was cloned from cDNA prepared from U-2OS cells with primers "ATGCGCTCCCTCCTG" and "CATCTTGTCACCCTTAGG". HSP47-APEX2 (HSP47ΔRDEL-GSlinker-FLAG-APEX2) was cloned into the Lentiviral transfer vector pLenti-puro, HSP47ΔRDEL-StrepII was cloned into pcDNA4. TANOG1-FLAG in pcDNA3.1 was a gift from Vivek Malhotra lab (CRG-Centre de Regulacio Genomica, Barcelona, Spain), 3xFLAG-SEC12 in p3xFLAG CMV10 plasmid was gifted from Kota Saito lab (Univeristy of Tokyo, Tokyo, Japan). Site directed mutagenesis was used to clone out the cytosolic domain of SEC12 and introduce I41A and N43A mutations.

Cell culture

Human lung fibroblasts IMR-90 and svIMR-90 (IMR-90 immortalized with SV-40) were obtained from Coriell Cell Repositories at the National Institute on Aging, Coriell Institute for Medical Research. Human osteosarcoma Saos-2 and U-2OS and human fibrosarcoma HT-1080 were obtained from ATCC. IMR-90, svIMR-90, Saos-2, U-2OS, and HT-1080 were maintained in DMEM plus 10% FBS (GE Healthcare). The construction and maintenance of HTPC1.1 and KI6 were described in Jin et al., 2012 and Gorur et al., 2017. HTPC1.1 that stably expresses COL1A1 was constructed from HT-1080 and the doxycycline-inducible KLHL12-3xFLAG stable cell line (KI6) was constructed from HTPC1.1.

Lenti virus production and transduction

Standard 2nd generation procedure was used to produce, store, and transduce. Early passaged HEK293T cells were transfected with equal molar ratio of transfer vector (pLenti_puro_HSP47ΔRDEL-GSlinker-FLAG-Apex2), packaging

plasmid (pxPAX2), and envelope plasmid (pMD2.G). The media was changed after 24 h, and media supernatant containing virus was harvested after 48 h by passing through a 44 μm filter. To transduce in IMR-90 cells, I replaced cultured media with 50% fresh media and 50% viral supernatant. Culture media was replaced after 24 h, and cells were harvested after 48 h for assays. Using this protocol, more than 70% of cells were transduced.

APEX2 proximity labeling

Immunofluorescence and the immunoprecipitation procedure was followed exactly as described by Hung et al., 2016. For electron microscopy, cells were processed as described in Lam et al., 2015 with the following modifications suggested by Jeffrey Martel and Alice Ting. A monolayer of cells was fixed by warm 2% Glutaraldehyde solution (EMS) in 0.1M sodium cacodylate (SC) buffer pH 7.4 for 5 min, then replaced with fresh 2% glutaraldehyde solution for 1 h. Fixed cells were washed 3 x with cold SC buffer, quenched with 20 mM glycine solution for 5 min on ice, then wash 3 x with cold SC buffer, followed by incubation with freshly prepared DAB/H_2O_2 solution (0.5 mg/ml DAB, 1 mM H_2O_2) for 30 min on ice. The reaction was halted by replacing media with SC buffer and processed for thin-section electron microscopy described in Gorur et al., 2017.

Immunofluorescence, immunoblotting, and antibodies

Immunofluorescence (IF) for confocal microscopy and STORM and immunoblotting (IB) analyses were performed as described in Gorur et al., 2017. For immunoblotting detection of TANGO1 in reconstituted vesicles, I used transfer buffer containing 0.1% SDS. The following antibodies were used: mouse anti-PC1 (clone 42024; QED Biosciences; 1:200 for IF); rabbit anti-PC1 (LF-41, 1:5000 for IB) was a gift of Larry Fisher (NIH, Bethesda, MD); rabbit anti-SEC31A (Bethyl Laboratories; for IF, at 1:200 for confocal and 1:2,000 for STORM); mouse anti-FLAG (Thermo Fisher Scientific; 1:5,000 for IB); goat anti-FLAG (Novus Biologicals; for IF at 1:1,000 for confocal and 1:5,000 for STORM); mouse anti-HSP47 (Enzo Life Sciences; at 1:200 for IF and 1:5,000 for IB); Rab anti-Calnexin (Abcam, 1:500 for IF, 1:5000 for IB), Rab anti-TANGO1 (Sigma, 1:200 for IF, 1:1000 for IB); Rab anti-cTAGE5 (Sigma, 1:2000 for IB); Rab anti-GFP (Tory Pines, 1:2000 for IB); Goat anti-SEC12 (R&D, 1:1000 for IB. Note: this is only used for vesicles purified by density gradient flotation due to a major

unrelated cytosolic band); Rat anti-SEC12 was purified from hybridoma clone 6B3 gifted from Kota Saito lab (University of Tokyo, Tokyo, Japan). For visualizing biotinylated proteins by microscopy or on a transferred blot, I used streptavidin-488 (Invitrogen) or streptavidin-HRP (Pierre) at the same time as secondary antibodies.

Vesicle budding reaction

The PC1 budding reaction was performed as described in Gorur et al., 2017. To separate COPII coated PC1 carriers and regular COPII vesicles, I scaled up the budding reactions 4-fold. In a polycarbon 11 x 34 mm ultracentrifugation tube (Beckman Coulter), I placed 500 μl of 18% (w/v) OptiPrep in B88 (20 mM HEPES, pH 7.2, 250 mM sorbitol, 150 mM KOAc, 5 mM $Mg(OAc)_2$) at the bottom of the tube, overlayed with 400 μl 7.5% (w/v) OptiPrep (Sigma-Aldrich) in B88, then 350 μl 7,000 g supernatant of the reaction. The OptiPrep gradient was centrifuged at 250,000 g for 1 h at 4°C (Beckman TLS-55) with slow acceleration and deceleration, after which 100 μl fractions were collected from the top. Desired fractions were subjected to flotation: 85 μl of each sedimentation fraction was gently mixed with 50 μl of 60% (w/v) OptiPrep until the sample was homogeneous, placed at the bottom of a 7 × 20 mm tube (Beckman Coulter), and overlaid with 100 μl of 18% (w/v) and 10 μl of 0% OptiPrep in B88. The OptiPrep gradient was centrifuged at 250,000 g for 1 h at 4°C (Beckman TLS-55 with adaptors for 7 × 20-mm tubes) with slow acceleration and deceleration, after which 40-μl was collected from the top and mixed with sample buffer for immunoblotting analysis.

Tryptophan fluorescence assay

The tryptophan fluorescence assay was performed at 37°C in a stirred-cuvette as described in Futai et al., 2004 and Fromme et al., 2007 with slight modifications. To HKM buffer (20 mM HEPES pH 7.2, 160 mM KOAc, 1 mM $Mg(OAc)_2$), I added an indicated amount of WT, I41A, or N43A SEC12-cyto, followed by 2 μM SAR1BΔN (the N-terminal amphipathic helix was omitted because it does not affect GTP/GDP binding as described in Lee et al., 2005), then 30 μM GTP. When GTP hydrolysis was tested, 0.7 μM SEC31A (950-1220) was added before the addition of SAR1BΔN, and after the exchange of GDP for GTP completed, 110 nM of SEC23A/24D was added to induce GTP hydrolysis.

PC1 secretion assay

Indicated combinations of plasmids and Lipofectamine3000 (Invitrogen) were used to transfect svIMR90 cells (30% confluent). Media was changed to OptiMEM 16 h after transfection and further incubated of 4 h. Media was harvested by careful removal of the supernatant fraction after 300 g centrifugation for 5 min. Cells were washed then lysed in PBST (PBS, 0.5% Triton), and the supernatant carefully recovered after 300 g centrifugation for 5 min. Sample buffer was added to media and lysate, which were then heated at 65°C and samples taken for immunoblotting analyses.

Figures

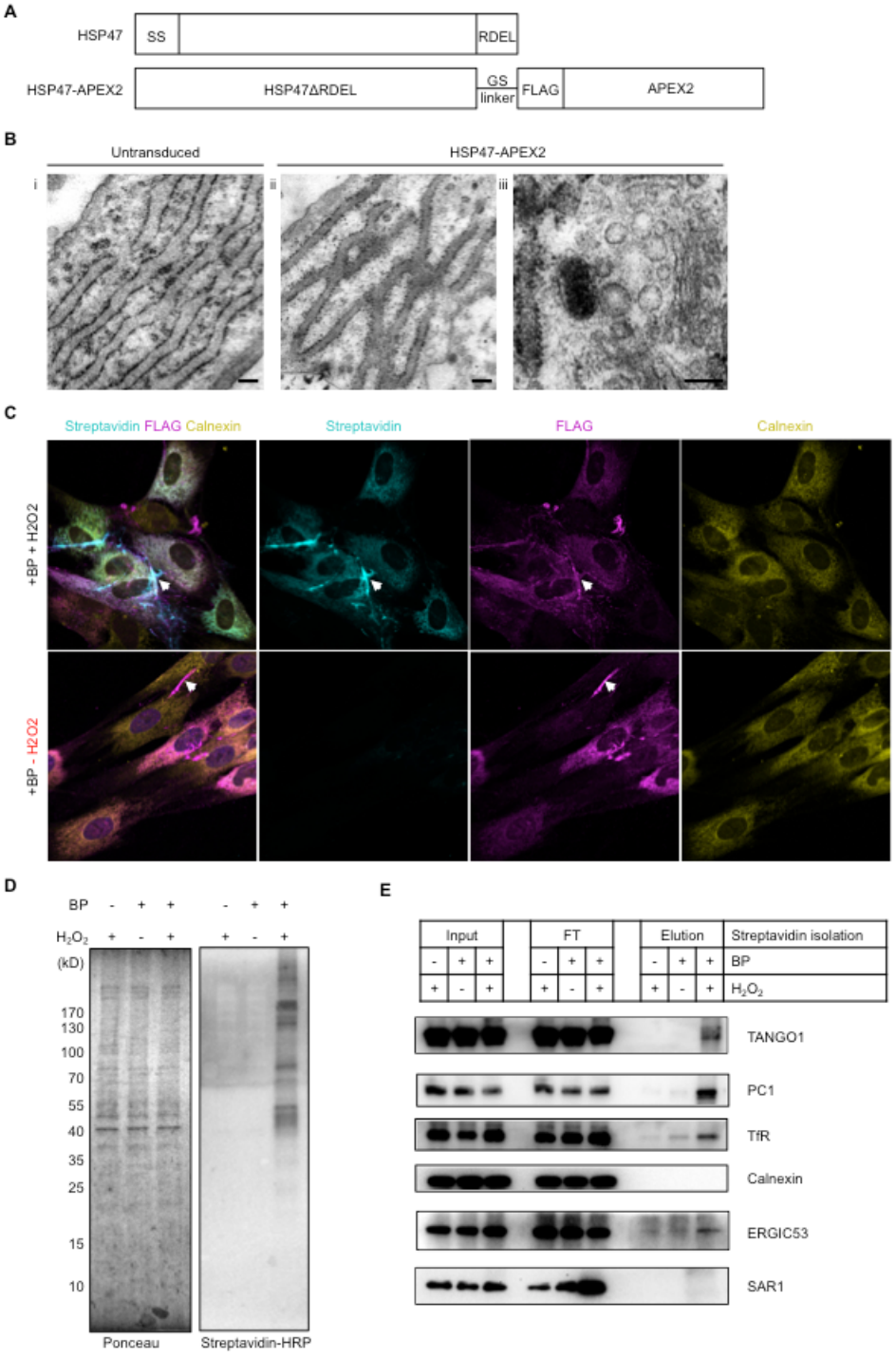

Figure 3.1. Proximity labeling of the PC1 secretory pathway.

(A) Schematic diagram of HSP47 and HSP47-APEX2 not drawn to scale. HSP47 without the C-terminal RDEL was cloned to the N-terminal coding sequence of APEX2, followed by a GS linker and FLAG tag. (B) Thin-section EM images of IMR-90 untransduced (i) or transduced with HSP47-APEX2 (ii,iii) and labeled with DAB. Dark regions indicated proximity labeling by APEX2 in ER (ii) or large COPII (iii). Scale bars: 0.2 μm. (C) Proximity biotinylation in IMR-90 cells expressing HSP47-APEX2 induced by biotin-phenol (BP) and H_2O_2. Cells not incubated with H_2O_2 were used as a negative control (bottom row). Biotinylated proteins were visualized by confocal microscopy after labeling with streptavdin-488 (teal). Immunofluorescence of calnexin (yellow) and FLAG (magenta), which targets the HSP47-APEX2 construct, were used as a control for transduction efficiency. Arrows point to secreted HSP47-APEX2 and biotinylated proteins in the extracellular matrix. (D) Streptavidin blotting of endogenous proteins biotinylated by HSP47-APEX2 in IMR-90 cells. Samples without BP or H_2O_2 were used as negative controls. Lysates were separated by SDS-PAGE and analyzed by blotting with streptavidin-HRP. Total protein on the same membrane was visualized by Ponceau staining. (E) Streptavidin enrichment of proteins biotinylated by HSP47-APEX2 from lysates prepared as in (D) using streptavidin-coated magnetic beads. Biotinylated proteins were eluted by heating SDS and biotin in sample buffer at 100 °C for 5 min and analyzed by immunoblotting against secretory protein markers. Proteins with known interactions were used as positive controls: PC1 and TANGO1. The cytosolic COPII protein SAR1 was used as a negative control. Proximity with the following proteins that contain large luminal or extracellular domains was probed: calnexin, ERGIC53, and transferrin receptor (TfR).

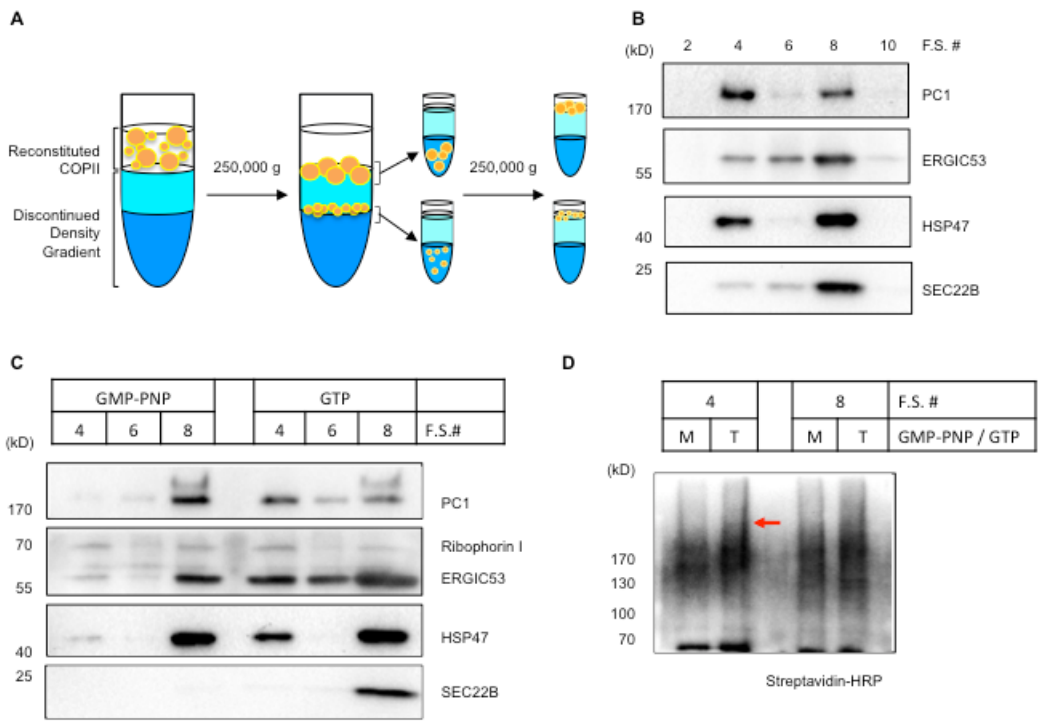

Figure 3.2. Fractionation of large and regular COPII by rate-zonal sedimentation.

(A) Schematic representation of the fractionating procedure. Supernatant (350 μl after 7000xg centrifugation) from a vesicle budding reaction was overlaid onto a step gradient consisting of 500 μl 18% and 400 μl 7.5% OptiPrep. The gradient was centrifuged at 250,000 g for 1 h at 4°C to separate large from regular COPII. Fractions taken after sedimentation were used as inputs for flotation to separate vesicles from soluble contents. (B) Immunoblotting against the large cargo PC1 and regular COPII cargos ERGIC53 and SEC22B in density gradient buoyant membrane (FS) fractions. (C) Vesicle budding reactions supplemented with GTP or GMP-PNP were fractionated, where GMP-PNP was used as a negative control for COPII budding. (D) Streptavidin blotting for biotinylated proteins in large or regular COPII. Donor membrane expressing HSP47-APEX2 was used for vesicle budding reaction, and buoyant membrane fractions were incubated with BP and H_2O_2 to induce proximity biotinylation. Arrow points to a high molecular weight band that was unique to the PC1 carrier fraction (FS fraction 4) in a GTP-supplemented vesicle budding reaction.

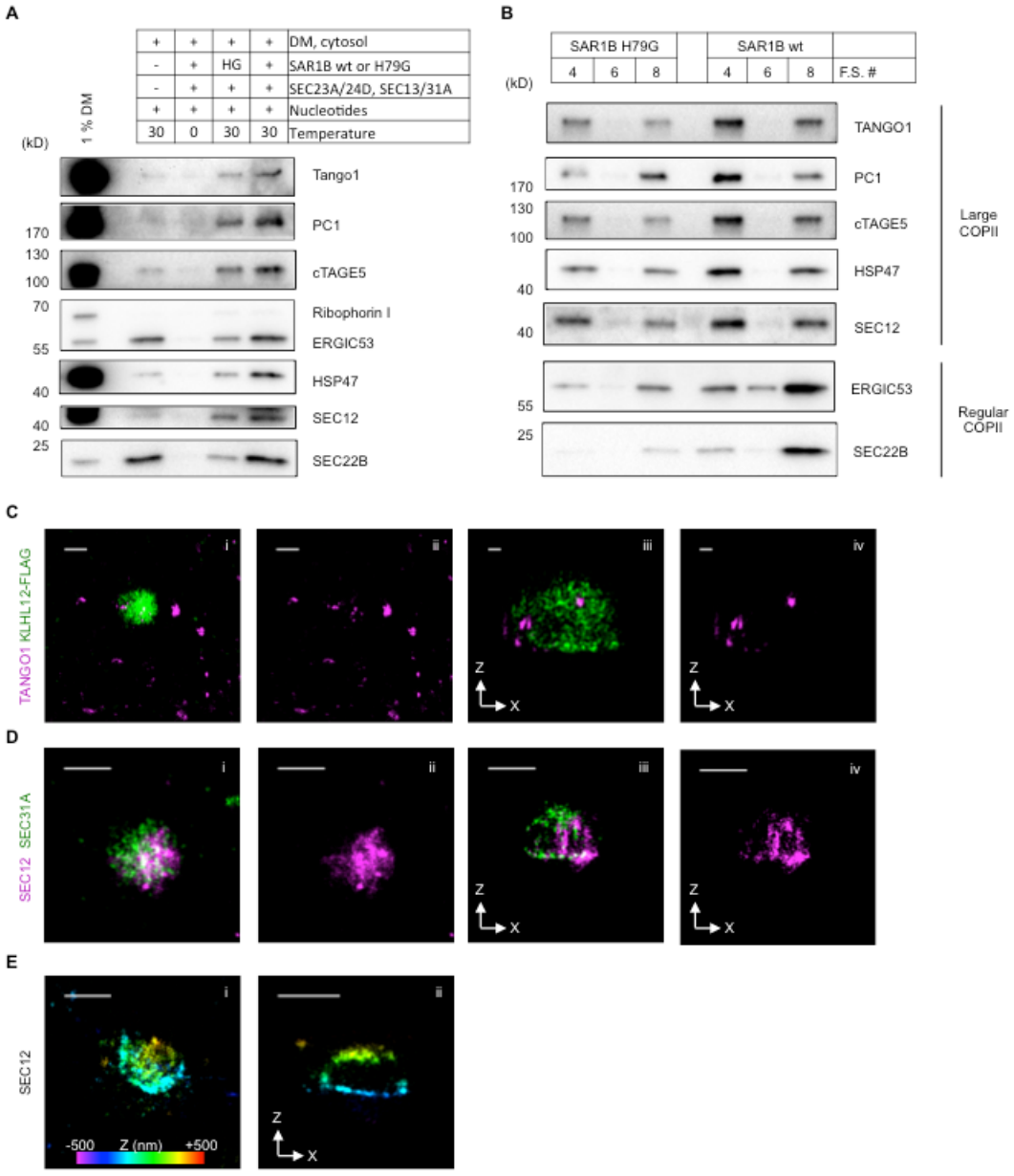

Figure 3.3. TANGO1/cTAGE5/SEC12 exit the ER in large COPII coated PC1 carriers.

(A) Immunoblotting of the buoyant membrane fractions from vesicle budding reactions incubated under different conditions. TANGO1, cTAGE5, and SEC12 were probed in addition to the large cargo PC1 and PC chaperone HSP47. ERGIC53 and SEC22B were used as markers for regular COPII and ribophorin I was used as an ER marker. (B) Immunoblotting of floated sedimentation (FS)

fractions 4, 6, 8 from incubation with wild-type (WT) or H79G mutant SAR1B. (C,D) STORM images of large COPII coated vesicles in KI6 cells after KLHL12 overexpression was induced for 8 h. TANGO1 (magenta in C) or SEC12 (magenta in D) co-localized with markers for large COPII: KLHL12-FLAG (green in C), SEC31A (green in D). (i,ii) XY maximum projections or (iii, iv) XZ cross-sections. (E) Large SEC12 puncta observed in Saos-2 cells without any overexpression were resolved by STORM. Magnified maximum XY projection (i) and visual cross-section of this structure in XZ (ii) are shown. Position in depth (z axis) is represented by color according to the color bar in Ei. Scale bars: 500 nm in Ci,ii, D, and E; 100 nm in Ciii,iv.

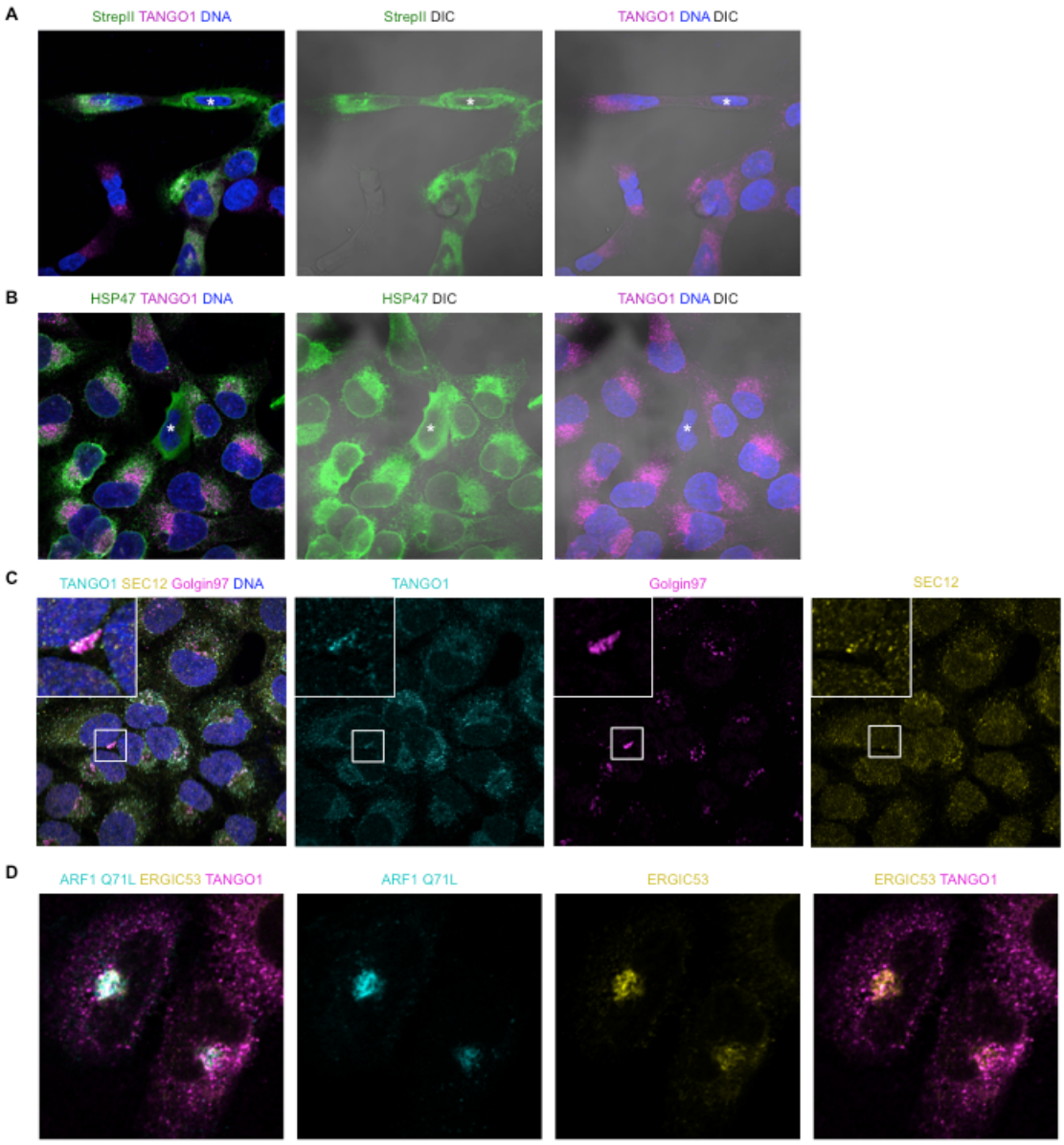

Figure 3.4. TANGO1 is recycled back to the ER via HSP47.
HSP47ΔRDEL-StrepII was overexpressed in U-2OS cells (A-C), StrepII (green in A), HSP47 (green in B) and TANGO1 (magenta in A, B) were immunofluorescently labeled. (A,B) DAPI staining was used to show the nucleus and DIC images were taken to show cell morphology. Cells indicated by the star symbol (*) had secreted HSP47ΔRDEL-StrepII and showed abnormally low signal of TANGO1. (C) U-2OS cells overexpressing HSP47ΔRDEL were shifted to 19.5°C for 3 h to block cargo proteins in the Golgi. Immunofluorescence microscopy of TANGO1 (teal), SEC12 (yellow) and a medial Golgi marker Golgin97 (magenta). Inserts showed enlarged regions within the box. (D)

Confocal images of U-2OS cells transfected with ARF1 Q71L (teal), and visualized for ERGIC53 (yellow), and TANGO1 (magenta). The pinhole was opened to 3 au in A,B to show the loss of intracellular signal of TANGO1 and secreted HSP47. A restricted pinhole of 0.6 au was used in C,D to confidently show co-localization between markers.

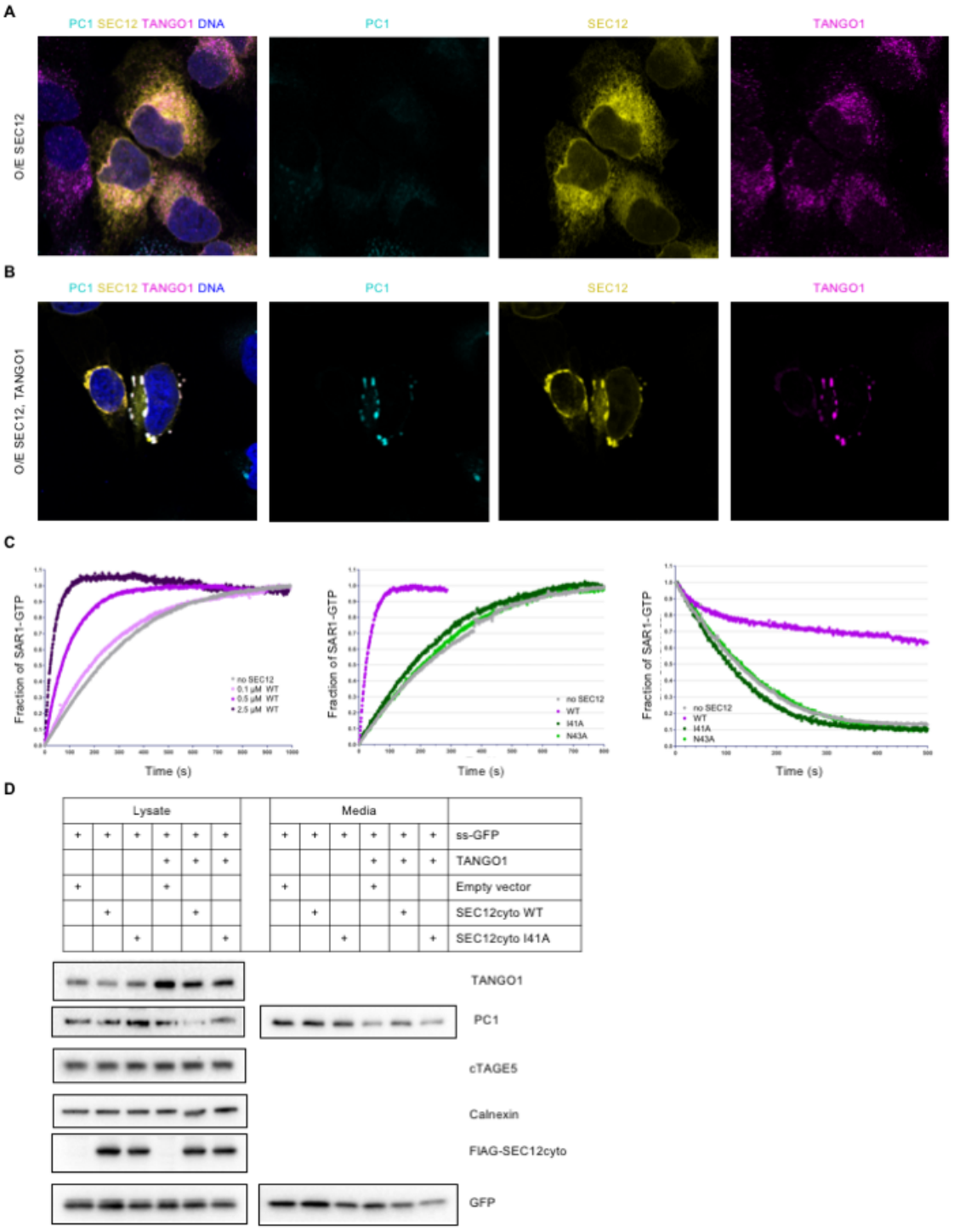

Figure 3.5. TANGO1 recruits SEC12 to generate large PC1 carriers.
(A-B) Confocal microscopy of U-2OS cells immunofluorescently labeled for PC1 (teal), SEC12 (yellow), and TANGO1 (magenta). SEC12 was co-overexpressed with an empty plasmid (A) or TANGO1 and cTAGE5 (B). (C) GTPase activity

assays to test the recombinant cytosolic domain of human SEC12. Changes in tryptophan fluorescent intensity was measured with time as an indicator of the nucleotide associated with SAR1 (Antonny et al., 2001). Fraction of SAR1-GTP was calculated by normalizing against total increase of tryptophan fluorescence after GDP was exchanged to GTP. GDP to GTP exchange occurred naturally (grey) or in the presence of GEF deficient mutants I41A or N43A (green) or was accelerated by WT SEC12 (magenta). GTP hydrolysis was also recorded in the presence or absence of WT, I41A, N43A SEC12. SAR1B (2.0 μM) was used in all reactions and 2.5 μM of WT or mutant SEC12 were used in (ii-iii) or as indicated in (i). (D) PC1 secretion assay where svIMR90 cells were transfected with ssGFP, TANGO1, SEC12 WT or I41A as indicated. The amounts of PC1 in the lysate and media were analyzed by immunoblotting. TANGO1, and FLAG were used as transfection controls. Calnexin and GFP was used as loading controls.

Chapter 4: The role of SEC31A in intracellular collagen trafficking

Introduction

The COPII complex plays an important role in the ER to Golgi transport of large cargos such as PC1. Of the five main components of COPII, SEC31 is the only subunit that has not been examined directly for its role in large cargo secretion by gene knockouts. Nevertheless, data from several published studies have implicated the importance of SEC31A in this process.

When SEC13 is knocked down in cultured human cells or zebrafish, the expression of SEC31A also decreases (Townley et al., 2008). SEC13 knockdown in primary fibroblasts results in decreased deposition of PC1 in the ECM. Suppression of Sec13 expression in Zebrafish leads to craniofacial abnormalities that are characteristic of defective collagen secretion seen in CLSD patients and *crusher* mutants, both of which are due to mutations in Sec23A (Townley et al., 2008).

One of the CLSD causing point mutations in SEC23A, F382L, results in selective inhibition of procollagen secretion (Boyadjiev et al., 2006). In homozygous F382L mutant fibroblasts, SEC31A localizes diffusely in the cytoplasm in contrast to its ER exit site localization in wild-type cells (Boyadjiev et al., 2006). Recombinant SEC23A F382L also failed to recruit SEC13/31A to SAR1B-decorated liposomes in vitro (Fromme et al., 2007). As a result, the budding efficiency of ERGIC53 is lowered when SEC23A F382L is supplemented to a cell-free COPII budding reaction with SAR1B in comparison to wild-type SEC23A and this deficiency can be rescued with a 6-fold higher concentration of SEC13/31A (Fromme et al., 2007). The importance of SEC13/31A recruitment in PC secretion suggests that SEC13/31A is more indispensable for large cargo secretion than regular cargos.

In addition to recruitment, post-translational modification of SEC31A is also implicated in the regulation of COPII size and PC1 secretion. SEC31A is a monoubiquitylation substrate of the E3 ubiquitin ligase CUL3 and the substrate adaptor KLHL12 (Jin et al., 2012). Overexpression of KLHL12 accelerates the ER to Golgi trafficking of PC1, it also results in large intracellular puncta that are positive for both KLHL12 and SEC31A (Jin et al., 2012). At moderate levels of overexpression of KLHL12, PC1 was resolved by STORM imaging to be

encapsulated inside of large SEC31A and KLHL12-coated carriers (Gorur et al., 2017).

In this chapter, the role of SEC31A in collagen secretion was examined by constructing SEC31A knockout cell lines. The SEC31A knockout cells accumulated PC1 intracellularly, which could be rescued by overexpressing SEC31A but not KLHL12, which confirmed the importance of SEC31 in PC1 secretion. Moreover, ubiquitylation sites were identified at the C-terminus of SEC31A in the active fragment that is known to accelerate the GTP hydrolysis of SAR1-GTP. The monoubiquitylated SEC31A was less efficient at stimulating the GAP activity of SEC23, providing a working model on how monoubiquitylation of SEC31A could modify the size of the COPII coat.

Results

Knockout of SEC31A inhibits PC1 secretion

To investigate the role of SEC31A directly, I constructed SEC31A knockout (KO) clones using CRISPR/Cas9 from two PC1 secreting cell lines: a human fibrosarcoma cell line that stably overexpresses *COL1A1*, HTPC1.1, and a human osteoscarcoma cell line U-2OS. Because only 20% of U-2OS cells express endogenous PC1, single clones of wild-type (WT) and KO cells were selected for uniform endogenous PC1 expression by immunoblotting.

The efficiency of PC1 secretion was examined by immunofluorescence microscopy with the same parameters across all samples. SEC31A KO HTPC1.1 cells show accumulation of intracellular PC1 in over 80% of cells compared to less than 40% of WT cells that show comparable level of intracellular PC1 (Fig. 4.1 A-B, 4.S1). Because ascorbate treatment stimulates PC1 secretion and KLHL12 was shown to accelerate PC1 secretion kinetics upon ascorbate treatment, response of WT and SEC31A KO cells to ascorbate was analyzed. After 1 h of ascorbate addition, most WT cells show little intracellular PC1 as previously observed, whereas PC1 can be observed in most SEC31A KO cells localized to large puncta (Fig. 4.1 A-B, 4.S1). The inefficient PC1 secretion phenotype was rescued by overexpressing SEC31A but not an empty plasmid (Fig. 4.1 C-D). SEC31A KO U-2OS cells also showed similar accumulation phenotypes (Fig. 4.S1).

However, PC1 can still be detected in the media of SEC31A KO cells by immunoblotting suggesting that SEC31A is not essential in PC1 secretion (data not shown). Moreover, the abovementioned PC1 accumulation phenotype decreased in severity as KO cells were passaged, possibly due to a compensatory increase of SEC31B. Although compensation has not been tested due to the lack of a reliable SEC31B antibody, overexpressing SEC31B-HA in SEC31A KO cells showed rescue of PC1 accumulation phenotype (data not shown).

KLHL12 regulate PC1 secretion through SEC31A

Overexpression of KLHL12 promotes PC1 export in human fibroblasts (IMR-90) through its interaction with SEC31A, as seen by the effect of the SEC31A interaction defective mutant KLHL12 FG289AA does not promote the secretion of PC1 (Jin et al., 2012). This phenotype was confirmed in WT HTPC1.1 cells (Fig. 4.2 A,B), and the effect of KLHL12 overexpression was tested on SEC31A KO cells (Fig. 4.2 C,D). Neither KLHL12 WT nor FG289AA mutant were able to promote the clearance of intracellular PC1 in SEC31A KO cells, showing that KLHL12 requires SEC31A to accelerate PC1 secretion (Fig. 4.2 C-D). Both WT and the FG289AA mutant co-localized with PC1 independent of the expression of SEC31A, suggesting that KLHL12 is not recruited to cargo-loaded ER regions by SEC31A (Fig. 4.2 B-D). It is worth mentioning that giant KLHL12 structures (distinct from large COPII, as these structures are much larger in size and often not co-localized with PC1) were also observed in SEC31A KO cells (Fig. 4.2 C), however, I failed to observe these structures in cells expressing the KLHL12 FG289AA mutant protein. This suggests that SEC31A is not required for KLHL12 to form giant inclusion body-like structures in the cell and FG289AA is not prone to such aggregation. The self-aggregating property of KLHL12 is also evident during the purification of recombinant KLHL12 from *E coli* (Fig. 4.S2 A-C). After cleavage of the MBP tag from purified MBP-KLHL12, a size exclusion column Superdex 200 was used to separate KLHL12 and MBP where KLHL12 was found excluded in the void fraction thus exceeding the estimated exclusion size of 600 kD, well beyond the molecular weight and dimensions of KLHL12 dimers. Thus, I obtained a low yield (typically 0.25-0.5% of the yield of this method) of purified, active KLHL12 (Fig. 4.S2 D).

The SEC31A C-terminal α-solenoid contains a novel binding site for KLHL12

Because the interaction between SEC31A and KLHL12 is important for promoting PC1 secretion, the KLHL12 interaction domain on SEC31A was investigated using co-immunoprecipitation. SEC31A comprises three major domains: the N-terminal cage-forming region (1-799aa) that interacts with SEC13 to form the COPII cage (Fath et al., 2007); the proline rich domain (PRD, 800-1092aa); and the C-terminal α-solenoid (1092-1220aa) (Fig. 4.3 A). These SEC31A domains were overexpressed in KI6 cells where KLHL12-FLAG expression was also induced. KLHL12-FLAG was isolated and the amount of co-immunoprecipitated SEC31A domains were assessed by immunoblotting (Fig. 4.3 B,C). Using the full-length SEC31A as a positive control, the cage forming region (1-799aa) and the C-terminal α-solenoid (1092-1220aa and 1114-1220aa) were co-immunoprecipitated with KLHL12. Our result confirmed a previously published interaction site in the N-terminal region of SEC31A and revealed another novel binding site at the C-terminus (Jin et al., 2012).

To confirm the binding between the C-terminal α-solenoid and KLHL12, I asked whether purified recombinant SEC31A fragment 950-1220aa, which contains the C-terminal α-solenoid (1114-1220aa) and a portion of the PRD, would interact with KLHL12 directly in vitro. Recombinant full length SEC13/31A was used as a positive control and the KLHL12 FG289AA mutant defective in SEC31A interaction was used as negative control. The SEC31A fragment 950-1220aa, which contained the C-terminal α-solenoid, interacted with KLHL12 WT but not FG289AA, whereas the active fragment 975-1040aa of PRD did not show interaction (Fig. 4.3 D).

CUL3-KLHL12 monoubiquitylates the C-terminus of SEC31A

SEC31A is monoubiquitylated by CUL3-KLHL12 in the cell and this process has been reconstituted in vitro (Jin et al., 2012). Because the ubiquitylation reaction requires binding of KLHL12 and SEC31A, I next tested whether the C-terminus of SEC31A (950-1220) can be monoubiquitylated by CUL3-KLHL12. Immunoblotting of SEC31A (950-1220) in completed reactions revealed unmodified and lower-mobility bands that had a difference of about 8.5 kD, the molecular weight (MW) of ubiquitin (Fig. 4.4 A). Formation of the lower-mobility band depended on the addition of essential components of an ubiquitylation reaction. Ubiquitylation was also confirmed by a monoclonal antibody that targets ubiquitin conjugates (both poly- and mono-) but not free ubiquitin.

Interestingly, the 947-1179aa fragment of SEC31B that is homologous to SEC31A (950-1220) was not monoubiquitylated by CUL3-KLHL12 (Fig. 4.4 B). Although there was a ubiquitin conjugate band at the putative migration of monoubiquitylated SEC31B (947-1179), it also appeared in the lane where the substrate was excluded and likely represented the ubiquitylated E2 conjugating enzyme UBCH5.

In an effort to find the ubiquitylation site at the C-terminus of SEC31A, an open-source sequence alignment software Clustal Omega was used to analyze the conservation between SEC31A and SEC31B. The PRDs were the least conserved between the paralogs, whereas the N-terminal cage-forming region and the C-terminal α-solenoid are relatively well-conserved. There are five lysines within the PRD of SEC31A (950-1220): four consecutive lysines at 1006-1009aa and a lysine at 1081aa. To test which sites were monoubiquitylated, I constructed lysine to arginine mutants of SEC31A (950-1220) and purified the mutant proteins for evaluation using the in vitro ubiquitylation reaction (Fig. 4.4. C-D). When an 8-16% gel was used instead of 4-20%, two monoubiquitylated species were resolved and the K to R mutations at 1006-1009aa ablated the higher-mobility species of the two monoubiquitylation bands. Therefore, the four lysines at 1006-1009aa accounted for one of the ubiquitylation sites at the C-terminus of SEC31A. Moreover, the short SEC31A fragment 975-1040aa that contained only four lysines at 1006-1009aa was also monoubiquitylated, albeit at much lower efficiency possibly due to the lack of the KLHL12 interaction site in 1114-1220aa.

Monoubiquitylation of the C-terminus of SEC31A inhibits its ability to accelerate SAR1 GTP hydrolysis

The four consecutive lysines at 1006-1009aa are part of the active fragment, which is sufficient to accelerate SAR1-GTP hydrolysis by potentiating the GTPase Activating Protein (GAP) activity of SEC23A (Bi et al., 2007). Therefore, we tested whether monoubiquitylation would have an effect on the rate of SAR1-GTP hydrolysis. A completed ubiquitylation reaction that contained about 15% of monoubiquitylated SEC31A was supplemented with SAR1-GTP, after which SEC23A/24D was added to induce GTP hydrolysis (Fig 4.5 A). Compared to the negative controls where a ubiquitylation reaction excluding ubiquitin was used, the presence of monoubiquitylated SEC31A decelerated SAR1-GTP hydrolysis.

The active fragment of SEC31A stimulates the GAP activity of SEC23 by orienting key residues of SEC23 into the active site of SAR1 (Bi et al., 2007). We tested the interaction dynamics between different COPII components in a binding assay. SEC31A (950-1220) was isolated from ubiquitylation reactions by affinity beads, which were then incubated with SEC23A/24D or SAR1 or both in the presence of GDP or GMP-PNP followed by co-immunoprecipitation analyses (Fig. 4.5 B). Because the interaction between SEC31A (950-1220) and SAR1 was weak, the amount of SAR1 that co-immunoprecipitated in the presence of SEC23 reflected how strongly SAR1 and SEC23 interacted. This was seen by the stronger SAR1 band co-precipitated in the presence of GMP-PNP, as SAR1-GTP binds SEC23 much stronger than SAR1-GDP (Fig. 4.5 B). Monoubiquitylation of SEC31A weakened the interaction between SEC23A and SAR1-GTP, which is consistent with the decrease in Sar1-GTP hydrolysis rate.

Discussion

The importance of SEC31A in large cargo secretion has been implicated in several published reports, here we investigated the role of SEC31A by creating KO clones using CRISPR/Cas9. Intracellular accumulation of PC1 was observed in SEC31A KO cells, and the PC1 secretion in response to ascorbate stimulation was markedly reduced (Fig. 4.1 A,B). This phenotype can be rescued by overexpressing SEC31A but not KLHL12 confirming the role of SEC31A during collagen secretion (Fig. 4.1 D, Fig. 4.2).

The interaction between SEC31A and KLH12 was shown to be important for the monoubiquitylation of SEC31A, enlargement of COPII, and accelerated PC1 secretion (Jin et al., 2012). I hypothesize that these correlated events are causative of each other: monoubiquitylation stimulates the enlargement of COPII vesicles which allowed the packaging of PC1. Although there is a logical relationship between the sizes of transport vehicles and cargos, the role of monoubiquitylation in regulating the size of COPII vesicles remains unexplained.

Here we propose a speculative mechanism by which monoubiquitylation of SEC31A may increase the size of a COPII vesicle. A novel KLHL12 binding site was identified in the C-terminal α-solenoid (1092-1220aa) of SEC31A (Fig 4.3 B-D), which allowed monoubiquitylation of one of the four consecutive lysine residues at 1006-1009aa of SEC31A (Fig 4.4 A, C-E). The crystal structure of the

active fragment of Sec31 in complex with Sar1 and Sec23 showed that residues 1006-1009 of the yeast Sec31 bind Sec23 and helps positioning side chains of Sec23 into the active pocket of Sar1-GTP to stimulate GTP hydrolysis (Bi et al., 2007). The presence of even just 15% of monoubiquitylated SEC31A (950-1220) resulted in a consistent decrease in SAR1-GTPase activity, possibly due to weakening of the SEC23A/SAR1-GTP interaction (Fig. 4.5).

The exchange of GDP to GTP activates SAR1, which exposes an amphipathic helix that intercalates into and induces membrane curvature (Futai et al., 2004; Lee et al., 2005). The withdrawal of the amphipathic helix during SAR1-GTP hydrolysis was implicated in membrane scission (Bacia et al., 2011). Regulating the rate of SAR1-GTP hydrolysis could change the timing of membrane scission and vesicle size. This is supported by the discovery of Sec24p-m11, a mutant that heightens the Sar1-GTPase activity and generates smaller COPII vesicles (Kung et al., 2012). Moreover, a mechanistic study of the CLSD causing mutation SEC23A M702V showed that procollagen packaging requires slower GTP hydrolysis (Kim et al., 2012). Interestingly, an N-terminal amphipathic helix on the clathrin adaptor CALM was recently identified and shown to play a central role in regulating the size of clathrin coated pits and vesicles, demonstrating a conserved mechanism in an independent pathway (Miller et al., 2015).

Besides monoubiquitylation, KLHL12 may induce large COPII formation through its ability to polymerize and associate with lipid in the membrane (Fig. 4.2 C; Fig. 4.S2). Because KLHL12 is recruited to large collagen puncta independent of SEC31A (Fig. 4.2), it could be recruited prior to SEC31A recruitment and its polymerization on membrane could provide a scaffold to allow the formation of a large SEC31A coat independent of the timely GTPase activity of the COPII complex. This hypothesis can be tested with mutant KLHL12 deficient in polymerization and normal in SEC31A binding.

Compared to the importance of TANGO1 in steady state collagen secretion, the KLHL12-SEC31A interaction seems to be more pertinent when the cell is in need of secreting large amounts of collagen in a short period of time (Jin et al., 2012). Timely collagen secretion is probably necessary at specific stages during development. As an example, the UPR transducer BBF2H7 was shown to increase the transcription of KLHL12 and other proteins involved in PC secretion in a developmental stage-specific manner (Ishikawa et al., 2017). Large COPII vesicles induced by KLHL12 overexpression often exceeded 300 nm and appeared less selective, as most of them were not positive for PC1 by

immunofluorescence microscopy. The potential excess of space and sacrifice in selectivity may be beneficial in the interest of speed.

Materials and methods

Antibodies

Commercially available antibodies used for immunofluorescence (IF) and immunoblotting (IB) were as follows: mouse anti-PC1 (clone 42024; QED Biosciences; 1:200 [1 mg/ml stock concentration] for IF); rabbit anti-SEC31A (Bethyl Laboratories; 1:200 for IF); mouse anti-SEC31A (BD, 1:5,000 for IB); mouse anti-FLAG (Thermo Fisher Scientific; 1:5,000 for IB); goat anti-FLAG (Novus Biologicals; for IF at 1:1,000); rab anti StrepII (abcam, 1:2,000 for IB); mouse anti mono- and polyubiquitylated conjugates (clone FK2; Enzo lifesciences; for IB at 1:2,000); mouse anti actin (abcam, 1:5,000 for IB). Rabbit anti–SAR1, SEC23A, and SEC24D were made in-house and used at 1:5,000 for IB.

Plasmids

For overexpression in human cells, SEC31A domains (1-799, 800-1091, 800-1113, 1092-1220, 1114-1220)-strepII were cloned into a pcDNA4 plasmid. Full length SEC31A/B-HA were cloned into pCS2+ plasmids. KLHL12 WT and FG289AA were cloned into a pcDNA5 vector and were gifts from Michael Rape's lab. For expression in *E coli*, SEC31A (950-1220)-FLAG/strepII, SEC31A (975-1040)-FLAG/strepII, SEC31B (948-1179)-strepII were cloned into pGex-2t. The mutations KKKK1006RRRR, K1081R, and KKKK1006RRRR+K1081R were introduced by site directed mutagenesis. MBP-TEV-KLHL12-His was a gift from Michael Rape's lab.

Cell culture, transfection, and drug treatments

Human osteosarcoma U-2OS and human fibrosarcoma HT-1080 were obtained from ATCC and maintained in DMEM plus 10% FBS (GE Healthcare). The construction and maintenance of HTPC1.1 and KI6 were described in Jin et al., 2012 and Gorur et al., 2017. HTPC1.1 stably expresses of COL1A1 was constructed from HT-1080 and the doxycycline-inducible KLHL12-3xFLAG

stable cell line (KI6) was constructed from HTPC1.1. Cells were kept in a 37°C incubator with 5% CO2. Transfection of DNA constructs was performed using Lipofectamine 2000 as detailed in the manual provided by Invitrogen. Ascorbate treatment used 0.25 mM ascorbic acid (Sigma-Aldrich) and 1 mM ascorbic-2-phosphate (Sigma-Aldrich). This concentration was in addition to the amount of ascorbic acid present in FBS (0.08 mM) as supplied by the manufacturer. Doxycycline (Sigma-Aldrich) was used at 1 μg/ml.

Construction of SEC31A KO cells

Standard CRISPR KO protocol was used to knockout SEC31A in HTPC1.1 and U-2OS cells. Briefly, two CRISPR guides were designed to target the first coding exon (exon2) of the human *SEC31A* gene: "AGTAGATCGTACAGCCATGCAGG" and "CTAGGTAAATGGGGTGATTCTGG". HTPC1.1 or U-2OS cells were transfected with pX330-Venus plasmids that carry the CRISPR guides, and single clones of Venus positive cells were sorted into 96-well plates. Clones were screened for the loss of SEC31A expression, and U-2OS clones were also screened for the endogenous expression of PC1 by immunoblotting. Candidate clones were genotyped with primers: "ATCTGTGTTCTGTGTTAGAC" and "TCTTCTCTCCTTTGAACTTACC", and those that carried only null alleles were kept as KO clones.

Immunofluorescence

The immunofluorescence protocol and imaging acquisition were described in Gorur et al., 2017. For characterizing SEC31A KO phenotype, a 20x air objective and pin hole of 3 au were used. Areas of comparable cell density were randomly selected through the DAPI channel, imaged with the same laser power and processed with the same parameter across all samples for unbiased comparison.

Immunoblotting

Polyacrylamide (4-20%) gels (Invitrogen) were used for most electrophoresis and 8-16% gels (Bio-Rad Laboratories) were used to resolve monoubiquitylated SEC31A (950-1220). Gels were transferred to PVDF (EMD Millipore) at a constant 0.4 A for 2 h. The PVDF membrane was incubated with antibodies (primary overnight at 4°C and secondary for 1 h at RT), and bound antibodies were visualized by the enhanced chemiluminescence method (Thermo Fisher

Scientific) on a ChemiDoc Imaging System (Bio-Rad Laboratories) with ImageLab software v4.0 (Bio-Rad Laboratories).

Co-immunoprecipitation

For co-immunoprecipitation from lysates, KI6 cells were transiently transfected with different SEC31A-StrepII domain constructs for 48 h. In the last 24 h, doxycycline was added to induce the overexpression of KLHL12. Cells were lysed in lysis buffer (PBS, 0.5% (v/v) Triton, proteinase inhibitors (Roch)). After centrifuging at 16,000 g for 10 min, the supernatant was incubated with pre-washed Strep-Tactin beads (IBA lifesciences) at 4°C for 3 h. Strep-Tactin beads were centrifuged and washed 4 times using lysis buffer, and proteins were eluted in sample buffer and heated at 65°C for 10 min for immunoblotting analyses.

For the in vitro binding assay, equal molar amount of recombinant wild-type or FG289AA mutant KLHL12 were incubated with equal molar amounts of full length, 950-1220aa or 975-1040aa of SEC31A-StrepII, and prewashed Strep-Tactin beads in binding buffer (20 mM HEPES, pH 7.2, 160mM KoAc, 0.1% Triton, 0.1 mg/ml BSA) at 4°C for 2 h. Strep-Tactin beads were centrifuged and washed 6 times with the binding buffer and proteins were eluted in sample buffer and heated at 65°C for 10 min followed by immunoblotting analyses.

For the COPII interaction assay, SEC31A (950-1220)-FLAG was isolated from complete ubiquitylation reactions by incubating with prewashed FLAG affinity beads at 4°C for 4 h. Sedimented beads were washed 6 times with 1x UBA buffer and further incubated with 5 ng/µl SEC23A/24D, 5 ng/µl SAR1A, 0.1mM GDP or GMP-PNP in the indicated combinations in binding buffer for 90 min at 4°C. Beads were washed 4 times with the binding buffer and proteins eluted in sample buffer and heated at 65°C for 10 min followed by immunoblotting analyses.

Protein purification

COPII proteins were purified as described previously in Kim et al., 2005 and Fromme et al., 2007. SAR1 and C-terminus of SEC31A (950-1220) or (975-1040) were purified from *E coli* with glutathione beads (GE) and cleaved with thrombin. SEC23A/24D, SEC13/31A were purified form sf9 cells with Ni-NTA followed by a monoQ column. Ubiquitylation proteins were described previously in Jin et al., 2012 and McGourty et al., 2016. KLHL12 was purified from *E coli* by affinity

binding to amylose resin and cleaved with MBP-TEV then purified again with Ni-NTA. CUL3/RBX1 was purified from *E coli* using the "split-n-coexpress" system as described in Zhuang et al., 2009 with glutathione resin, followed by TEV cleavage and the size exclusion column Superdex 200. UBA3, Ube2M, ubiquitin E1, UBCH5 were gifts from Michael Rape's lab. Nedd8 and ubiquitin were purchased from BostonBiochem.

In vitro ubiquitylation

The in vitro ubiquitylation reaction was performed as described in McGourty et al., 2016. To a neddylation reaction, 5 μM CUL3/RBX1, 63 μM Nedd8, 0.7 μM UBA3, 0.8 μM Ube2M, ATP regeneration system (1 mM ATP, 40 mM creatine phosphate, and 0.2 mg/ml creatine phosphokinase) were combined in 1X UBA buffer (50 mM Tris-HCl pH 7.5, 50 mM NaCl, 10 mM MgCl) and incubated at 30°C for 5 min. To an ubiquitylation reaction, 200 nM E1, 5 μM UBCH5, 1 μM $CUL3^{N8}$/RBX1, 1 μM KLHL12, 67 μM ubiquitin, 47 μM SEC31A (950-1220), ATP regeneration system, and 1mM DTT were added to 1 x UBA buffer and incubated at 30°C for 1hr. Ubiquitylation reactions were stopped by shifting to ice, and 1 μl of the reaction was diluted 50x with 1x sample buffer and 5 μl was used for immunoblotting. Small aliquots of complete ubiquitylation reactions were flash frozen in liquid nitrogen and stored at -80°C for use in other experiments.

GTPase activity assay

The tryptophan fluorescence assay was performed at 37°C as described in Fromme et al., 2007, using major-minor mix synthetic liposomes in a stirred-cell cuvette. To 0.3 mM liposomes in HKM buffer (20 mM HEPES pH 7.2, 160 mM KOAc, 1 mM $Mg(OAc)_2$), I added SAR1A to a final concentration of 2 μM. One min later, GTP was added to 30 μM. After spontaneous exchange of GDP for GTP was complete (another 15-30 min), 15 μl of completed ubiquitylation reactions containing 1.23 μM SEC31A (950-1220) was added where indicated, followed by the addition of 110 nM of SEC23A/24D complex.

Figures

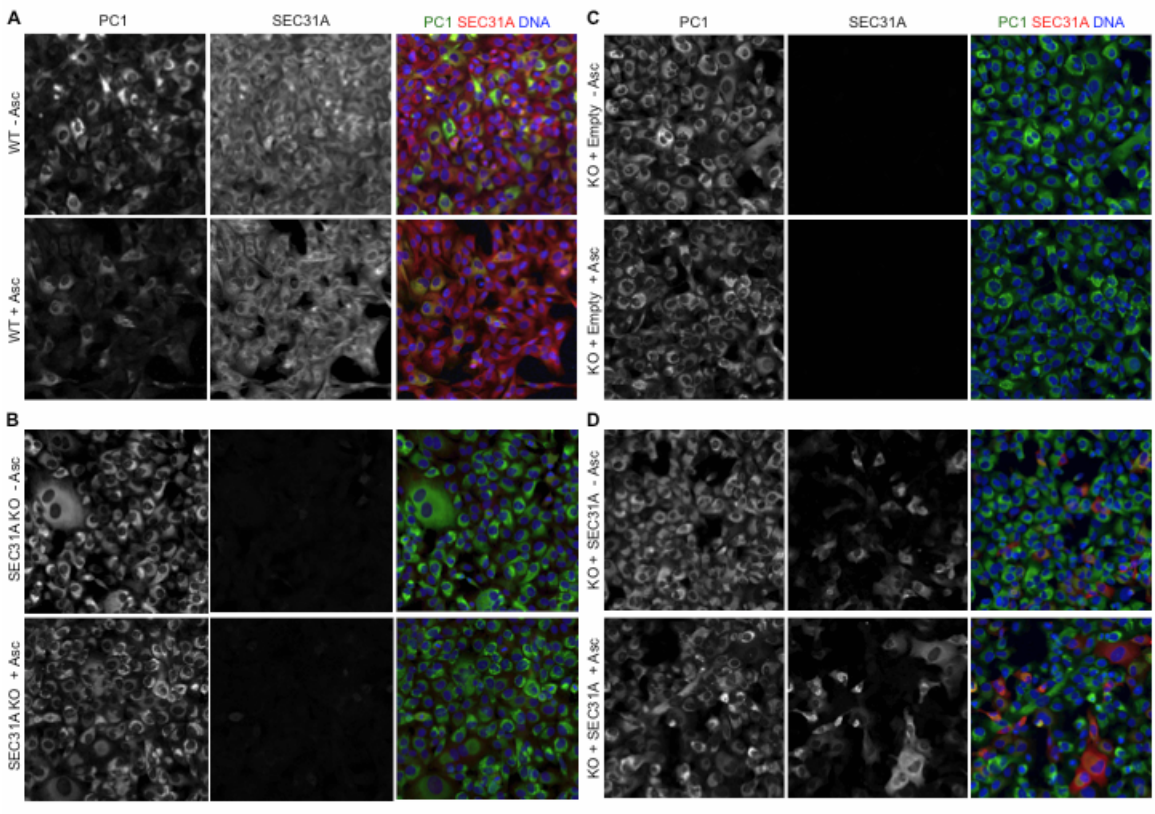

Figure 4.1. Knockout of SEC31A results in intracellular accumulation of PC1. Confocal images of wildtype (A) or SEC31A KO HTPC1.1 cells (B-D) immunofluorescently labeled for PC1 (green) and SEC31A (red), and DAPI stained for DNA (blue). SEC31A KO cells were transiently transfected with an empty construct (C) or one that coded for SEC31A (D). Cells in top fields of each panel were cultured in regular conditions (-Asc) and the ones in bottom fields were treated with ascorbate (+Asc) for 1 h prior to fixation.

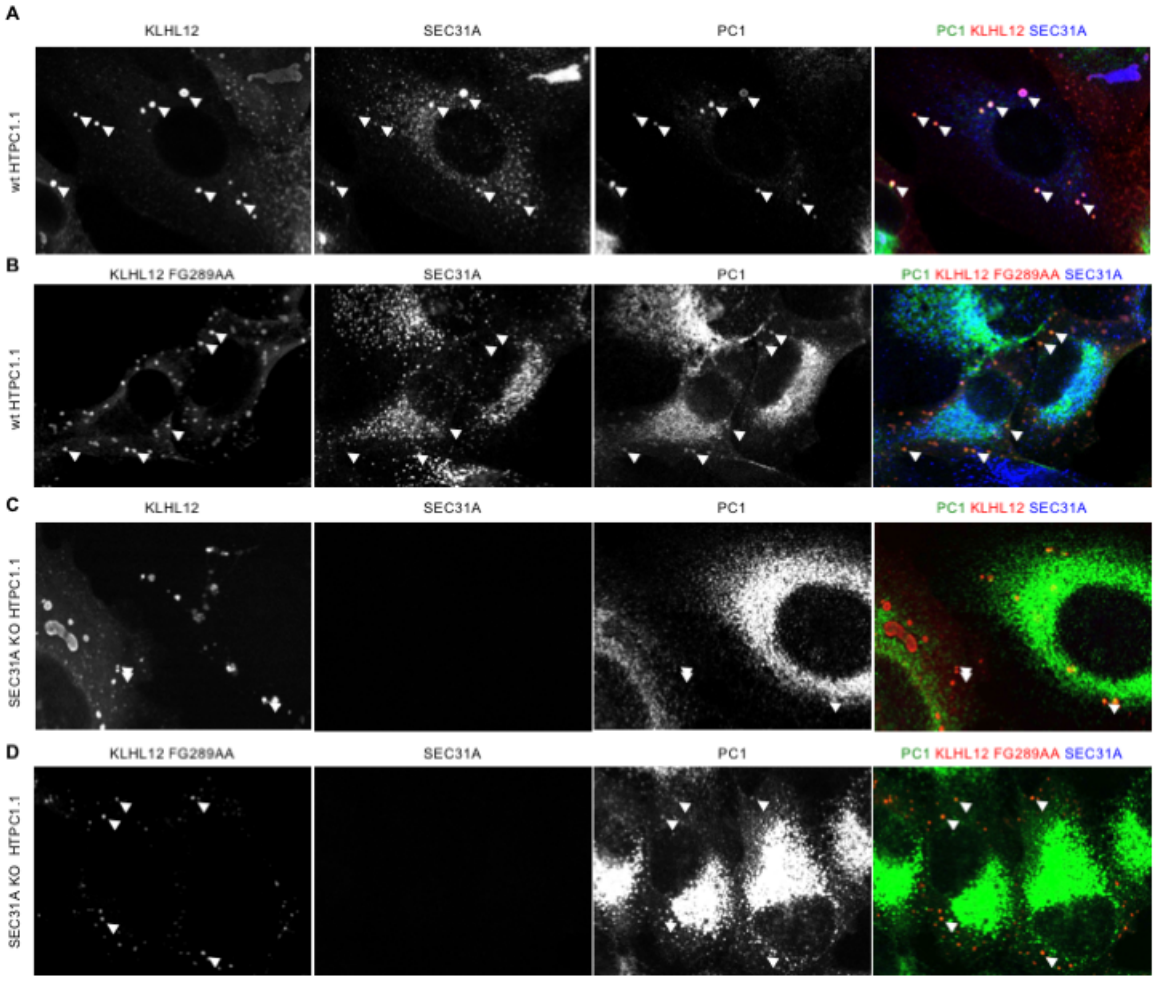

Figure 4.2. KLHL12 fails to regulate PC1 secretion in SEC31A KO cells. Confocal images of wild-type (A-B) or SEC31A KO HTPC1.1 cells (C-D) that were transiently transfected with wild-type KLHL12-FLAG (A, C) or KLHL12 FG289AA-FLAG mutant that is deficient in SEC31A binding (B, D) and immunofluorescently labeled against PC1 (green), FLAG (red), and SEC31A (blue). Arrows indicate co-localization between KLHL12 and PC1 regardless of the presence of SEC31A or the ability of KLHL12 to interact with SEC31A.

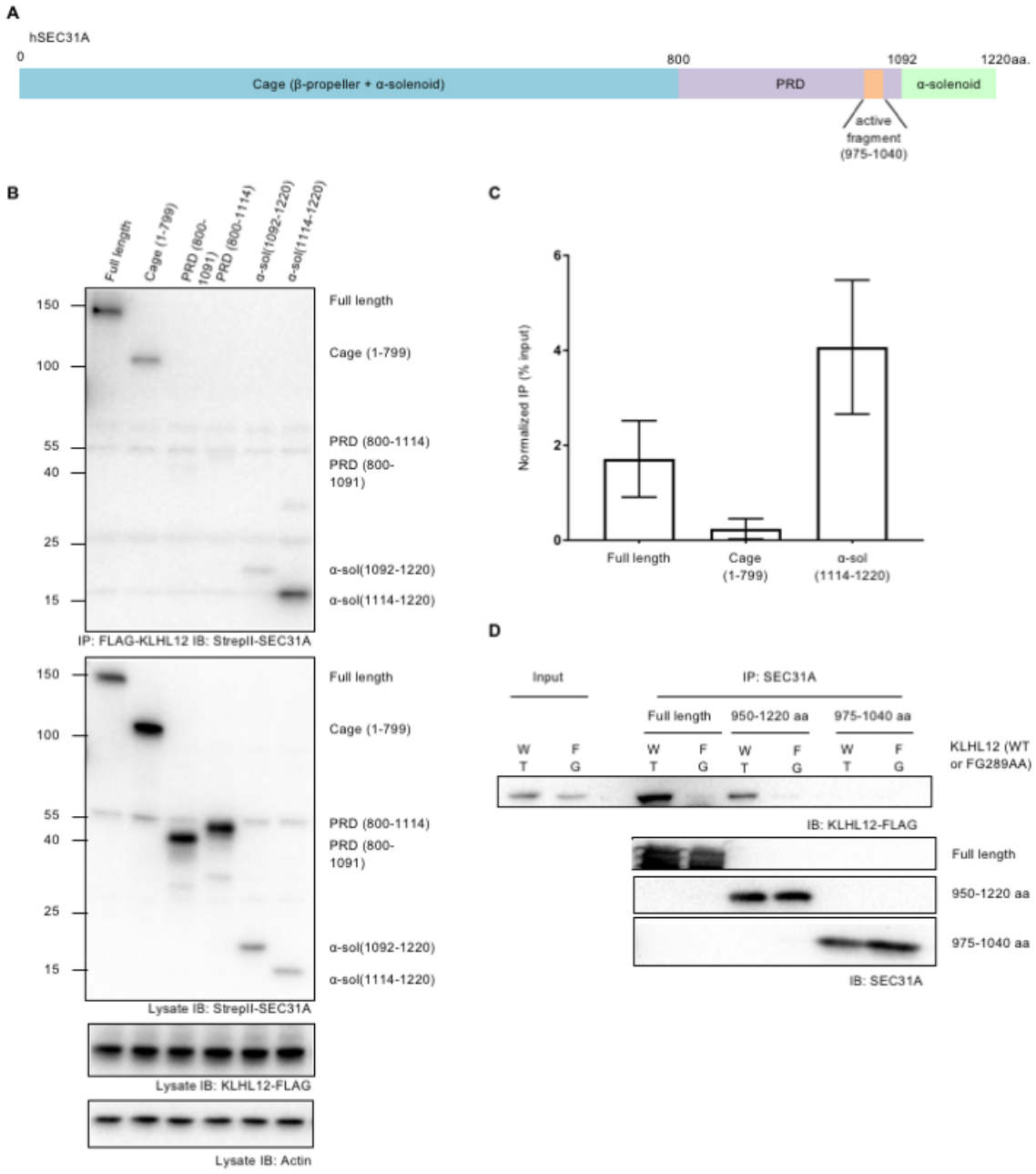

Figure 4.3. The C-terminal α-solenoid of SEC31A contains a novel binding site for KLHL12.

(A) Schematic representation of the domain structures of human SEC31A. The first 799aa makes up the outer cage with SEC13 (Fath et al., 2008). The unstructured proline rich domain (PRD) contains a small active fragment that accelerates SAR1-GTP hydrolysis (Bi et al., 2007). The C-terminal α-solenoid (α-sol) is defined as 1092-1220aa by UniProt, but helices starts from 1114aa accordingly to Phire2 structure prediction. (B) KI6 cells was transfected with full

length SEC31A, cage forming region (1-799aa), PRD (800-1092aa or 800-1113aa), C-terminal α-solenoid domain (1092-1220aa or 1114-1220aa) and induced for KLHL12-FLAG overexpression. KLHL12 was isolated from lysates and SEC31A domains that co-immunoprecipitated were analyzed by immunoblotting. The exposure was the same for the IP blot as the input (1.3%) blot. (C) Band intensities of co-immunoprecipitated SEC31A domains were normalized against their respective band intensities in the 1.3% input and plotted as a percentage of input (n=4, error bar: s.d.). (D) Immunoblotting analysis of recombinant wild-type or FG289AA mutant KLHL12 that co-immunoprecipitated with recombinant full length, 950-1220aa, or 975-1040aa of SEC31A.

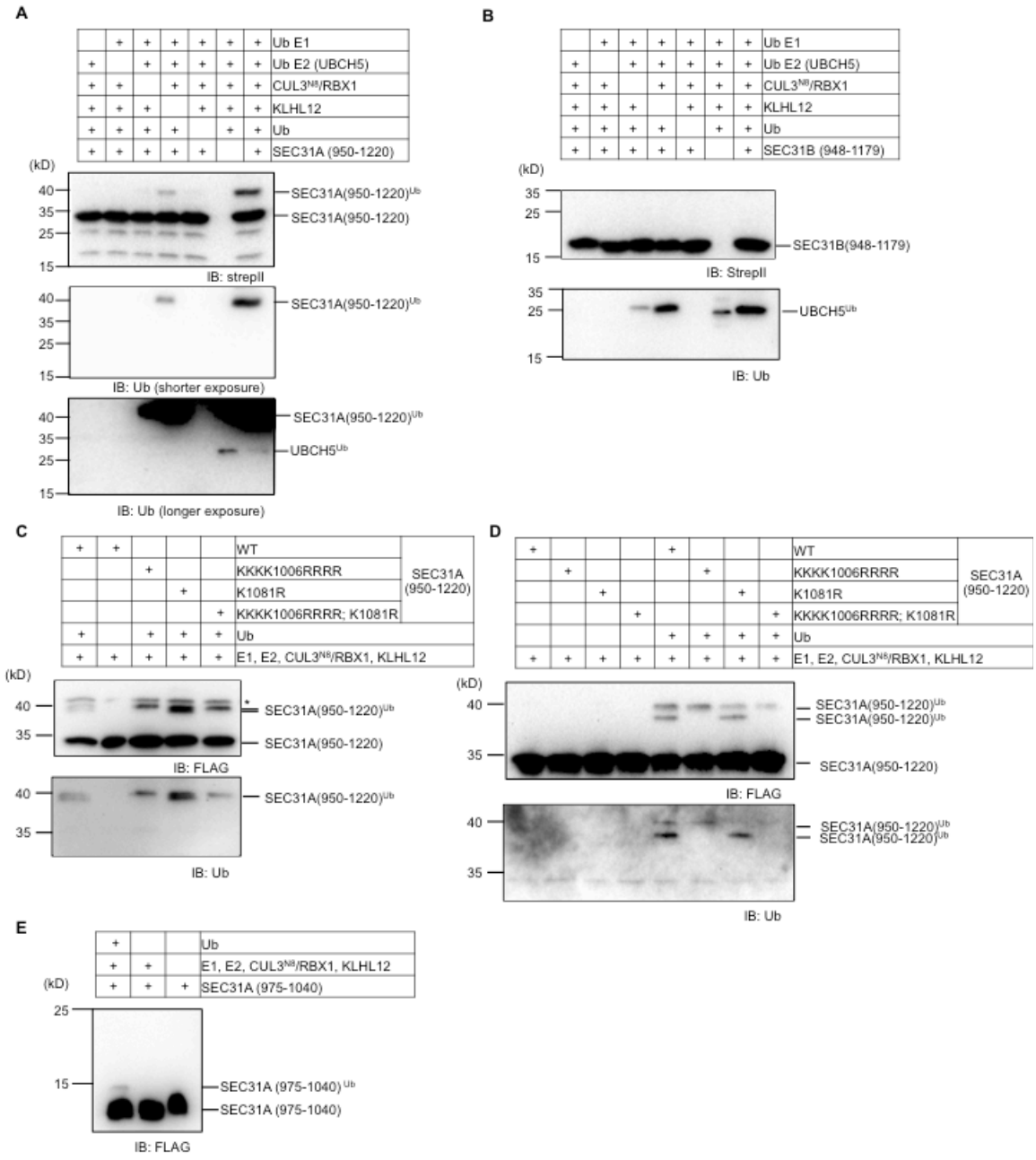

Figure 4.4. CUL3-KLHL12 monoubiquitylates lysines at 1006-1009aa of SEC31A in vitro.

(A) Monoubiquitylation of recombinant SEC31A (950-1220) in vitro under different conditions. Antibodies targeting SEC31A (950-1220)-strepII or ubiquitylated conjugates (ub) were used for Immunoblotting. (B) Recombinant SEC31B (948-1179) was not ubiquitylated by CUL3-KLHL12 in vitro. The

ubiquitylation band around 25 kD represents the 17 kD E2 UBCH5 conjugated with ubiquitin (8.5 kD) as evidenced by its presence when the substrate was omitted, which can also be detected in the corresponding control lane in (A). (C,D) In vitro ubiquitylation of purified recombinant K to R mutants of SEC31A (950-1220). Two monoubiquitylation bands of slightly different mobility were better resolved when 8-16% gel was used (D) comparing to 4-20% gel (C). *: An irrelevant band due to the use of a polyclonal FLAG antibody raised in goat, other experiments used a monoclonal FLAG antibody did not produce this band. (E) In vitro ubiquitylation of the recombinant SEC31A (975-1040), which contains only four lysines at 1006-1009aa.

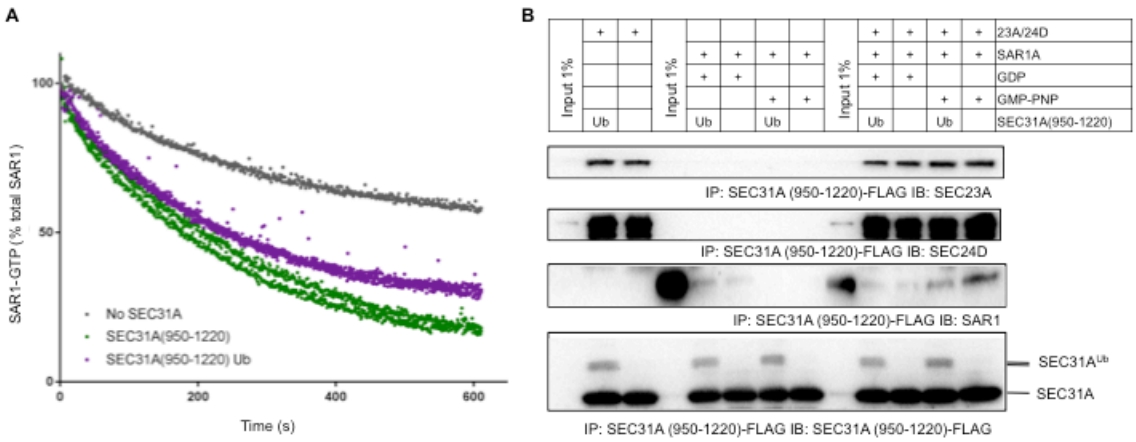

Figure 4.5. Monoubiquitylation inhibits SEC31A (950-1220) from accelerating SAR1-GTP hydrolysis.

(A) Tryptophan fluorescent intensity was measure against time as an indicator of the nucleotide associated with SAR1 (Antonny et al., 2001). Percentage of SAR1-GTP was calculated by normalizing the decrease in tryptophan fluorescence during GTP hydrolysis against total increase of tryptophan fluorescence after GDP was exchanged to GTP. To a sample containing GTP loaded SAR1A, a completed in vitro ubiquitylation reaction of SEC31A (950-1220) that contained 15% monoubiquitylated SEC31A (950-1220) was added (duplicates, both are in Purple). After the fluorescence reading stabilized, SEC23A/24D was added to trigger GTP hydrolysis. As controls, an ubiquitylation reaction that omitted ubiquitin (duplicates, both are in green) or no SEC31A was added (grey). (B) Monoubiquitylated SEC31A (950-1220)-FLAG was isolated from ubiquitylation reactions with FLAG affinity beads, which was subsequently incubated with SEC23A/24D or SAR1 or both and supplemented with GDP or GMP-PNP at 4°C for 90 min. SEC23A and SAR1 co-immunoprecipitated with monoubiquitylated SEC31A (950-1220) under different incubation conditions were compared with samples using SEC31A (950-1220) isolated from negative control ubiquitylation reactions as baits.

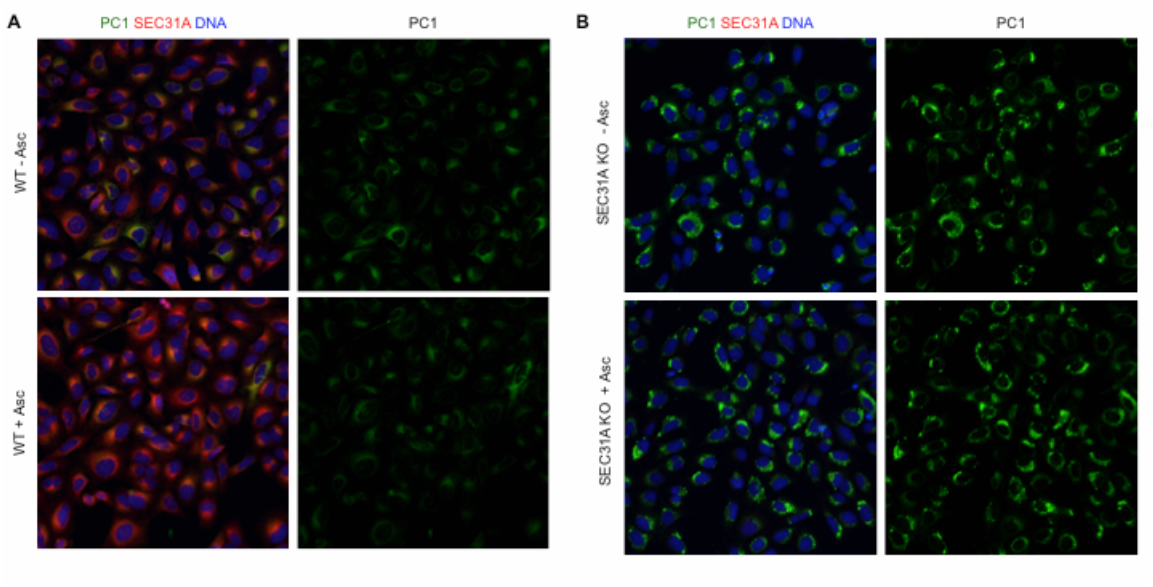

Figure 4.S1. Knockout of SEC31A leads to intracellular accumulation of endogenous PC1.

Confocal images of wildtype (A) or SEC31A KO U-2OS cells (B) clonally selected for comparable endogenous PC1 expression. Samples were immunofluorescently labeled for PC1 (green) and SEC31A (red), and DAPI stained for DNA (blue). Cells in top fields of each panel were cultured in regular conditions (-Asc) and the ones in bottom fields were treated with ascorbate (+Asc) for 1 h prior to fixation.

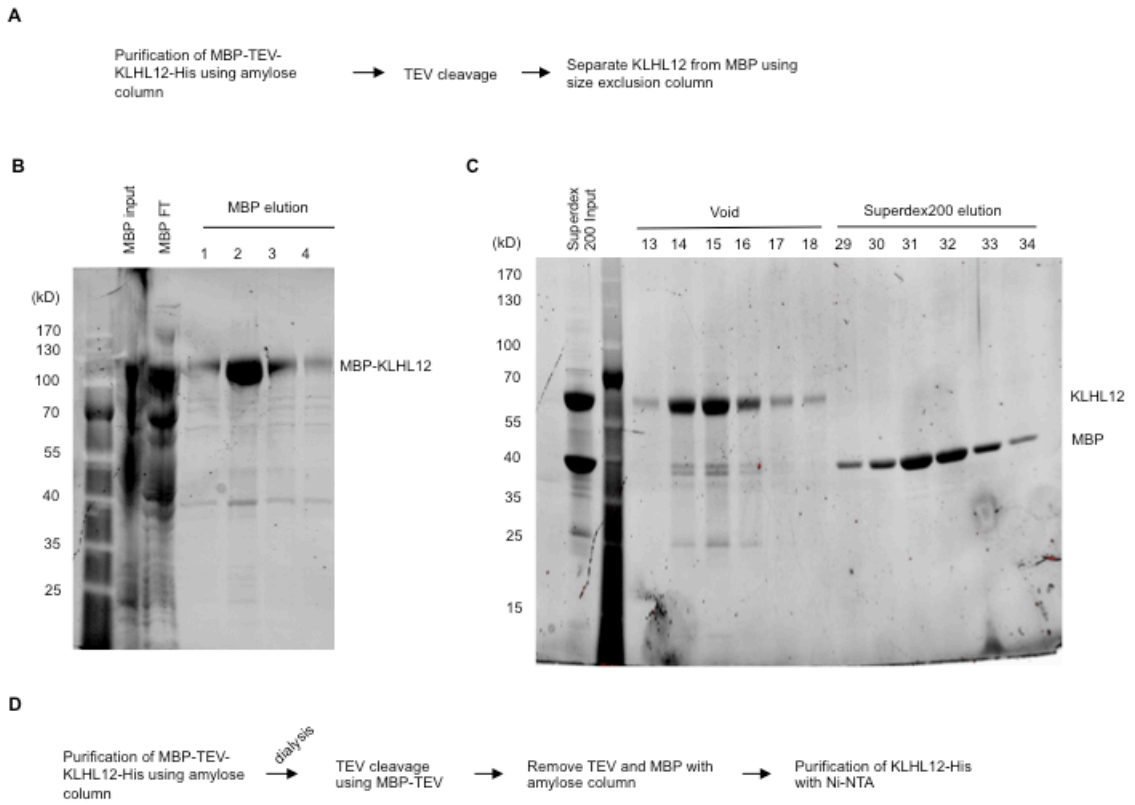

Figure 4.S2. Purification of KLHL12 from *E coli*.
(A) Schematic representation of the purification protocol that lead to the discovery of KLHL12 aggregates. The yield of KLHL12 from this method was 110 mg from 6 L of *E coli*. (B) Sypro-red protein staining of fractions taken from the amylose purification step. (C) Sypro-red protein staining of fractions taken from the Superdex 200 column. (D) Purification scheme that produces active KLHL12 developed by Colleen A. McGourty in Michael Rape's lab. The yield of KLHL12 using this method ranged between 0.25-0.5 mg from 6 L of *E coli*.

References

Antonny B., Madden D., Hamamoto S., Orci L., Schekman R. 2001. Dynamics of the COPII coat with GTP and stable analogues. *Nat. Cell Biol*. 3, 531–537

Bacia, K., E. Futai, S. Prinz, A. Meister, S. Daum, D. Glatte, J.A. Briggs, and R. Schekman. 2011. Multibudded tubules formed by COPII on artificial liposomes. *Sci Rep*. 1:17. doi:10.1038/srep00017.

Bächinger, H.P., K.J. Doege, J.P. Petschek, L.I. Fessler, and J.H. Fessler. 1982. Structural implications from an electron microscopic comparison of procollagen V with procollagen I, pC-collagen I, procollagen IV, and a Drosophila procollagen. *J. Biol. Chem.* 257:14590–2.

Bard, Casano, Mallabiabarrena, Wallace, Saito, Kitayama, Guizzunti, Hu, Wendler, Dasgupta, Perrimon, and Malhotra. 2006. Functional genomics reveals genes involved in protein secretion and Golgi organization. *Nature*. doi:10.1038/nature04377. 439:604–7.

Barlowe, and Helenius. 2015. Cargo Capture and Bulk Flow in the Early Secretory Pathway. *Annual Review of Cell and Developmental Biology*. doi:10.1146/annurev-cellbio-111315-125016. 32:1–26.

Barlowe, C., L. Orci, T. Yeung, M. Hosobuchi, S. Hamamoto, N. Salama, M.F. Rexach, M. Ravazzola, M. Amherdt, and R. Schekman. 1994. COPII: a membrane coat formed by Sec proteins that drive vesicle budding from the endoplasmic reticulum. *Cell*. 77:895–907.

Barlowe, and Schekman. 1993. SEC12 encodes a guanine-nucleotide-exchange factor essential for transport vesicle budding from the ER. *Nature*. doi:10.1038/365347a0. 365:347–349.

Bernstein, E.F., Y.Q. Chen, J.B. Kopp, L. Fisher, D.B. Brown, P.J. Hahn, F.A. Robey, J. Lakkakorpi, and J. Uitto. 1996. Long-term sun exposure alters the collagen of the papillary dermis. Comparison of sun-protected and photoaged skin by northern analysis, immunohistochemical staining, and confocal laser scanning microscopy. *J. Am. Acad. Dermatol.* 34:209–18.

Bi X., Mancias J.D., and Goldberg J. 2007. Insights into COPII coat nucleation from the structure of Sec23.Sar1 complexed with the active fragment of Sec31. Dev. Cell. 13:635–645. 10.1016/j.devcel.2007.10.006

Bossi, M., J. lling, V.N. Belov, V.P. Boyarskiy, R. Medda, A. Egner, C. Eggeling, A. nle, and S.W. Hell. 2008. Multicolor far-field fluorescence nanoscopy through isolated detection of distinct molecular species. *Nano letters*. 8:2463–2468. doi:10.1021/nl801471d.

Boyadjiev, S.A., J.C. Fromme, J. Ben, S.S. Chong, C. Nauta, D.J. Hur, G. Zhang, S. Hamamoto, R. Schekman, M. Ravazzola, L. Orci, and W. Eyaid. 2006. Cranio-lenticulo-sutural dysplasia is caused by a SEC23A mutation leading to abnormal endoplasmic-reticulum-to-Golgi trafficking. *Nat. Genet.* 38:1192–7. doi:10.1038/ng1876.

Chaumont, D.F., S Dallongeville, and N Chenouard. 2012. Icy: an open bioimage informatics platform for extended reproducible research. *Nature Methods.* 9: 690-96. doi:10.1038/nmeth.2075.

Dragovic, R., C. Gardiner, A. Brooks, D. Tannetta, D. Ferguson, P. Hole, B. Carr, C. Redman, A. Harris, P. Dobson, P. Harrison, and I. Sargent. 2011. Sizing and

phenotyping of cellular vesicles using Nanoparticle Tracking Analysis. *Nanomedicine Nanotechnol Biology Medicine*. 7:780–788. doi:10.1016/j.nano.2011.04.003.

Fath S, Mancias JD, Bi X, Goldberg J. Structure and organization of coat proteins in the COPII cage. Cell. 2007 Jun 29;129(7):1325-36.

Fisher, L.W. 1995. Antisera and cDNA probes to human and certain animal model bone matrix noncollagenous proteins. *Acta Orthopaedica Scandinavica*. 66:61–65.

Fisher, L.W., W. Lindner, M.F. Young, and J.D. Termine. 1989. Synthetic peptide antisera: their production and use in the cloning of matrix proteins. *Connective tissue research*. 21:43–50. doi:10.3109/03008208909049994.

Foellmer, H., K. Kawahara, J. Madri, H. Furthmayr, R. Timpl, and L. Tuderman. 1983. A Monoclonal Antibody Specific for the Amino Terminal Cleavage Site of Procollagen Type I. *Eur J Biochem*. 134:183–189. doi:10.1111/j.1432-1033.1983.tb07549.x.

Fromme, J.C., and R. Schekman. 2005. COPII-coated vesicles: flexible enough for large cargo? *Curr. Opin. Cell Biol.* 17:345–52. doi:10.1016/j.ceb.2005.06.004.

Fromme JC, Ravazzola M, Hamamoto S, Al-Balwi M, Eyaid W, Boyadjiev SA, Cosson P, Schekman R, Orci L.2007. The genetic basis of a craniofacial disease provides insight into COPII coat assembly. *Dev. Cell 13*, 623-634. DOI: 10.1016/j.devcel.2007.10.005

Futai, Hamamoto, Orci, and Schekman. 2004. GTP/GDP exchange by Sec12p enables COPII vesicle bud formation on synthetic liposomes. *The EMBO journal*. doi:10.1038/sj.emboj.7600428. 23:4146–55.

Garbes, L., K. Kim, A. Rieß, H. Hoyer-Kuhn, F. Beleggia, A. Bevot, M.J. Kim, Y.H. Huh, H.-S.S. Kweon, R. Savarirayan, D. Amor, P.M. Kakadia, T. Lindig, K.O. Kagan, J. Becker, S.A. Boyadjiev, B. Wollnik, O. Semler, S.K. Bohlander, J. Kim, and C. Netzer. 2015. Mutations in SEC24D, encoding a component of the COPII machinery, cause a syndromic form of osteogenesis imperfecta. *Am. J. Hum. Genet.* 96:432–9. doi:10.1016/j.ajhg.2015.01.002.

Gorur A, Yuan L, Kenny SJ, Baba S, Xu K, Schekman R. 2017. COPII-coated membranes function as transport carriers of intracellular procollagen I. J Cell Biol. Apr 20. pii: jcb.201702135. doi: 10.1083/jcb.201702135.

Huang, B. 2008. Three-Dimensional Super-Resolution Imaging by Stochastic Optical Reconstruction Microscopy. *Science*. 319.

Hung, Lam, Udeshi, Svinkina, Guzman, Mootha, Carr, and Ting. 2017. Proteomic mapping of cytosol-facing outer mitochondrial and ER membranes in living human cells by proximity biotinylation. *eLife*. doi:10.7554/eLife.24463. 6.

Hung, Udeshi, Lam, Loh, Cox, Pedram, Carr, and Ting. 2016. Spatially resolved proteomic mapping in living cells with the engineered peroxidase APEX2. Nature protocols. doi:10.1038/nprot.2016.018. 11:456–75.

Ishida, Y., H. Kubota, A. Yamamoto, A. Kitamura, H. Bächinger, and K. Nagata. 2006. Type I Collagen in Hsp47-null Cells Is Aggregated in Endoplasmic Reticulum and Deficient in N-Propeptide Processing and Fibrillogenesis. *Mol Biol Cell*. 17:2346–2355. doi:10.1091/mbc.E05-11-1065.

Ishida, Y., and K. Nagata. 2011. Hsp47 as a collagen-specific molecular chaperone. *Meth. Enzymol.* 499:167–82. doi:10.1016/B978-0-12-386471-0.00009-2.

Ishikawa, Y., S. Ito, K. Nagata, L.Y. Sakai, and H.P. Bächinger. 2016. Intracellular mechanisms of molecular recognition and sorting for transport of large extracellular matrix molecules. *Proc. Natl. Acad. Sci. U.S.A.* 113:E6036–E6044. doi:10.1073/pnas.1609571113.

Ishikawa, Toyama, Nakamura, et al (2017) UPR transducer BBF2H7 allows export of type II collagen in a cargo- and developmental stage-specific manner. The Journal of cell biology 216:1761–1774. doi: 10.1083/jcb.201609100

Jin, L., K.B. Pahuja, K.E. Wickliffe, A. Gorur, C. Baumgärtel, R. Schekman, and M. Rape. 2012. Ubiquitin-dependent regulation of COPII coat size and function. *Nature*. 482:495–500. doi:10.4161/cl.20372

Kim, S.-D.D., K.B. Pahuja, M. Ravazzola, J. Yoon, S.A. Boyadjiev, S. Hammamoto, R. Schekman, L. Orci, and J. Kim. 2012. SEC23-SEC31 interface plays critical role for export of procollagen from the endoplasmic reticulum. *J. Biol. Chem.* 287:10134–44. doi:10.1074/jbc.M111.283382.

Kim, J., S. Hamamoto, M. Ravazzola, L. Orci, and R. Schekman. 2005. Uncoupled packaging of amyloid precursor protein and presenilin 1 into coat protein complex II vesicles. *J. Biol. Chem.* 280:7758–68. doi:10.1074/jbc.M411091200.

Kung LF, Pagant S, Futai E, D'Arcangelo JG, Buchanan R, Dittmar JC, Reid RJ, Rothstein R, Hamamoto S, Snapp EL, Schekman R, Miller EA. 2012. Sec24p and Sec16p cooperate to regulate the GTP cycle of the COPII coat. EMBO J. 31, 1014-27

Lam, Martell, Kamer, Deerinck, Ellisman, Mootha, and Ting. 2015. Directed evolution of APEX2 for electron microscopy and proximity labeling. *Nature methods*. doi:10.1038/nmeth.3179. 12:51–4.

Lang, R.,M. Lapierre, A., L, Frotscher., M, Goldenring., R., J and E. W. Knapik. 2006. Secretory COPII coat component Sec23a is essential for craniofacial chondrocyte maturation. *Nature Genetics*. 38: 1198-1203. doi:10.1038/ng1880

Lee, M.C.S., Orci, L., Hamamoto, S., Futai, E., Ravazzola, M., and Schekman, R. 2005. Sar1p N-terminal helix initiates membrane curvature and completes the fission of a COPII vesicle. Cell 122, 605-617

Ma, W., and J. Goldberg. 2016. TANGO1/cTAGE5 receptor as a polyvalent template for assembly of large COPII coats. *Proc National Acad Sci*. 113:10061–10066. doi:10.1073/pnas.1605916113.

Maeda, Katada, and Saito. 2017. TANGO1 recruits Sec16 to coordinately organize ER exit sites for efficient secretion. The Journal of cell biology. doi:10.1083/jcb.201703084.216:1731–1743.

Maeda, Saito, and Katada. 2016. Distinct isoform-specific complexes of TANGO1 cooperatively facilitate collagen secretion from the endoplasmic reticulum. Molecular biology of the cell. doi:10.1091/mbc.E16-03-0196. 27:2688–96.

Malhotra, V. & Erlmann, P. The pathway of collagen secretion. *Annu. Rev. Cell Dev. Biol.***31**, 109–24 (2015).

Matsuoka, K., L. Orci, M. Amherdt, S.Y. Bednarek, S. Hamamoto, R. Schekman, and T. Yeung. 1998. COPII-coated vesicle formation reconstituted with purified coat proteins and chemically defined liposomes.*Cell*. 93:263–75. doi:10.1016/S0092-8674(00)81577-9.

Mancias J. D., Goldberg J. 2008. Structural basis of cargo membrane protein discrimination by the human COPII coat machinery. EMBO J. 27, 2918–2928

McCaughey, J., V.J. Miller, N.L. Stevenson, A.K. Brown, A. Budnik, K.J. Heesom, D. Alibhai, and D.J. Stephens. 2016. TFG Promotes Organization of Transitional ER and Efficient Collagen Secretion. *Cell Reports*. 15:1648–1659. doi:10.1016/j.celrep.2016.04.062.

McGourty, C.A., D. Akopian, C. Walsh, A. Gorur, A. Werner, R. Schekman, D. Bautista, and M. Rape. 2016. Regulation of the CUL3 Ubiquitin Ligase by a CalciumDependentCoadaptor. *Cell*.167:525538.e14.doi:10.1016/j.cell.2016.09.026.

Merte, J., D. Jensen, K. Wright, S. Sarsfield, Y. Wang, R. Schekman, and D.D. Ginty. 2010. Sec24b selectively sorts Vangl2 to regulate planar cell polarity during neural tube closure. *Nat. Cell Biol.*12:41–6; sup pp 1–8. doi:10.1038/ncb2002.

Miller, Beilharz, Malkus, Lee, Hamamoto, Orci, and Schekman. 2003. Multiple cargo binding sites on the COPII subunit Sec24p ensure capture of diverse membrane proteins into transport vesicles. *Cell*. 114:497–509.

Miller, Sahlender, Graham, and Höning. 2011. The molecular basis for the endocytosis of small R-SNAREs by the clathrin adaptor CALM. doi:10.1016/j.cell.2011.10.038.

Mironov, A.A., A.A. Mironov, G.V. Beznoussenko, A. Trucco, P. Lupetti, J.D. Smith, W.J. Geerts, A.J. Koster, K.N. Burger, M.E. Martone, T.J. Deerinck, M.H. Ellisman, and A. Luini. 2003. ER-to-Golgi carriers arise through direct en bloc protrusion and multistage maturation of specialized ER exit domains. *Dev. Cell*. 5:583–94. doi:10.1016/S1534-5807(03)00294-6.

Mironov, A.A., G.V. Beznoussenko, A. Luini, and R.S. Polishchuk. 2005. Visualizing Intracellular Events In Vivo by Combined Video Fluorescence and 3 D Electron Microscopy. *Methods in enzymology*. 404:43–57.

Nagai, N., M. Hosokawa, S. Itohara, E. Adachi, T. Matsushita, N. Hosokawa, and K. Nagata. 2000. Embryonic lethality of molecular chaperone hsp47 knockout mice is associated with defects in collagen biosynthesis. *J. Cell Biol.* 150:1499–506.

Nakano, Brada, and Schekman. 1988. A membrane glycoprotein, Sec12p, required for protein transport from the endoplasmic reticulum to the Golgi apparatus in yeast. doi:10.1083/jcb.107.3.851.

Noble, A.J., Q. Zhang, J. O'Donnell, H. Hariri, N. Bhattacharya, A.G. Marshall, and S.M. Stagg. 2013. A pseudoatomic model of the COPII cage obtained from cryo-electron microscopy and mass spectrometry. *Nat. Struct. Mol. Biol.* 20:167–73. doi:10.1038/nsmb.2467.

Nogueira, C., P. Erlmann, J. Villeneuve, A.J.J. Santos, E. Martínez-Alonso, J.Á.Á. Martínez-Menárguez, and V. Malhotra. 2014. SLY1 and Syntaxin 18 specify a distinct pathway for procollagen VII export from the endoplasmic reticulum. *Elife*. 3:e02784. doi:10.7554/eLife.02784.

Oecal, S., E. Socher, M. Uthoff, C. Ernst, F. Zaucke, H. Sticht, U. Baumann, and J.M. Gebauer. 2016. The pH-dependent Client Release from the Collagen-specific Chaperone HSP47 Is triggered by a Tandem Histidine Pair. *J. Biol. Chem.* 291:12612–26. doi:10.1074/jbc.M115.706069.

Ono, T., T. Miyazaki, Y. Ishida, M. Uehata, and K. Nagata. 2012. Direct in vitro and in vivo evidence for interaction between Hsp47 protein and collagen triple helix. *J. Biol. Chem.* 287:6810–8. doi:10.1074/jbc.M111.280248.

Pastor-Pareja, JC, and T Xu. 2011. Shaping cells and organs in Drosophila by opposing roles of fat body-secreted Collagen IV and perlecan. *Developmental cell*.

Pautke, C., M. Schieker, T. Tischer, A. Kolk, P. Neth, W. Mutschlet, and S. MILZ. 2004. Characterization of osteosarcoma cell lines MG-63, Saos-2 and U-2 OS in comparison to human osteoblasts. *Anticancer research*. 24:3743–3748

Petley-Ragan, L., E. Ardiel, C. Rankin, and V. Auld. 2016. Accumulation of Laminin Monomers in Drosophila Glia Leads to Glial Endoplasmic Reticulum Stress and Disrupted Larval Locomotion. *J Neurosci*. 36:1151–1164. doi:10.1523/J Neurosci.1797-15.2016.

Presley, J.F., N.B. Cole, T.A. Schroer, K. Hirschberg, K.J. Zaal, and J. Lippincott-Schwartz. 1997. ER-to-Golgi transport visualized in living cells. *Nature*. 389:81–5. doi:10.1038/38001.

Raote, Bellido, Pirozzi, Zhang, Melville, Parashuraman, Zimmermann, and Malhotra. 2017. TANGO1 assembles into rings around COPII coats at ER exit sites. *The Journal of cell biology*. doi:10.1083/jcb.201608080. 216:901–909.

Roberts, B., C. Clucas, and I.L. Johnstone. 2003. Loss of SEC-23 in Caenorhabditis elegans causes defects in oogenesis, morphogenesis, and extracellular matrix secretion. *Molecular biology of the cell*. 14:4414–4426.

Rust, M., M. Bates, and X. Zhuang. 2006. Sub-diffraction-limit imaging by stochastic optical reconstruction microscopy (STORM). *Nat Methods*. 3:793–796. doi:10.1038/nmeth929.

Saito, K., M. Chen, F. Bard, S. Chen, H. Zhou, D. Woodley, R. Polischuk, R. Schekman, and V. Malhotra. 2009. TANGO1 facilitates cargo loading at endoplasmic reticulum exit sites. *Cell*. 136:891–902. doi:10.1016/j.cell.2008.12.025.

Saito, K., K. Yamashiro, Y. Ichikawa, P. Erlmann, K. Kontani, V. Malhotra, and T. Katada. 2011. cTAGE5 mediates collagen secretion through interaction with TANGO1 at endoplasmic reticulum exit sites.*Mol. Biol. Cell*. 22:2301–8. doi:10.1091/mbc.E11-02-0143.

Saito, K., K. Yamashiro, N. Shimazu, T. Tanabe, K. Kontani, and T. Katada. 2014. Concentration of Sec12 at ER exit sites via interaction with cTAGE5 is required for collagen export. *J. Cell Biol.* 206:751–62. doi:10.1083/jcb.201312062.

Santos, A.J.J., C. Nogueira, M. Ortega-Bellido, and V. Malhotra. 2016. TANGO1 and Mia2/cTAGE5 (TALI) cooperate to export bulky pre-chylomicrons/VLDLs from the endoplasmic reticulum. *J. Cell Biol.*213:343–54. doi:10.1083/jcb.201603072.

Sarmah, S, A Barrallo-Gimeno, and DB Melville. 2010. Sec24D-dependent transport of extracellular matrix proteins is required for zebrafish skeletal morphogenesis. *PloS one*. doi:10.1371/journal.pone.0010367.

Satoh, M., K. Hirayoshi, S. Yokota, N. Hosokawa, and K. Nagata. 1996. Intracellular interaction of collagen-specific stress protein HSP47 with newly synthesized procollagen. *J. Cell Biol.* 133:469–83. doi:10.1083/jcb.133.2.469.

Scales, S.J., R. Pepperkok, and T.E. Kreis. 1997. Visualization of ER-to-Golgi transport in living cells reveals a sequential mode of action for COPII and COPI. *Cell*. 90:1137–48. doi:10.1016/S0092-8674(00)80379-7.

Shima, D.T., S.J. Scales, T.E. Kreis, and R. Pepperkok. 1999. Segregation of COPI-rich and anterograde-cargo-rich domains in endoplasmic-reticulum-to-Golgi transport complexes. *Curr. Biol.*9:821–4. doi:10.1016/S0960-9822(99)80365-0.

Siddiqi, S.A., F.S. Gorelick, J.T. Mahan, and C.M. Mansbach. 2003. COPII proteins are required for Golgi fusion but not for endoplasmic reticulum budding of the pre-chylomicron transport vesicle. *J. Cell. Sci.* 116:415–27. doi:10.1242/jcs.00215.

Siddiqi, S., U. Saleem, N.A. Abumrad, N.O. Davidson, J. Storch, S.A. Siddiqi, and C.M. Mansbach. 2010. A novel multiprotein complex is required to generate the prechylomicron transport vesicle from intestinal ER. *J. Lipid Res.* 51:1918–28. doi:10.1194/jlr.M005611.

Stephens, D.J., N. Lin-Marq, A. Pagano, R. Pepperkok, and J.P. Paccaud. 2000. COPI-coated ER-to-Golgi transport complexes segregate from COPII in close proximity to ER exit sites. *J. Cell. Sci.*113:2177–85.

Stephens, D.J., and R. Pepperkok. 2002. Imaging of procollagen transport reveals COPI-dependent cargo sorting during ER-to-Golgi transport in mammalian cells. *J. Cell. Sci.* 115:1149–60.

Tasab, M., M.R. Batten, and N.J. Bulleid. 2000. Hsp47: a molecular chaperone that interacts with and stabilizes correctly-folded procollagen. *EMBO J.* 19:2204–11. doi:10.1093/emboj/19.10.2204.

Tasab, M., L. Jenkinson, and N.J. Bulleid. 2002. Sequence-specific recognition of collagen triple helices by the collagen-specific molecular chaperone HSP47. *J. Biol. Chem.* 277:35007–12. doi:10.1074/jbc.M202782200.

Testa, I, CA Wurm, R Medda, and E Rothermel. 2010. Multicolor fluorescence nanoscopy in fixed and living cells by exciting conventional fluorophores with a single wavelength. *Biophysical journal*. doi:10.1016/j.bpj.2010.08.012.

Townley, A.K., Y. Feng, K. Schmidt, D.A. Carter, R. Porter, P. Verkade, and D.J. Stephens. 2008. Efficient coupling of Sec23-Sec24 to Sec13-Sec31 drives COPII-dependent collagen secretion and is essential for normal craniofacial development. *J. Cell. Sci.* 121:3025–34. doi:10.1242/jcs.031070.

Venditti, R., T. Scanu, M. Santoro, G. Tullio, A. Spaar, R. Gaibisso, G.V. Beznoussenko, A.A. Mironov, A. Mironov, and L. Zelante. 2012. Sedlin controls the ER export of procollagen by regulating the Sar1 cycle. *Science*. 337:1668–1672.

Weissman, Plutner, and Balch. 2001. The mammalian guanine nucleotide exchange factor mSec12 is essential for activation of the Sar1 GTPase directing endoplasmic reticulum export. *Traffic (Copenhagen, Denmark)*. doi:10.1034/j.1600-0854.2001.20704.x. 2:465–75.

Widmer, C., J.M. Gebauer, E. Brunstein, S. Rosenbaum, F. Zaucke, C. Drögemüller, T. Leeb, and U. Baumann. 2012. Molecular basis for the action of the collagen-specific chaperone Hsp47/SERPINH1 and its structure-specific

client recognition. *Proc. Natl. Acad. Sci. U.S.A.* 109:13243–7. doi:10.1073/pnas.1208072109.

Wilson, D.G., K. Phamluong, L. Li, M. Sun, T.C. Cao, P.S. Liu, Z. Modrusan, W.N. Sandoval, L. Rangell, R.A. Carano, A.S. Peterson, and M.J. Solloway. 2011. Global defects in collagen secretion in a Mia3/TANGO1 knockout mouse. *J. Cell Biol.*193:935–51. doi:10.1083/jcb.201007162.

Zanetti, G., K.B. Pahuja, S. Studer, S. Shim, and R. Schekman. 2012. COPII and the regulation of protein sorting in mammals. *Nat. Cell Biol.* 14:20–8. doi:10.1038/ncb2390.

Zhuang M, Calabrese MF, Liu J, Waddell MB, Nourse A, Hammel M, Miller DJ, Walden H, Duda DM, Seyedin SN, Hoggard T, Harper JW, White KP, Schulman BA. 2009. *Mol Cell.* 36(1):39-50*.* doi:10.1016/j.molcel.2009.09.022.

Zhu, M., J. Tao, M.P. Vasievich, W. Wei, G. Zhu, R.N. Khoriaty, and B. Zhang. 2015. Neural tube opening and abnormal extraembryonic membrane development in SEC23A deficient mice. *Scientific reports*. 5:15471. doi:10.1038/srep15471.